การสำรวจการเคลื่อนตัวของLNAPLในตัวกลางพรุนชนิดไม่อิ่มตัวด้วยน้ำในห้องปฏิบัติการ

นายสุวสันต์ สุดแสง

วิทยานิพนธ์นี้เป็นส่วนหนึ่งของการศึกษาตามหลักสูตรปริญญาวิศวกรรมศาสตรดุษฎีบัณฑิต

สาขาวิชาวิศวกรรมโยธา ภาควิชาวิศวกรรมโยธา

คณะวิศวกรรมศาสตร์ จุฬาลงกรณ์มหาวิทยาลัย

ปีการศึกษา 2554

LABORATORY INVESTIGATION OF LNAPL MIGRATION IN UNSATURATED POROUS MEDIA

Mr. Suwasan Sudsaeng

A Dissertation Submitted in Partial Fulfillment of the Requirements
for the Degree of Doctor of Philosophy Program in Civil Engineering
Department of Civil Engineering
Faculty of Engineering
Chulalongkorn University
Academic Year 2011

Thesis Title	LABORATORY INVESTIGATION OF LNAPL MIGRATION IN UNSATURATED POROUS MEDIA
By	Mr. Suwasan Sudsaeng
Field of Study	Civil Engineering
Thesis Advisor	Associate Professor Suched Likitlersuang, D.Phil

---

Accepted by the Faculty of Engineering, Chulalongkorn University in Partial Fulfillment of the Requirements for the Doctoral Degree

……Dean of the Faculty of Engineering
(Associate Professor Boonsom Lerdhirunwong, Dr.Ing.)

THESIS COMMITTEE

…….. Chairman
(Associate Professor Boonsom Lerdhirunwong, Dr.Ing.)

……..……. Thesis Advisor
(Associate Professor Suched Likitlersuang, D.Phil)

…….. Thesis Co-advisor
(Professor Takeshi Katsumi, D.Eng)

…….. Examiner
(Associate Professor Supot Teachavorasinskun, D.Eng)

…….. Examiner
(Associate Professor Tirawat Boonyatee, D.Eng.)

…….. External Examiner
(Assistant Professor Siam Yimsiri, Ph.D.)

สุวสันต์ สุดแสง: การสำรวจการเคลื่อนตัวของ LNAPL ในตัวกลางพรุนชนิดไม่อิ่มตัวด้วยน้ำในห้องปฏิบัติการ (Laboratory investigation of LNAPL migration in unsaturated porous media) อ. ที่ปรึกษาวิทยานิพนธ์หลัก: รศ. ดร. สุเชษฐ์ ลิขิตเลอสรวง, 115 หน้า.

ปัญหาน้ำใต้ดินและดินปนเปื้อนด้วยสารเคมีที่ไม่ละลายน้ำหรือละลายน้ำได้น้อยที่เรียกกันว่า NAPL (Non-Aqueous Phase Liquid) มักพบบ่อยในแหล่งปนเปื้อน และ การกระบวนการบำบัดสารปนเปื้อนจำพวกนี้มีความซับซ้อนเป็นอย่างยิ่ง ในการศึกษาครั้งนี้จะใช้น้ำมันดีเซลซึ่งจัดเป็น NAPL ชนิดที่มีความหนาแน่นน้อยกว่าน้ำหรือ LNAPL (Light Non-Aqueous Phase Liquid) และใช้ทรายออตตาวาเบอร์ 3820 และเบอร์ 3821 เป็นตัวกลางพรุน การศึกษานี้เป็นการศึกษาทดลองถึงผลกระทบของการไหลของน้ำใต้ดินที่มีผลต่อการเคลื่อนตัวของน้ำมันดีเซลในตัวกลางพรุนชนิดไม่อิ่มตัวด้วยน้ำ วิธีSimplified image analysis method (SIAM) (Flores, 2010)ใช้ในการหาค่าการกระจายตัวของระดับการอิ่มตัวด้วยของเหลว ซึ่งก่อนดำเนินการศึกษาทดลองต้องทำการพิสูจน์ว่าตัวกลางพรุนที่ใช้มีความสัมพันธ์ระหว่างอัตราความเข้มแสงเฉลี่ย ระดับการอิ่มตัวด้วยน้ำ และระดับการอิ่มตัวด้วยน้ำมันดีเซลมีความสัมพันธ์กันเป็นแบบเชิงเส้น วิธี SIAM จึงจะสามารถนำมาใช้ในการศึกษาทดลองได้ คอลัมภ์อะคริลิคหนึ่งมิติ ขนาด 3.5 ซม. x 3.5 ซม. x 110 ซม. ใช้ในการศึกษาถึงผลกระทบของการขึ้นลงของน้ำใต้ดินที่มีต่อการเคลื่อนตัวของน้ำมันดีเซลและ แทงค์อะคริลิคสองมิติ ขนาด 3.5 ซม. x 50 ซม. x 60 ซม.ใช้ในการศึกษาถึงผลกระทบของการขึ้นลงของน้ำใต้ดินและการไหลของน้ำใต้ดินที่มีต่อการเคลื่อนตัวของน้ำมันดีเซล ดำเนินการทดลองทั้งสิ้นใน 8 คอลัมภ์ และ 12 แทงค์ โดยดำเนินการทดลองทั้งในตัวกลางพรุนเนื้อเดียวและตัวกลางพรุนเนื้อผสม ผลการศึกษาทดลองพบว่า การขึ้นลงของน้ำใต้ดินมีอิทธิพลอย่างมีนัยสำคัญในการกระจายของระดับการอิ่มตัวด้วยน้ำมันดีเซล ทั้งในเขตอิ่มน้ำและเขตอิ่มอากาศ และอัตราการไหลของน้ำใต้ดินที่สูงมีผลทำให้การกระจายตัวของน้ำมันดีเซลได้มากกว่า อัตราการไหลของน้ำใต้ดินที่ต่ำ ก่อให้เกิดการปนเปื้อนของน้ำมันดีเซลในชั้นดินได้ในวงกว้าง

ภาควิชา วิศวกรรมโยธา ลายมือชื่อนิสิต .....

สาขาวิชา วิศวกรรมโยธา ลายมือชื่อ อ.ที่ปรึกษาวิทยานิพนธ์หลัก .....

ปีการศึกษา 2554

497 18360 21: MAJOR CIVIL ENGINEERING
KEYWORDS: LNAPL / DIESEL / SIMPLIFIED IMAGE ANALYSIS METHOD / UNSATURATED POROUS MEDIA / SATURATION

SUWASAN SUDSAENG: LABORATORY INVESTIGAION OF LNAPL MIGRATION IN UNSATURATED POROUS MEDIA. ADVISOR: ASSOC. PROF. SUCHED LIKITLERSUANG, D.Phil., 115 pp.

Soil and groundwater contamination with non aqueous phase liquids (NAPLs) are often found at contaminated sites and it lead sophisticated procedure for remediation. This research experimentally investigates the effects of groundwater movement on the migration of LNAPL in the subsurface. Diesel was selected as LNAPL and it can be classified as a light non-aqueous phase liquid (LNAPL) because of its lower density than water. Ottawa#3820 sand and Ottawa#3 sand were used as porous media. The Simplified Image Analysis Method (SIAM) (Flores, 2010) is used as a non-intrusive and non-destructive technique to measure temporal and spatial distribution of fluid saturations in a whole domain. Linear relationships between average optical density (AOD) and degree of water saturation (S_w) and Degree of diesel saturation (S_o) for Ottawa#3820 sand and Ottawa#3821 sand were established as required by SIAM. One-dimensional column (3.5 cm x 3.5 cm x 110 cm transparent acrylics column) is used to study the effects of water table fluctuation and Two-dimensional tank (3.5 cm x 50 cm x 60 cm transparent acrylic tank) is used to study totally effects of groundwater level fluctuation and horizontal groundwater flow. 8 one-dimensional column tests and 12 two-dimensional tank tests in homogeneous and heterogeneous porous media were conducted. The results show that the water table fluctuation significantly affects the LNAPL distribution in the ground to the full range of the water saturated zone and vadose zone. A higher horizontal groundwater flow rate renders the larger diesel-contaminated area comparing with lower flow rate also results in a larger area of diesel contamination.

Department : Civil Engineering Student's Signature .....

Field of Study : Civil Engineering Advisor's Signature .....

Academic Year : 2011

ACKNOWLEDGEMENTS

First I would like express my sincere thanks to AUN-Seed Net in the Collaboration with Thailand Commission of Higher Education (CHE) to support me for the PhD. Scholarship.

I would like to express my sincere appreciate to my Advisor, Associate Professor Dr. Suched Likitlersuang, for all the supports and guidance throughout my studies.

Greatest gratitude to my co-advisor, Professor Takeshi Katsumi for his support and guidance throughout the research. His continued support led me to the right track and thank you very much again for taking care of me during my stay in your laboratory. I will never forget the motto “Work hard and no sleep”.

Deeply grateful to Assistant Professor Dr.Siam Yimsiri who bring me back to the academic world for his support and guidance throughout my study and never give up on me.

My sincere appreciation is extended to my supervisor and my first teacher in Image Analysis Method who I was lucky enough to work with, Dr.Giancarlo Flores for his generous advice, inspiring guidance and encouragement throughout my research. Thank you for never giving up on me. Muchas Gracias!

Special thanks to Associate Professor Dr.Toru Inui and Assistant Professor Atsushi Takai, for all the support, guidance and valuable comments during my stay in Japan.

Special acknowledgement to Dr.Zhenze Li for invaluable academic and personal discussion.

Last but not least, gratefully thanks to my father Sunan and my mother Pilaiporn for their continuous supports, encouragement and love. My beloved wife Thansita, without you I could not have successfully gone through all the difficulty I faced. Unforgettable my beloved sons, True Bhakawat and Tide Bhuriwatch, I love you both!

CONTENTS

Page

Page

LIST OF TABLES

LIST OF FIGURES

Page

Page

Page

Page

Page

LIST OF SYMBOLS

D_i	Average optical density
S_w	Degree of water saturation (%)
S_o	Degree of oil saturation (%)
Max	Mass of contaminant transport by advection in x direction, kg/day
C	Concentration of contaminant in the fluid, kg/m^3
Ks	Saturated hydraulic conductivity, m /day
A_x	Cross sectional area of the flow, m^2
V_x	Darcy velocity, m/day
$\frac{\partial h}{\partial x}$	Hydraulic gradient
Mdx	Mass of contaminant transport by diffusion, kg/day
Dm	Effective diffusion coefficient, m^2/day
$\frac{\partial C}{\partial x}$	Concentration gradient, kg/m^3-m
Do	Diffusion coefficient, m^2/day
A_x	Cross sectional area of the flow, m^2
n	Porosity of the medium
Sr	Degree of saturation
τ	Tortuosity
M'_{dx}	Mass of contaminant transport by mechanical dispersion, kg/day
D'_m	Mechanical dispersion coefficient, m^2/day
$\frac{\partial C}{\partial x}$	Concentration gradient, kg/m^3-m
Sw	Saturation of aqueous phase
Sa	Saturation of gas phase
Sn	Saturation of NAPL phase
σ_{ij}	Interfacial tension between substance i and j (i&j =solid, liquid A&B)
θ	Interfacial angle between two fluids

P_C	Capillary pressure (Pa)
P_{NW}	Non-wetting phase pressure (Pa)
P_W	Wetting phase pressure (Pa)
A	Optical density
P	Intensity
a	Absorptivity
b	Length of the beam in the absorbing medium
c	Concentration of the absorbing species
P_o	Radiant power
ρ	Reflectance
I^r	Intensity of reflected light
I^0	Intensity of the reflected light from ideal white surface
D_i^{nl}	Average optical density across the area of interest
β_i^{nl}	Average optical density for a dry porous medium
D_{450}	Average optical density at wavelength = 450 nm
D_{640}	Average optical density at wavelength = 640 nm
$[D_i^{00}]_{mn}$	Average optical density at wavelength i of each mesh element for dry sand
$[D_i^{10}]_{mn}$	Average optical density at wavelength i of each mesh element for fully water saturated sand
$[D_i^{01}]_{mn}$	Average optical density at wavelength i of each mesh element for fully diesel saturated sand

CHAPTER I

INTRODUCTION

1.1 Research background

Soil and groundwater contamination with non aqueous phase liquids (NAPLs) are often found at contaminated sites and it lead to sophisticated procedure for remediation. Numerous processes affect the concentration of such chemicals in aquifers. Generally, these processes include infiltration of the NAPLs through the unsaturated zone of the subsurface, spreading of the NAPLs pool at the water table, dissolution of slightly soluble species from the NAPLs into the water, transport of these chemicals with the groundwater towards potential point of contact such as a groundwater well and losses such as sorption or biodegradation

With high consumptions of petroleum product in Thailand, the total of 20,087 service stations (DOEB, 2010) located throughout the country. There are both standard and non-standard fuel service stations where entrepreneurs have to be responsible by themselves for petroleum storage. If they ignore checking of underground storage system, it is expected that there would be numerous releases of those products from underground storage tank and piping system. The leak will contaminate the environment through contamination with soil, groundwater and sources of surface water. Part of it may evaporate into atmosphere. The petroleum's contamination with environment is really detrimental as normally soil, water and air are vital factors for human's living.

Diesel is a pollutant which presents as liquid, that is immiscible with water. It can be classified as a light non-aqueous phase liquid (LNAPL) because of its lower density than water. When released into the ground, it can persist in the environment unless removed by some remediation techniques. Therefore, it can continue to degrade the ground and groundwater quality for many years through dissolution due to its toxicity and low water solubility. When LNAPL is discharged into the subsurface through spill or leak, if the amount of product is small, the

LNAPL will flow into the unsaturated zone until residual saturation is reached and the LNAPL will become discontinuous and immobile. A larger spill will result in product reaching the water table. The dissolved components of the infiltrating LNAPL precede the product and may change the wetting properties of the water, causing a reduction in the residual water content and a collapse of the capillary fringe and depression of the water table. If the flow from the LNAPL source stops, it will flow through the vadose zone until residual saturation is reached. The LNAPL will tend to spread laterally along the top of the capillary fringe. Draining of the upper portions of the vadose zone reduces the total head at the interface between the LNAPL and the groundwater, allowing the water table to slightly rebound. However, product remains in the aquifer at residual saturation and is gradually released by dissolution as groundwater moves through this zone (Boulding and Ginn, 2003).

All this process is further complicated by the fluctuations of water table due to seasonal changes of rainfall or groundwater extraction. This can be a situation commonly encountered in, e.g. coastal fuel depot, when contamination occurs. The fluctuation can cause vertical displacement and redistribution of LNAPL within the saturated and unsaturated zones.

This research experimentally investigates the effects of groundwater movements on the migration of diesel in the subsurface. One-dimensional column is used to study the effects of water table fluctuation. Two-dimensional tank test is used to study the coupling effects of groundwater level fluctuation and horizontal groundwater flow. The Simplified Image Analysis Method (Flores, 2010) is utilized as a tool to measure the distribution of water and diesel saturations in the porous media.

1.2 Research objectives

This research aims to investigate the behaviour of diesel migration in porous media with the effect of water fluctuation and horizontal groundwater flow. The main objectives can be summarised as follows:

(1) To verify the applicability of the Simplified Image Analysis Method (Flores, 2010) on Diesel and porous media by showing that a linear relationship exists between average optical density (D_i), saturation of water (S_w) and saturation of NAPLs (S_o) as predicted by the extension of the Beer-Lambert law of transmittance**.**

(2) To investigate the effects of water table fluctuation on the migration of diesel in homogeneous and heterogeneous porous media using one-dimensional column test.

(3) To investigate the effects of water table fluctuation and horizontal groundwater flow on the migration of diesel in homogeneous and heterogeneous porous media using two-dimensional tank test.

1.3 Outline of the dissertation

This dissertation has been divided in 5 chapters. The research flowchart and contents are shown in Figure 1.1

(1) Chapter 1 aims to clarify the objective and outline the contents of this dissertation

(2) Chapter 2 reviews basic concepts of NAPL migration in porous media and discussing some of the most important saturation measurement techniques available for measuring water and NAPL in soil samples

(3) Chapter 3 discusses the applicability testing of Simplified Image Analysis Method to Diesel and porous media and describes the experimental set-up for Two-Phase column experiment, Three-Phase column with homogeneous porous media and Three-Phase column with Heterogeneous porous media subject to fluctuating water table conditions.

(4) Chapter 4 presents two-dimensional tank test in both homogeneous and heterogeneous porous media subject to fluctuating water table and horizontal groundwater flow conditions

(5) Finally, Chapter 5 summarizes the results of this study and gives direction for further research.

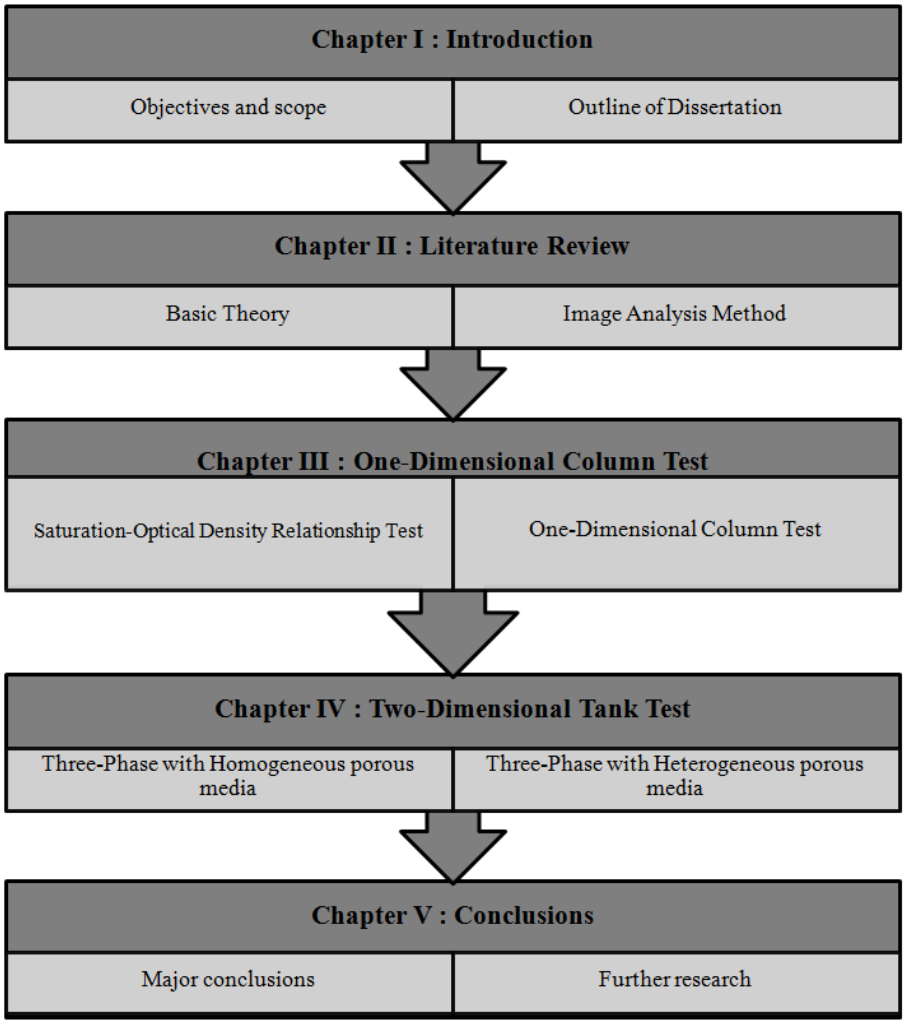

Figure 1.1 Outline of dissertation

CHAPTER II

LITERATURE REVIEW

2.1 Introduction

It is already known that there would be numerous releases of LNAPL at service stations, distribution terminals or leaking from underground storage tank. In most cases, the lack of information from the regulatory of environment those controlling the investigation and remediation of LNAPL leaks and spills were insufficient. Benzene, a major constituent of petroleum product, has the potential to cause chromosome aberrations and cancer from a lifetime exposure at levels above the maximum contaminants level. Toluene has the potential to cause pronounced nervous disorders such as spasms, tremors, impairment of speech, hearing, vision, memory, and coordination; and lever and kidney damage from a lifetime exposure at level above the maximum contaminant levels. There are two major types of health effects from releases of petroleum product includes acute health effect and chronic health effect.

Acute health effects are immediate (within hours or days) effects that may result from exposure or accidental spills of chemical contaminants Inhalation of vapors can cause central nervous system depression, convulsion, loss of consciousness. Ingestion has symptoms similar to inhalation and aspiration hazard. Eye / Skin contact causes irritation. (PTT PLC, 2008)

Chronic health effects are the possible result of exposure over many years to domestic water contaminant at levels above its maximum level. Chronic health effects include dermatitis, nervous system, kidney, liver and Blood disorder. (PTT PLC, 2008)

Most of the chemicals used in industrial operations could be contaminated to large quantities of water even if only small amounts of a contaminant are present. Pollution Control Department of Thailand has been issued the soil and groundwater acceptable pollution standard to protect the public from side effects. Groundwater quality standard and soil quality standard for habitat and agriculture are showing in table 2.1 and 2.2 respectively.

quality standard and soil quality standard for habitat and agriculture are showing in table 2.1 and 2.2 respectively.

Table 2.1 Thailand soil quality standards for habitat and agriculture (Pollution Control Department, 2004)

No.	Parameter	Standard Value (mg/kg)
1	Benzene	≤ 6.5
2	Carbon Tetrachloride	≤ 2.5
3	1,2-Dichloroethane	≤ 3.5
4	1,1-Dichloroethylene	≤ 0.5
5	Cis-1,2-Dichloroethane	≤ 43
6	Trans-1,2-Dichloroethane	≤ 63
7	Dichloromethane	≤ 89
8	Ethylbenzene	≤ 230
9	Styrene	≤ 1,700
10	Tetrachloroethylene	≤ 57
11	Toluene	≤ 520
12	Trichloroethylene	≤ 28
13	1,1,1-Trichloroethane	≤ 630
14	1,1,2-Trichloroethane	≤ 8.4
15	Total Xylenes	≤ 2.1

Note: The analytical methods for all parameter are Gas Chromatography (GC) or Gas Chromatography/Mass Spectrometry (GC/MS) or other methods approved by PCD.

Table 2.2 Thailand groundwater quality standards (Pollution Control Department, 2007)

No.	Parameter	Standard Value (μg/l)
1	Benzene	≤ 5
2	Carbon Tetrachloride	≤ 5
3	1,2-Dichloroethane	≤ 5
4	1,1-Dichloroethylene	≤ 7
5	Cis-1,2-Dichloroethane	≤ 70
6	Trans-1,2-Dichloroethane	≤ 100
7	Dichloromethane	≤ 5
8	Ethylbenzene	≤ 700
9	Styrene	≤ 100
10	Tetrachloroethylene	≤ 5
11	Toluene	≤ 1,000
12	Trichloroethylene	≤ 5
13	1,1,1-Trichloroethane	≤ 200
14	1,1,2-Trichloroethane	≤ 5
15	Total Xylenes	≤ 10,000

Note: The analytical methods for all parameter are purge and trap Gas Chromatography (GC) or purge and trap Gas Chromatography/Mass Spectrometry (GC/MS) or other methods approved by PCD.

The following section will discuss some basic concepts on LNAPL migration in porous media and the image analysis techniques for measuring water and LNAPL saturation in soil samples in laboratory experiments.

2.2 Behavior of phases in porous media

Contaminant in the subsurface can remain in any phase such as vapor, dissolved or NAPL such that the subsurface transport of different phases will involve different governing factors. The following section provides the details of properties of fluid and of media associated with the migration of each phase.

2.2.1 Saturation

The saturation, S, of a fluid phase is the volume fraction of the total pore volume occupied by the relevant fluid in porous medium. This can vary from zero to unity. The summation of saturation of each phase must be equal to one.

$$S_w + S_a + S_n = 1 \tag{2.1}$$

Where,

S_w = Saturation of aqueous phase
S_a = Saturation of gas phase
S_n = Saturation of NAPL phase

Saturation is important, because some properties, such as capillary pressure and relative permeability, are function of saturation of fluid phase.

2.2.2 Interfacial tension and wettability

Interfacial tension refers to the tensile force that exists in the interface separating two immiscible fluid phases. A liquid in contact with another substance such as a solid, an immiscible liquid or gas forms interfacial energy. This is a result of the difference in the degree of attraction between molecules of the same substance and between those of different substances, at the liquid surface. This phenomenon is known as interfacial tension and can be defined as the amount of work required to separate a unit area of one substance from another.

The affinity of one immiscible fluid for a solid surface in the presence of a second or third immiscible fluid is referred as wettability. This depends on the

interfacial tension (Mercer and Cohen, 1990) Figure 2.1 illustrates a drop of liquid A resting on a solid surface in the presence of liquid B. The specific angle at which characterizes the wettability. The fluids in which the contact angle is measured to be less than 90^o are call wetting fluid (liquid A) and the fluid in which the angle is greater than 90^o is referred as non wetting fluid (liquid B). If the contact angle is between 70^o and 110^o, it is called neutral (Anderson, 1986).

The following equation gives the relationship between contact angle and the interfacial tensions for three interfaces.

$$\cos\theta = \frac{\sigma_{SB} - \sigma_{SA}}{\sigma_{BA}} \tag{2.2}$$

Where,

σ_{ij} = Interfacial tension between substance i and j (i&j =solid, liquid A&B)

θ = Interfacial angle between two fluids

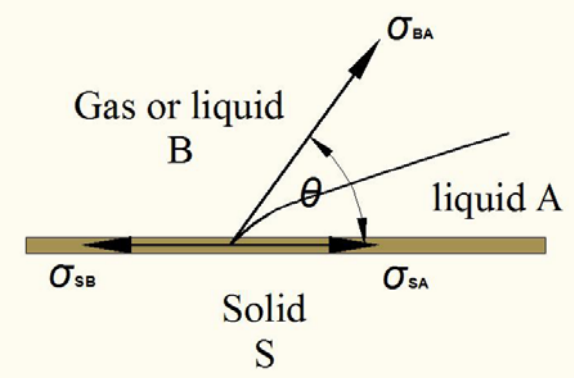

Figure 2.1 Interfacial tensions between a solid surface, a wetting fluid and a non wetting fluid

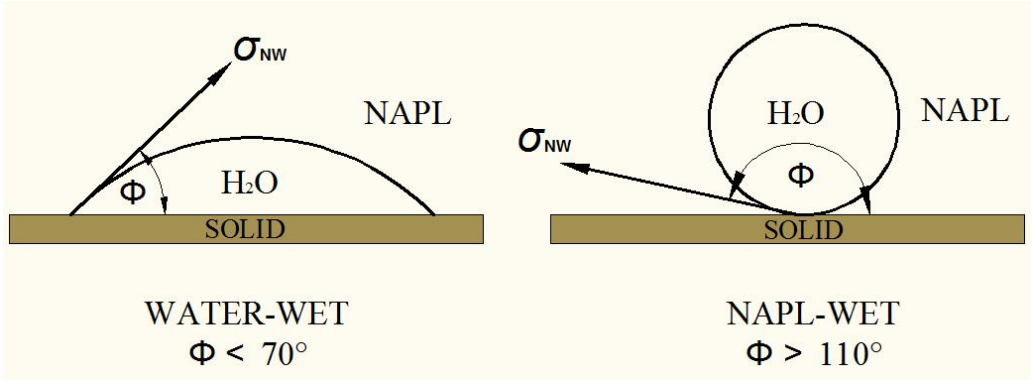

Figure 2.2 Wettability configurations (Mercer and Cohen, 1990)

2.2.3 Capillary pressure

A curved surface at the interface will develop when two immiscible liquids are in contact, as shown in Figure 2.1. The pressure difference near the curved interface is called the capillary pressure. This pressure difference exists due to the interfacial tension present in the fluid-fluid interface separating the two fluids. Capillary pressure is represented by the following equation.

$$P_C = P_{NW} - P_W \tag{2.3}$$

Where,

P_C = Capillary pressure (Pa)

P_{NW} = Non-wetting phase pressure (Pa)

P_W = Wetting phase pressure (Pa)

Figure 2.3 shows the radius of curvature, r' for the spherical air water interface in the possible porous material. Equation 2.4 gives the relationship of the capillary pressure, P_C the interfacial tension of two liquids, σ, and the radius of curvature.

$$P_C = -\frac{2\sigma}{r'}\cos\theta \tag{2.4}$$

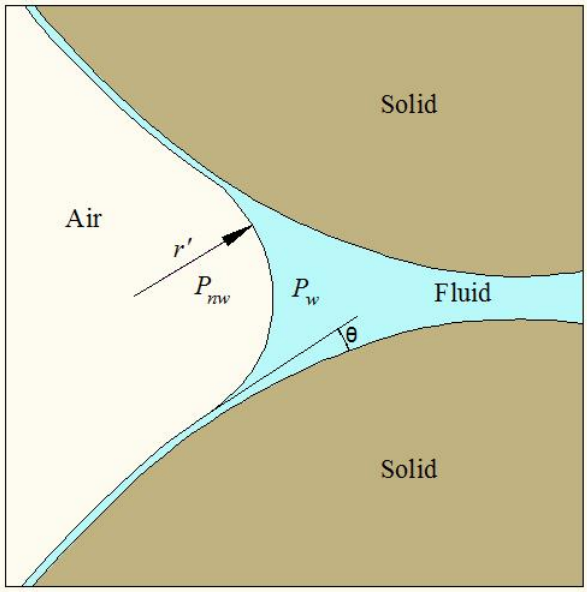

Figure 2.3 Radius of curvature for a spherical capillary interface (Fetter, 1993)

Accordingly, it can be seen that the capillary pressure is directly promotional to the interfacial tension and inversely proportional to the radius of curvature. The radius of curvature will be defined by the pore size of the material. This means that capillary pressure is a function of the properties of two immiscible liquids and the porous media, which leads to the development of a capillary pressure-saturation curve for the given porous material.

The pore space can be filled by different fluids (air, water, or LNAPL) that are not miscible with each other. The fraction of the pore space that is occupied by a given fluid phase is called the saturation. Saturation is either represented as a fraction or a percent. The sum of the fluid saturations should total 1, or 100%. Below the water table and in the absence of LNAPL, the water saturation is nearly one (1), and the air saturation is nearly zero (0).

Typically in the subsurface, water preferentially "wets," or adheres to, the solid media surface and occupies the smaller pores. It is called the wetting phase and wets the surface of the solid media in preference to air. Air is called the non-wetting phase. The implications of this relationship can be illustrated by a simple capillary rise experiment shown in figure 2.4.

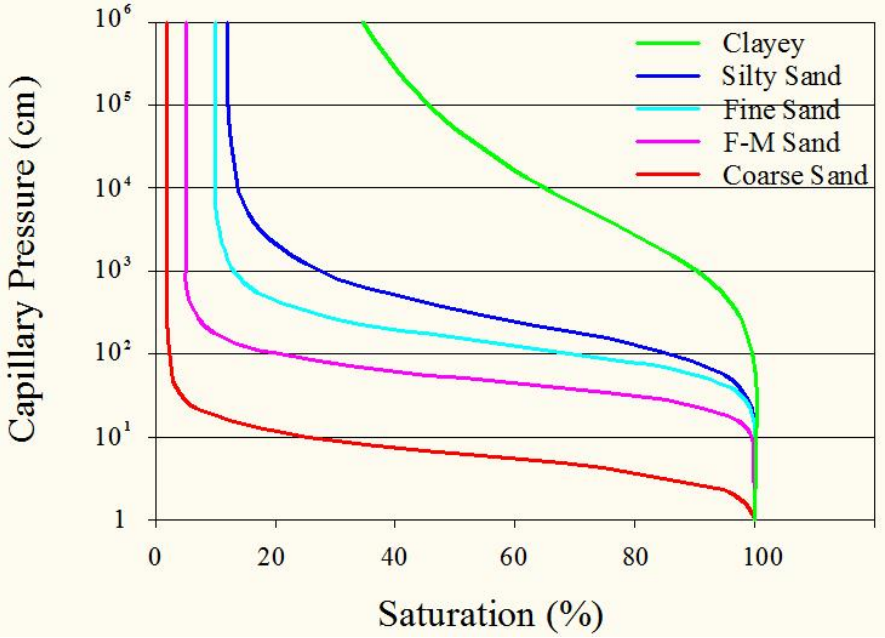

Figure 2.4 Capillary pressure curves

Figure 2.4 depicts ideal capillary pressure curves for different grain sizes. The X axis is water saturation. It ranges from 0, indicating that the pore space is completely filled with air, to 100 percent, indicating that the pore space is completely filled with water. The Y axis is the capillary pressure (or capillary suction pressure). This is related to the height of the water in the tube, as described in the capillary rise experiment. Smaller tubes exhibit greater capillary pressure, which results in a greater height of water. These capillary pressure curves illustrate two things: First, note that the capillary pressure in the coarse sand is much lower than the capillary pressure in the clay. This indicates that the pore sizes in the sand are larger than in the clay, Second, the coarse sand curve is very flat over a wide range of water saturations. This indicates that the pore size distribution is uniformly large.

2.3 Migration of Light Non-Aqueous Phase Liquids (LNAPLs)

LNAPL migration is affected by several factors, including its conductivity, the groundwater hydraulic gradient through Darcy's Law, the pore throat displacement entry pressure, and a fluctuating water table. LNAPL conductivity depends on its fluid properties, its relative permeability, and the conductivity of the porous media. Displacement entry pressure is a certain pressure needs to be applied to

the LNAPL for it to move through a pore throat. If the up gradient pressure is not sufficient at the leading edge of a plume to force LNAPL through the pore throats in the media, the LNAPL cannot migrate.

In clean coarse sand, the displacement entry pressure is lower, and the plume can spread more easily. In a very fine grained media, the displacement entry pressure can be quite high and effectively prevents the LNAPL from migrating. A fluctuating water table can prevent the LNAPL from migrating because, as the water table rises, the LNAPL can become trapped as residual.

For most of the last 20 years, groundwater scientists and engineers approached the evaluation and recovery of LNAPL with a conceptual model in which LNAPL floated on the water table like a pancake, displacing nearly all of the water and the air in the pore space of the aquifer. In this model, the result was a uniformly high saturation of LNAPL on the water table.

Although many people recognized that there was a difference between the thickness of LNAPL measured in a monitoring well and the actual thickness in the aquifer, the tools needed to understand this relationship and how it varied with the type of LNAPL and aquifer had yet to be developed. People believed that, when petroleum hydrocarbon was observed in the monitoring well, it was spreading. They also believed that LNAPL moved up and down with a fluctuating water table, always riding on the top of the water table.

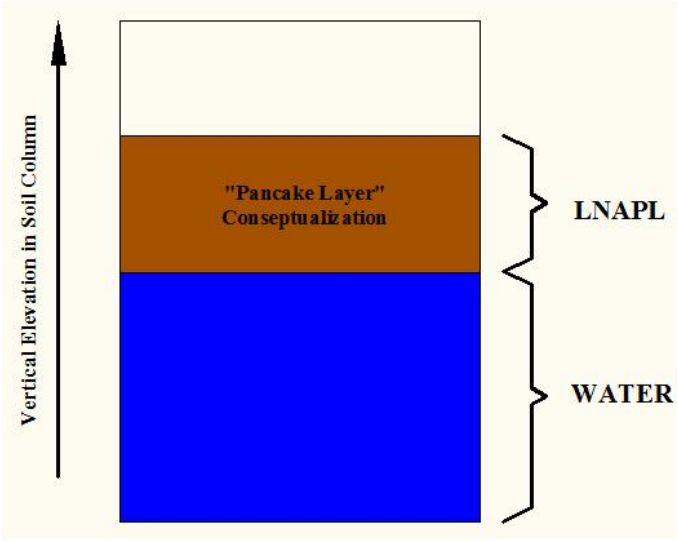

Figure 2.5 1980's pancake model

The quantitative understanding of petroleum distribution in subsurface media and its recovery was developed in the 1930s at Princeton and other universities. This understanding established the role of interfacial and capillary forces in determining the distribution of oil in subsurface media. It also led to the development of methods for describing the conductivity and recoverability of petroleum from oil reservoirs.

Farr *et al.* (1990) and Lenhard and Parker **(**1990) extended the understanding of LNAPL behavior developed for oil reservoirs in the 1930s to environmental applications of hydrocarbon spills and leaks. This research was the basis of a paradigm shift that occurred in the 1990s. The conceptual model resulting from the later research is shown in figure 2.6. Unlike in the old "pancake model" LNAPL is not continuous in the subsurface media matrix.

Simpler models have been developed. These models, combined with data gathered in the field, have helped to pull together a picture that can be applied to everyday situations. LNAPL co-exists with water in the pore network within the aquifer. It does not float on the water table. The degree of LNAPL saturation depends on the history, lithology, capillary parameters, and fluid properties of the site and the volume of LNAPL released. LNAPL only partially fills the aquifer pore space, and saturation decreases with depth until water fills all the pores.

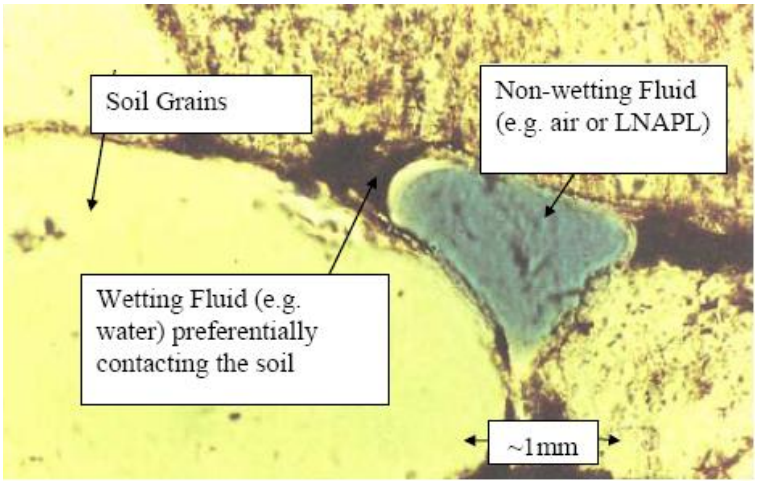

Figure 2.6 LNAPL co-exists with water in the pore network within the aquifer.

Light nonaqueous phase liquids are less dense than water. When spilled at the land surface, they migrate vertically in the vadose zone under the influence of gravity and capillary forces, just as water does. Unless the vadose zone is extremely dry, it will be water-wet and the LNAPL will be the non wetting phase.

Figure 2.7 shows the distribution of water in the vadose zone (Abdul, 1988). Notice that at the top of the vadose zone the water is held at the irreducible water saturation. The water held here is called pendular water. Below that is a zone where the water content is above the irreducible saturation; this is sometimes called funicular water. When close to 100% water saturation is reached, we find the capillary fringe. The air-water relationship of the vadose zone behaves as a two-phase immiscible flow, so there is residual air saturation in the capillary zone.

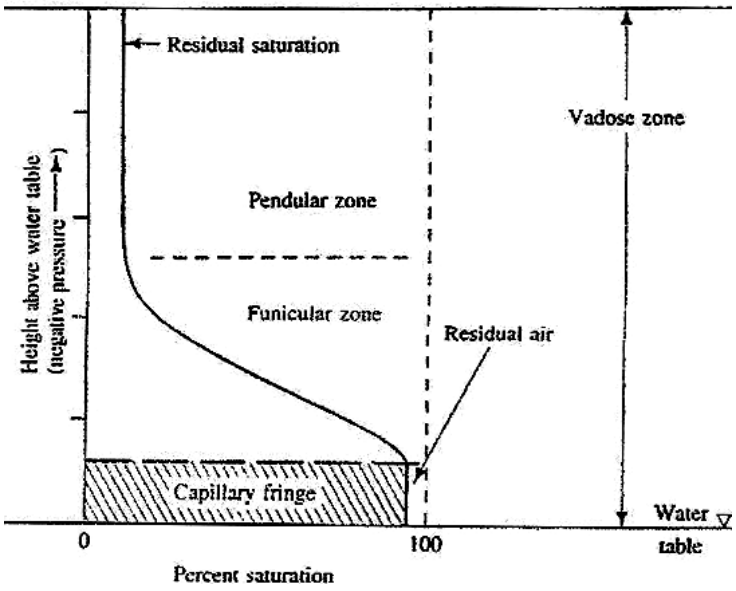

Figure 2.7 Distribution of water in the vadose zone in the absence of nonaqueous phase liquids (Fetter, 1993)

As LNAPL migrates through the vadose zone toward the capillary fringe, it displaces air, but generally not water, from the pore spaces. The LNAPL-filled pores drain slowly and can leave behind LNAPL globules trapped by capillary forces. If only a small volume of LNAPL is released, it may become entirely trapped in the vadose zone. If a greater volume is released, the LNAPL may migrate completely through the unsaturated zone and accumulate in a zone that is loosely constrained by the water table.

The LNAPL will travel vertically in the vadose zone. If a sufficient quantity is present so that the residual LNAPL saturation is exceeded, it will eventually reach the top of the capillary zone. However, much of the LNAPL may remain behind, trapped in the vadose zone. Eckberg and Sunada (1984) studied the distribution of oil in the vadose zone. Figure 2.8 shows the changes in the distribution of water and oil in a sand column into which a quantity of oil was added. Note that much of the oil remains throughout the thickness of the vadose zone as a residual oil.

In moving downward an LNAPL may displace some of the capillary water in the vadose zone, causing it to move ahead of the advancing LNAPL front. Once the capillary zone is reached. LNAPL will begin to accumulate. Initially, the LNAPL will be under tension, just as the water in the vadose zone is under tension. As additional LNAPL accumulates above the capillary zone, an "oil table" will develop, with some LNAPL having a positive pore pressure. The capillary zone will become thinner, and mobile, or "free" LNAPL will accumulate. Eventually, the capillary zone may disappear altogether and the oil table will rest directly on the water table. In the core of a thick zone of mobile LNAPL, the water table may be depressed by the weight of the LNAPL.

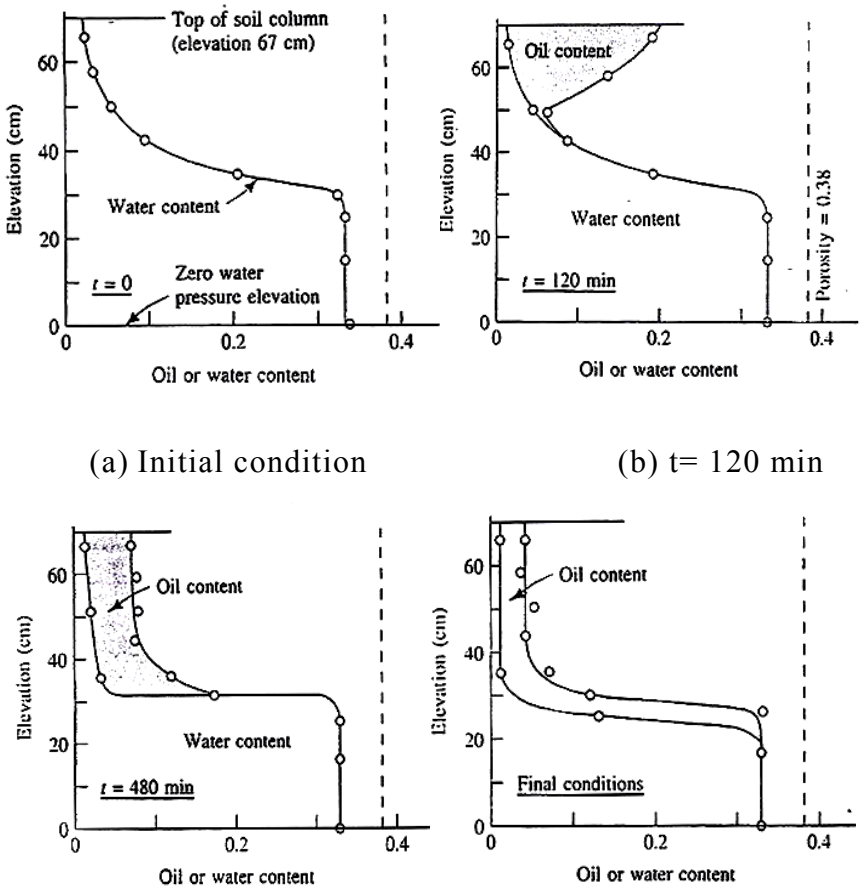

(a) Initial condition (b) t= 120 min

(c) t=480 min (d) final condition

Figure 2.8 Changes in the vertical distribution of oil with time after a slug of oil is added to the top of a column of sand. Oil content and water content are expressed as a fraction of the total volume of the porous media (Fetter, 1993)

2.4 Image analysis method

2.4.1 Multispectral image analysis method (MIAM)

Beer's Law states that for a parallel beam of monochromatic radiation passing through homogenous solutions of equal path length the absorbance is proportional to the concentration. Lambert's Law states that for a parallel beam of monochromatic radiation passing through homogenous solutions of equal concentration the absorbance is proportional to the path length. This comes to their relation stating that for a parallel beam of monochromatic radiation passing through a homogenous solution the absorbance is proportional to the product of the concentration and path length depending on the substance, the solvent, the wavelength and the units for concentration and path length. The laws of Lambert and Beer relate the radiant power in a beam of electromagnetic radiation, monochromatic light, to the length of the path of the beam in an absorbing medium and to the concentration of the absorbing species, respectively. The laws are normally combined in the relation Swinehart (1962)

$$A = -\log_{10}\frac{P}{P_0} = abc \tag{2.5}$$

Where,

A = optical density

P = intensity

a = absorptivity

b = length of the beam in the absorbing medium

c = concentration of the absorbing species

P_o = radiant power

Kecharvarzi *et al* (2000) presented a Multispectral Image Analysis Method (MIAM) to determine dynamic fluid saturation distributions of water, NAPL and air in two-dimensional intermediate-scale laboratory experiments. As with a Light Transmission Method and Light Reflection Method, this technique provides a non-destructive and non-intrusive tool for multifluid flow imaging for systems with rapid changes. Optical density (D) can be defined in terms of reflectance:

$$D = \log_{10}(\rho) \tag{2.6}$$

Reflectance is defined as;

$$\rho = \frac{I^r}{I^0} \tag{2.7}$$

Where I^r and I^0 are the intensity of the reflected light and the light that would be reflected by an ideal white surface, respectively.

Differences in reflectance of water and the LNAPL within the narrow spectral bands, measured with a spectrometer, formed the basis of the saturation determinations. Contrasted reflected light intensity between each spectral band depends on the quantity of each liquid present in the system. Digital images were obtained within these three spectral bands by placing band-pass interference filters in front of the camera lens. For calibration purposes, a large number of porous medium samples with varying fluid saturations and combinations of air-water, air-LNAPL, and air-water-LNAPL were prepared and photographed with a black-and-white digital near infrared camera. A gray scale was placed next to each sample to allow for correction of spatial and temporal lighting condition variations between images. The light intensity was divided into 4096 gray levels. Each sample contained a fixed area (fixed number of pixels on the image) of interest (AOI) for which the average optical density for the aqueous phase and LNAPL was determined from the following:

$$D = \frac{1}{N}\sum_{j=1}^{N} d_{ji} = \frac{1}{N}\sum_{j=1}^{N}\left[-\log_{10}\left[\frac{I_{ji}^r}{I_{ji}^0}\right]\right] \tag{2.8}$$

Where N is the number of pixels contained in the AOI for a given spectral band *i,* and d_{ji} is the optical density of the individual pixels. Plotting D values versus aqueous phase saturation, S_1, in the air-water systems, and versus saturation of the LNAPL saturation, S_n, in the air-LNAPL systems, resulted in the linear relationships

$$D_i^l = \lambda_i^l S_l + \beta_i^l \tag{2.9}$$

$$D_i^n = \lambda_i^n S_l + \beta_i^n \text{, i= 500, 760, 970 nm} \tag{2.10}$$

Where *1* and *n* refer to the water and LNAPL, respectively, *i,* refers to the centered wavelength of the three spectral bands, and λ and β are regression coefficients. Kecharvarzi *et al* (2000), discussed that λ depends on porosity and that, consequently the linear relationships only develops if the porosity is constant. It was also shown experimentally that values for β representing the reflectance of dry porous medium were hardly effected by variations in porosity. For three-fluid phase system, for each spectral band, the average optical density was a linear function of LNAPL saturation for fixed water saturations, from this the optical density in three phase systems can be written as

$$D_i^{nl} = \lambda_i^l S_l + \lambda_i^n S_n + \beta_i^{nl}, \text{ i= 500, 760, 970 nm} \qquad (2.11)$$

Where D_i^{nl} is the average optical density across the area of interest, and β_i^{nl} corresponds to the average optical density for a dry porous medium. Considering that equation 2.11 applies to three spectral bands so we have three equations with the fluid saturations as the unknowns. Solving above equation for two spectral bands *i* and *k* gives us the equations

$$S_l = \frac{\lambda_i^n (D_k^{nl} - 2\beta_k^{nl}) - \lambda_k^n (D_k^{nl} - 2\beta_k^{nl})}{\lambda_k^n \lambda_i^l - \lambda_i^n \lambda_k^l}$$

$$S_n = \frac{\lambda_k^l (D_k^{nl} - 2\beta_k^{nl}) - \lambda_k^n (D_k^{nl} - 2\beta_k^{nl})}{\lambda_k^n \lambda_i^l - \lambda_i^n \lambda_k^l} \qquad (2.12)$$

i,k = 500, 760, 970 nm

To decrease the variance in the fluid saturations, the denominator of the equation 2.12 needs to be large. The λ coefficients need to be large as well as and should be as different as possible for the two chosen spectral bands. Based on data in Kecharvarzi *et al* (2000) it is obvious that either the combination i =500 and k= 760 nm or i = 500 and k = 970 nm should be selected. To solve the equation 2.51 all λ and β values can be obtained from two-fluid phase system and no three-fluid phase systems are needed. In image processing, it is important to overcome any uncertainty in uneven lighting across the experimental domain, must have constant lighting conditions.

The MIAM was applied to three infiltration and redistribution experiments with Soltrol 220 in partly saturated porous media. Fluid flow behavior in one of the experiments was described in detail by Kechavarzi *et al* (2005). For each of the porous media, extensive calibration procedures yielded the coefficient values needed to compute fluid saturations according to the equation 2.51. During the experimental phase of their study either 3 or 4 L of LNAPL was introduced in partially saturated sand, homogenous or layered, with the water table near the bottom and a capillary fringe height ranging from 20 to about 50 cm. Differences between applied and measured saturations varied from 2.8 to 10.5%, depending on the experiment.

2.4.2 Simplified image analysis method (SIAM)

The Simplified Image Analysis Method (Flores, 2010) similarly to Multispectral Image Analysis Method employs the extension of the Beer-Lambert Law of transmittance that a linear relationship exists between average optical density (D_i) and water and LNAPL saturation values (S_w and S_o). Used to calculate both water and LNAPL saturation distributions for porous subsurface domains subject to contamination by an LNAPL and to fluctuating groundwater conditions, under laboratory controlled environmental conditions. The SIAM accounts for the effects of the variable angle of incidence of the reflected light and eliminate the need to prepare the dozens of sample required for calibrating the regression linear plane while at the same time improving its accuracy for points far from the centre. The development of the Simplified Image Analysis Method was brought about by the simplification of the complex calibration process of MIAM. In simplifying the calibration process, the Simplified Image Analysis Method (SIAM) increases the mathematical complexity of the computational analysis by providing not one set of regression equations for the whole domain, but one set of equations for each mesh element of the whole domain. This increase in complexity improves the accuracy of the method by providing each mesh element with its own set of non related equations (from the images taken by two different spectral bands) that account for both spatial variations of light and other surface imperfections.

SIAM improves the instead of requiring the calibration with many different samples (~60 or more samples), a simplification of this method by shortening the calibration This new image analysis method only requires three calibration pictures with each of the two cameras obtained by filling the studied domain with sand under one of the following three limit conditions: dry sand (S_w = 0%; S_o = 0%); water saturated sand (S_w = 100%; S_o = 0%); NAPL saturated sand (S_w = 0%; S_o = 100%). These three conditions provide three non-linear points to recreate the linear regression plane (Figure 2.9). The following calibrated photos are the clearly seen in the linear regression plane (Figure 2.10) which can be plotted without the need to calibrate 60 different samples with varying degrees of water and LNAPL saturations. The following steps were presented by Flores (2010) for the Simplified Image Analysis Method procedure.

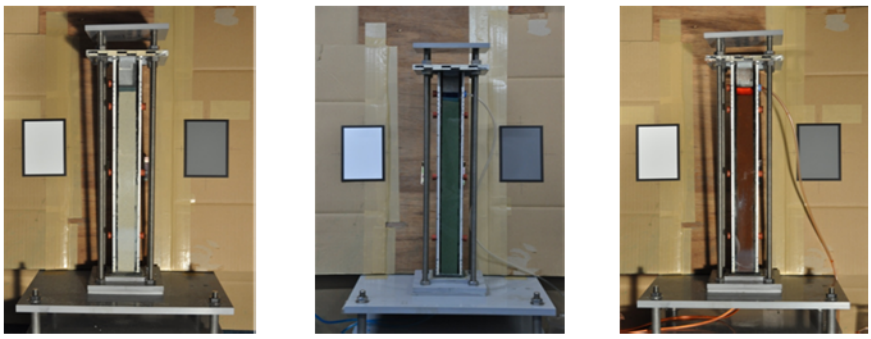

Figure 2.9 Experiment calibration photos

Flores (2010) confirms these three non-linear points as the best points selected to define the regression, recalling from Equation 2.13 the average optical density of the dry sand β_k^{nl} is one point, the second point is 100% water saturated sand (S_w) and the third point being 100% LNAPL saturated sand (S_o)

$$\begin{bmatrix} D_i \\ D_j \end{bmatrix}_{mn} = \begin{bmatrix} \left(D_i^{10} - D_i^{00}\right).S_w + \left(D_i^{01} - D_i^{00}\right).S_o + D_i^{00} \\ \left(D_j^{10} - D_j^{00}\right).S_w + \left(D_j^{01} - D_j^{00}\right).S_o + D_j^{00} \end{bmatrix}_{mn} \tag{2.13}$$

Where,

m and n are the dimensions of the matrix

$[D_i]_{mn}$ and $[D_j]_{mn}$ are the values of average optical density of each mesh element for wavelength *i* and *j*

$[D_i^{00}]_{mn}$ and $[D_j^{00}]_{mn}$ are the average optical density of each mesh element for dry sand

$[D_i^{10}]_{mn}$ and $[D_j^{10}]_{mn}$ are the average optical density of each mesh element for water saturated sand and

$[D_i^{01}]_{mn}$ and $[D_j^{01}]_{mn}$ are the average optical density of each mesh element for LNAPL saturated sand

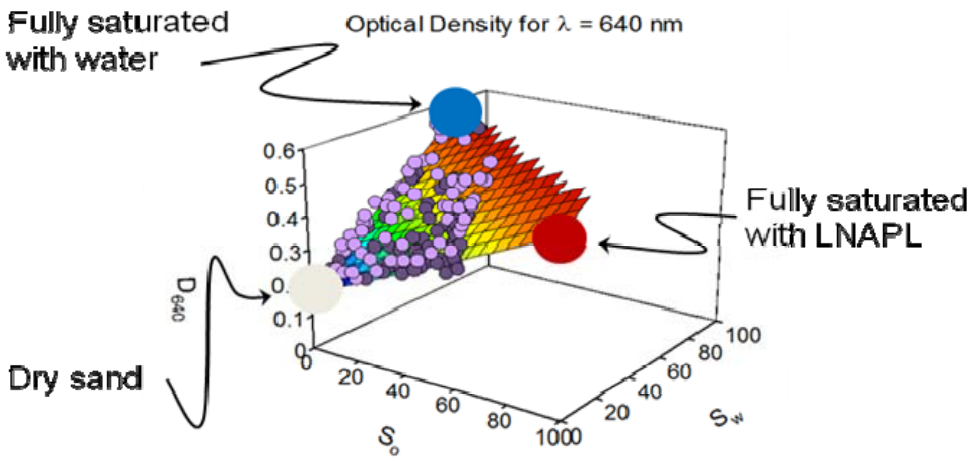

Figure 2.10 Linear regression plane

2.4.3 Differences between MIAM and SIAM

Luatua (2011) gives a summary of the difference between the two Image Analysis Methods, the MIAM is identified with its long and complex calibration stage, where as many as 40 or more samples are required to be prepared with different degrees of LNAPL and water saturations in order to calibrate the linear regression plane. Conversely, the SIAM only requires the photographing of 3 different conditions which gives the 3 non-linear points required to define the linear regression plane. Another notable difference is calculation of the Average Optical Density, in the MIAM procedure, Image subtraction of the same element of two different photographs taken at different times gives the values of water and LNAPL saturations. On the contrary the SIAM gives a set of equations for each mesh element of the studied domain giving the average optical density of each mesh disregarding

the need to apply image subtraction on the images. The summary of difference between the two image analysis methods is shown in Table 2.3

Table 2.3 Multispectral image analysis method vs. Simplified image analysis method (Luatua, 2011)

	Multispectral Image Analysis Method (MIAM)	**Simplified Image Analysis Method (SIAM)**
Average Optical Density Calculations	Image Subtraction	Each mesh element (matrix) have its own set of AOD equations
Cameras	1	2
Filters	3 Filters (500nm, 760nm, 970nm)*	2 Filters (450nm & 640nm)
Calibrated Sample	Sample container	Experimental Domain (1-D Column, 2-D Tank)
Experiment Calibration	>40 samples with different degrees of LNAPL saturation and water saturation (the more samples, the higher accuracy level)	3 Non-linear points to recreate linear regression plane taken from these pictures (S_w= 0% S_o = 0% Dry Sand S_w=100% S_o = 0% Sand fully saturated with water S_w= 0% S_o = 100% Sand fully saturated with LNAPL)

*only two are used for the calculations of S_o and S_w equations

CHAPTER III

ONE-DIMENSIONAL COLUMN TEST

3.1 Introduction

This chapter focuses on the verification of the Beer-Lambert Law of Transmittance by the existence of a linear relationship between diesel saturation, water saturation and average optical density in order to select the porous media to be used in one-dimensional column test. Diesel saturation and water saturation distribution in one-dimensional column in both homogenous and heterogeneous porous media will be compared to better understand their behavior under fluctuating water table conditions and Simplified Image Analysis Method will be used to obtain diesel saturation and water saturation in study domain. Totally 3 scenarios in 8 column test will be discussed.

i. Two phase one-dimensional column experiment: Diesel drainage test and water drainage test in Ottawa#3820 sand and Ottawa#3821 sand to study the soil liquid characteristic obtained from Simplified Image Analysis Method.

ii. Three phase one dimensional column in homogeneous porous media: water drainage following with diesel and air infiltration in Ottawa#3820 sand and Ottawa#3821 under the fluctuating of water table condition.

iii. Three phase one dimensional column in heterogeneous porous media: water drainage following with diesel and air infiltration in homogeneous porous media under the fluctuating of water table condition.

3.2 Saturation-optical density relationship test

Kechavazi *et al*. (2000) and Flores (2010) found a relationship exists between optical density, LNAPL and water saturation which is the main basis of Simplified Image Analysis Method that will be utilized as a tool to measure the distribution of water and diesel saturations in this study. Kechavarzi *et al*. (2000) used

a digital near infrared camera with three narrow spectral bands of visible and near infrared spectrum (10 nm large and centered at 500, 760, and 970nm) and two cameras with two different band pass filters were used (450nm and 640nm) by Flores (2010) which is similarly used in this research.

3.2.1 Materials

Ottawa#3820 sand, Ottawa#3821 sand, STS white sand, Chonburi sand and Toyoura sand were used as a porous media in this study. Porous media gradation curve and engineering properties are shown in Figure 3.1 and Table 3.1 respectively. Diesel was dyed red with Red Sudan III from Nacalai tesque, Japan (1:10000 by weight) and water was dyed blue with Brilliant Blue FCF from Nacalai tesque, Japan (1:10000 by weight) to enhance visual observation and increase their light absorbance properties. There is no noticeable change in the physical properties of water and diesel after being mixed with their respective dyes and the dyes do not migrate between water and diesel and are not absorbed by the soil particles. Properties of liquid used in this study is presented in Table 3.2

In order to conduct the saturation-optical density relationship test, evaporation analysis of diesel and water are required to confirm that diesel and water have none or negligible solubility in air, in both dyed and non-dyed conditions as required by Simplified Image Analysis method. Diesel and water were exposed to evaporate for 72 hours. Both liquid were contained in a 15 ml centrifuge tube (15 mm diameter and 118 mm height) and left exposed to constant room temperature of 20^{o} C and humidity of 70%, allowing for evaporate for up to 72 hours. Initial weight was measured and final weight at the end of 3 days was recorded and the results found that evaporation rate of both diesel and water are very low (less than 3%) and can be negligible. Evaporation rate of diesel and water are presented in Figure 3.2.

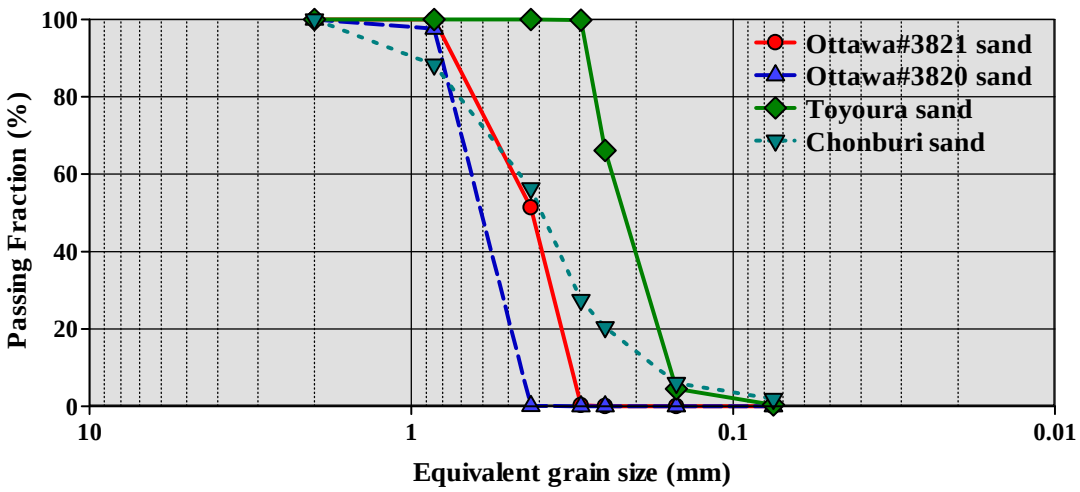

Figure 3.1 Grain size distributions of porous media

Table 3.1 Engineering properties of porous media

Properties	Ottawa#3820 sand	Ottawa#3821 sand	Chonburi sand	Toyoura sand
Soil particle density, ρ_s (g/cm^3)	2.64	2.63	2.66	2.61
Uniformity coefficient, C_u	1.47	1.56	2.68	1.51
Mean grain size (D_{50}), mm	0.643	0.422	0.397	0.224
Hydraulic conductivity, k (cm/s)	2.02×10^{-2}	1.80×10^{-2}	3.69×10^{-2}	2.01×10^{-3}
Diesel hydraulic conductivity, k_{diesel} (cm/s)	1.91×10^{-2}	1.58×10^{-2}	-	-
USCS	SP	SP	SP	SP

Table 3.2 Properties of liquids use in this study at 20 ^{o}C

Properties	**Water**	**Diesel**
Density, ρ_s (g/cm^3)	0.998	0.865
Viscosity, ν (mm^2/s)	1.00	4.10
Vapor pressure at 40^{o}C (mmHg)	7.37	3.75

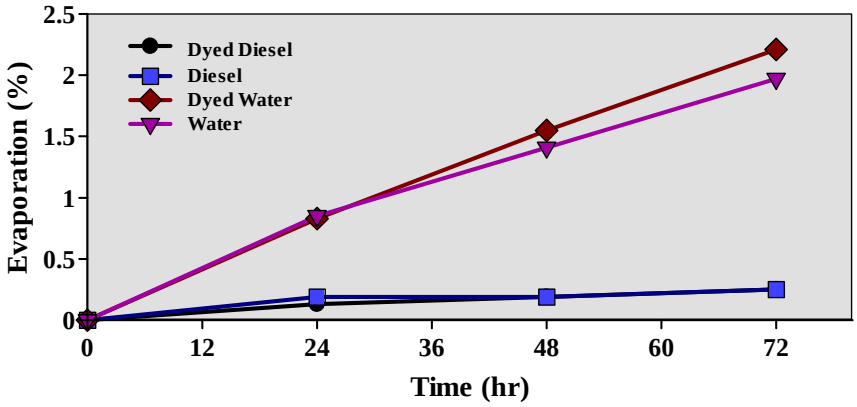

Figure 3.2 Evaporation rates of diesel and water

3.2.2 Equipments

Two cameras (Nikon D90) with the 450nm and 640nm band-pass filters were set to manual mode so that their aperture, shutter speed and white balance were kept constant. Both cameras were connected to a computer via USB cables and remotely controlled by Nikon Camera control Pro 2. X-Rite Gretagmacbeth ColorChecker white balance card was located next to the sample to provide a white and black reference. Two 30 W LED floodlights were used to illuminate the samples. Room temperature was kept at 20˚C and humidity at 70% following the experiment setup recommended by Flores (2010). Pictures were recorded in NEF format (Nikon 12-bit proprietary RAW format) and then were exported to TIFF format (Tagged Image File Format) using ViewNX 2.0. TIFF images were then analyzed by an ad-hoc program written in MATLAB Release 2007a. Equipments set up is shown in Figure 3.3

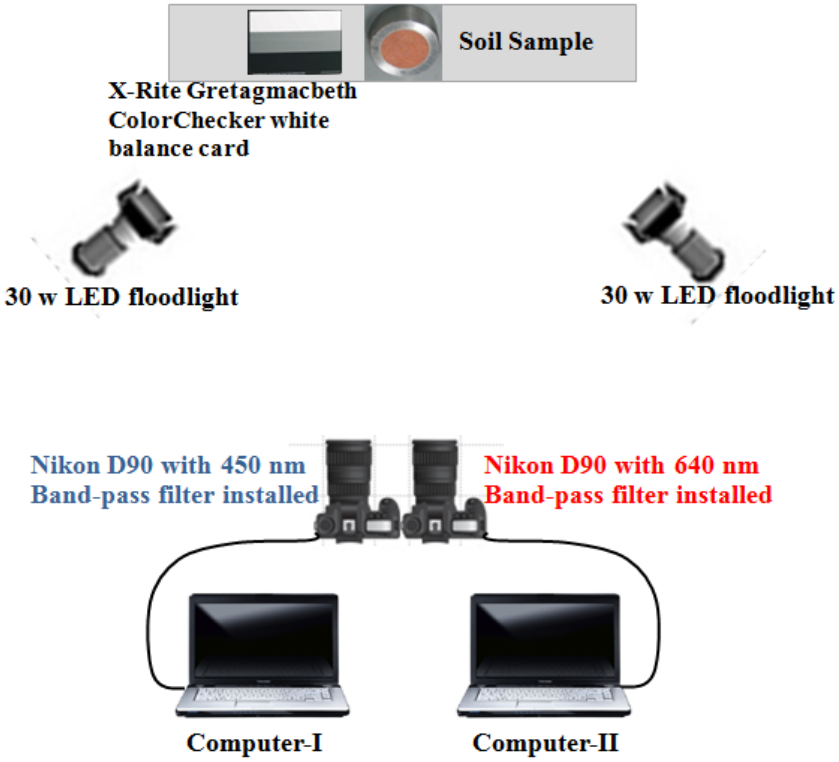

Figure 3.3 Saturation-Optical density Relationship Test Equipments set up

3.2.3 Method

Thirty soil samples were prepared with each porous media by mixing known amounts of water, diesel and porous media in 25 cm^3 cylindrical sample containers (*ø* = 40 mm, *h* = 20 mm). The prepared samples were positioned approximately 1.5 m in front of both cameras, the two 30 W LED floodlights were turned on, and one picture were taken with each camera. A Gretamacbeth white balance card was located next to the sample to provide a white and black reference and was part of each picture as well. Both cameras were set to manual mode so that aperture, shutter speed and white balance were kept constant. Room temperature was kept at 20 °C and humidity at 70%. Pictures were recorded in NEF format and then were exported to TIFF format using ViewNX 1.5.0. The TIFF images were then analyzed by an ad-hoc program written in MATLAB Release 2007a. Graphics were prepared for each porous media, comparing water and Diesel saturation versus Optical density values, for each wavelength.

3.2.4 Results and discussions

Relationship between Diesel saturation (S_o), Water saturation (S_w) and Average Optical Density (AOD) for the all porous media are shown in Figure 3.4-Figure 3.7

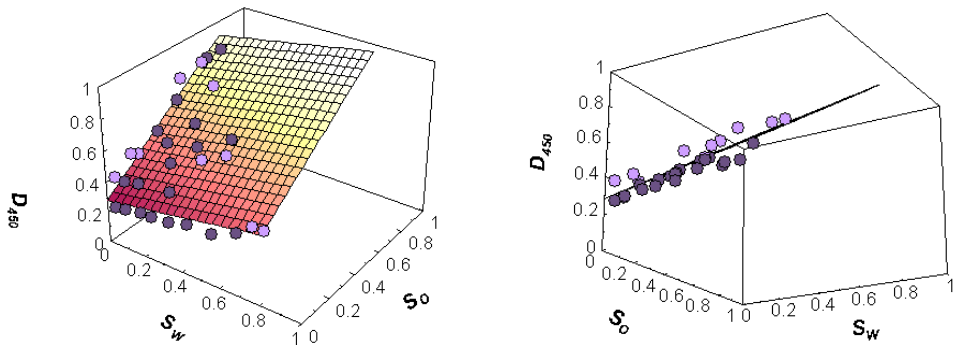

(a) (b)

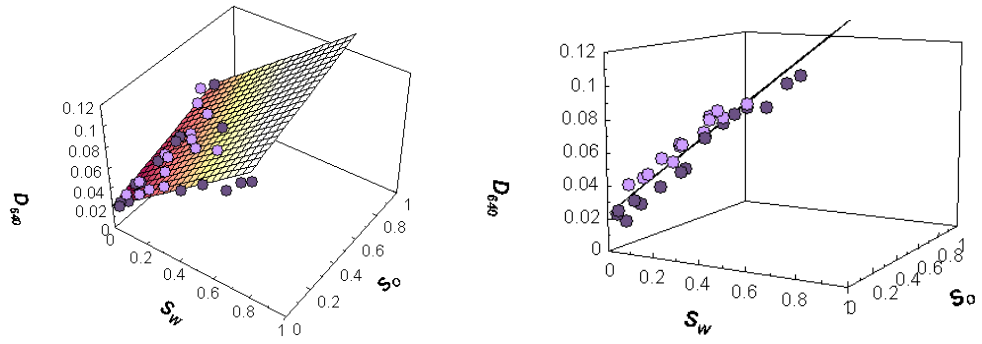

(c) (d)

Figure 3.4 Oattwa#3820 sand optical density, diesel and water saturation relationship for each wavelength. (a) Optical density for λ =450 nm (D_{450}), Diesel saturation (S_o) and water saturation (S_w) relationship. (b) Orthogonal view to regression plane of D_{450}, S_o and S_w. (c) Optical density for λ =640 nm (D_{640}), Diesel saturation (S_o) and water saturation (S_w) relationship. (d) Orthogonal view to regression plane of D_{640}, S_o and S_w.

$$D_{450} = 0.279 + 0.222S_w + 0.773S_o \qquad (R^2 = 0.91)$$
$$D_{640} = 0.230 + 0.128S_w + 0.047S_o \qquad (R^2 = 0.93) \tag{3.1}$$

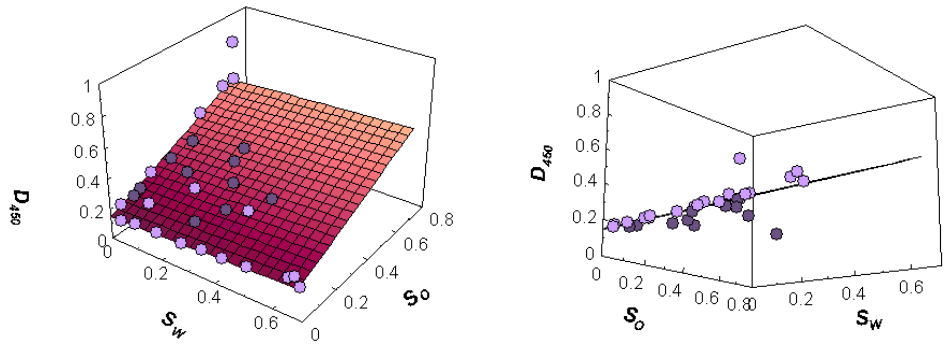

(a) (b)

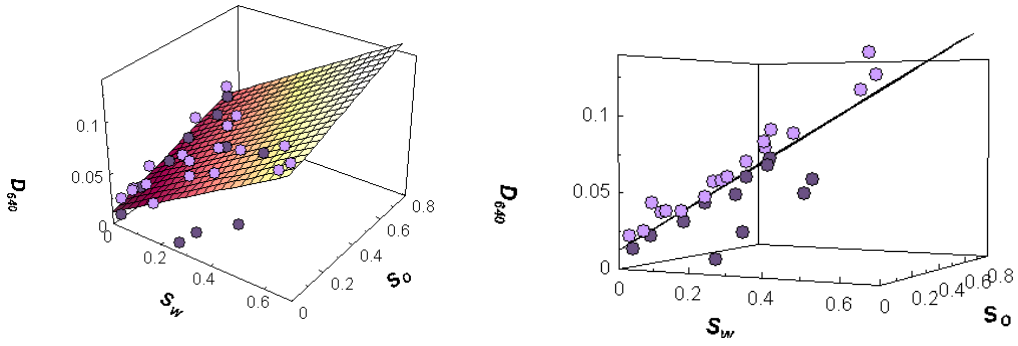

(c) (d)

Figure 3.5 Oattwa#3821 sand optical density, diesel and water saturation relationship for each wavelength. (a) Optical density for λ =450 nm (D_{450}), Diesel saturation (S_o) and water saturation (S_w) relationship. (b) Orthogonal view to regression plane of D_{450}, S_o and S_w. (c) Optical density for λ =640 nm (D_{640}), Diesel saturation (S_o) and water saturation (S_w) relationship. (d) Orthogonal view to regression plane of D_{640}, S_o and S_w.

$$D_{450} = 0.146 + 0.080S_w + 0.567S_o \qquad (R^2 = 0.71)$$
$$D_{640} = 0.012 + 0.148S_w + 0.061S_o \qquad (R^2 = 0.74) \tag{3.2}$$

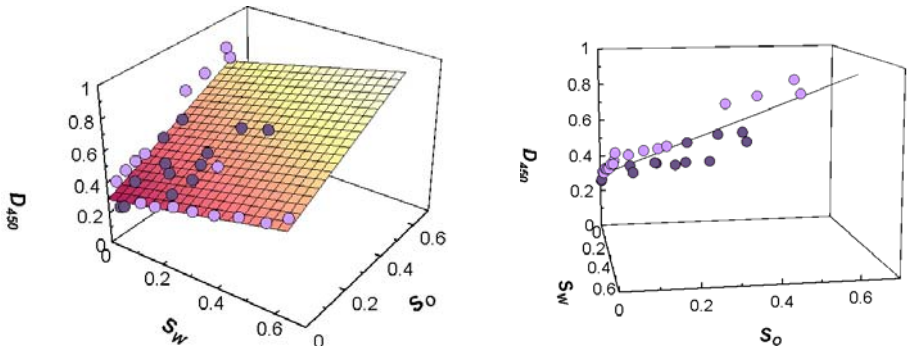

(a) (b)

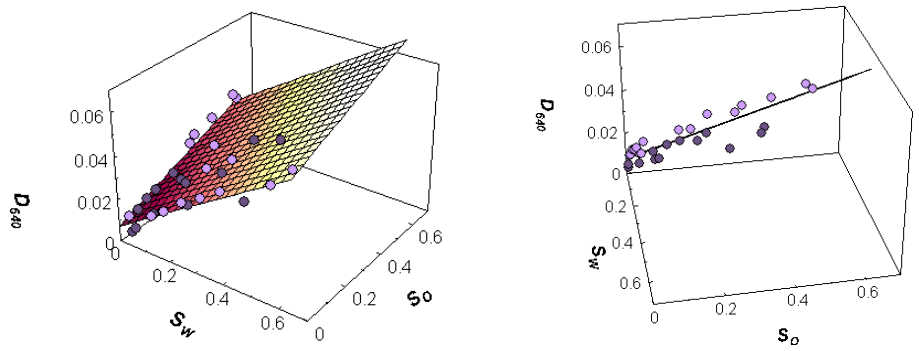

(c) (d)

Figure 3.6 Toyoura sand optical density, diesel and water saturation relationship for each wavelength. (a) Optical density for λ =450 nm (D_{450}), Diesel saturation (S_o) and water saturation (S_w) relationship. (b) Orthogonal view to regression plane of D_{450}, S_o and S_w. (c) Optical density for λ =640 nm (D_{640}), Diesel saturation (S_o) and water saturation (S_w) relationship. (d) Orthogonal view to regression plane of D_{640}, S_o and S_w.

$$D_{450} = 0.288 + 0.404S_w + 0.689S_o \qquad (R^2 = 0.73)$$
$$D_{640} = 0.007 + 0.812S_w + 0.040S_o \qquad (R^2 = 0.80) \tag{3.3}$$

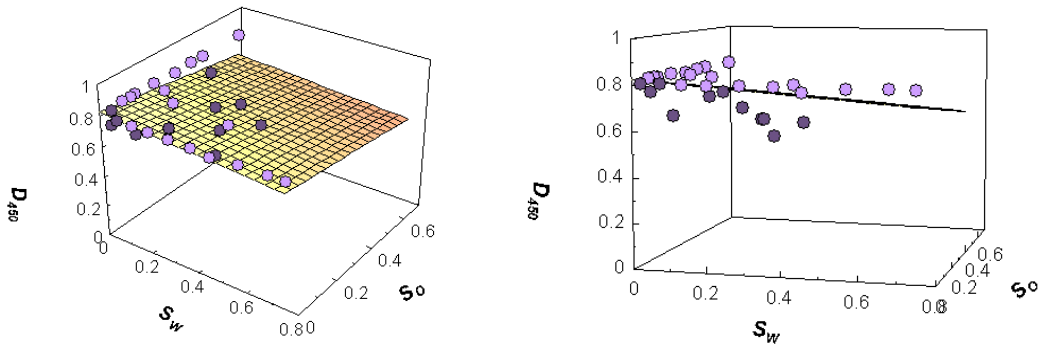

(a) (b)

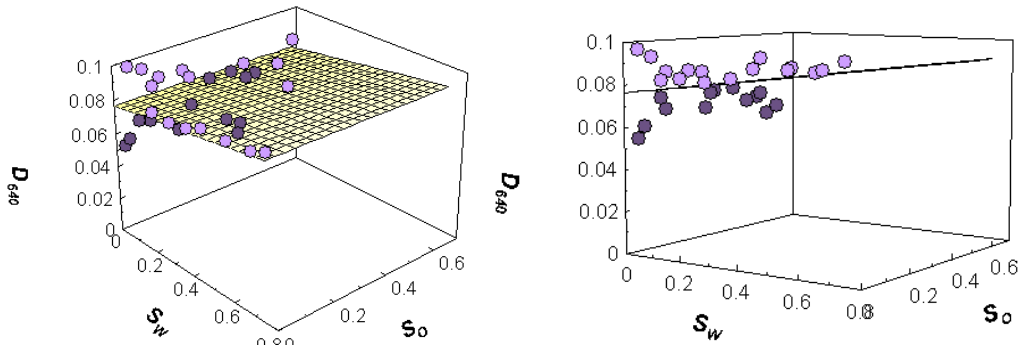

(c) (d)

Figure 3.7 Chonburi sand optical density, diesel and water saturation relationship for each wavelength. (a) Optical density for λ =450 nm (D_{450}), Diesel saturation (S_o) and water saturation (S_w) relationship. (b) Orthogonal view to regression plane of D_{450}, S_o and S_w. (c) Optical density for λ =640 nm (D_{640}), Diesel saturation (S_o) and water saturation (S_w) relationship. (d) Orthogonal view to regression plane of D_{640}, S_o and S_w.

$$D_{450} = 0.827 + 0.119S_w - 0.208S_o \qquad (R^2 = 0.19)$$
$$D_{640} = 0.076 + 0.019S_w - 0.001S_o \qquad (R^2 = 0.16) \tag{3.4}$$

From Saturation-Optical Density relationship test, a linear relationship exists between optical density and saturations of Diesel and water in Ottawa#3820 sand, Ottawa#3821 sand and Toyoura sand. Their coefficients of correlation (R^2) are in ranges between 0.73 and 0.93 therefore the produced regression equations are satisfactory. Only in Chonburi sand which is the highest in organic content, the relationship between saturation and optical density is nonlinear therefore Simplified Image Analysis Method is not applicable for this porous media.

3.2.5 Additional saturation-optical density relationship test

Only thirty soil samples were tested for each porous media in previous section and there is a potential to apply the Simplified Image Analysis Method on 3 porous media included Ottawa#3820 sand, Ottawa#3821 sand and Toyoura sand. Due to the availability of Toyoura sand in Thailand, only Ottwa#3820 and Ottawa#3821 will be used in the following test to confirm that the linear relationship exists between

saturation and optical density. As mentioned in Table 2.3, Calibration process of Multispectral Image Analysis Method required more than 40 samples with different degrees of LNAPL saturation and water saturation (the more samples, the higher accuracy level). Hundred and thirty five samples for each porous media (Ottawa#3820 sand and Ottawa#3821 sand) were prepared by mixing known amounts of water, diesel and porous media. Non dye water were used instead of Brilliant Blue FCF dyed water used in section 3.2.4 to test the possibility of using of non dye water in further 1-D Column and 2-D tank experiment. In this test 120 W LED floodlight were used to illuminate the samples. The result are shown in Figure 3.8-Figure 3.9

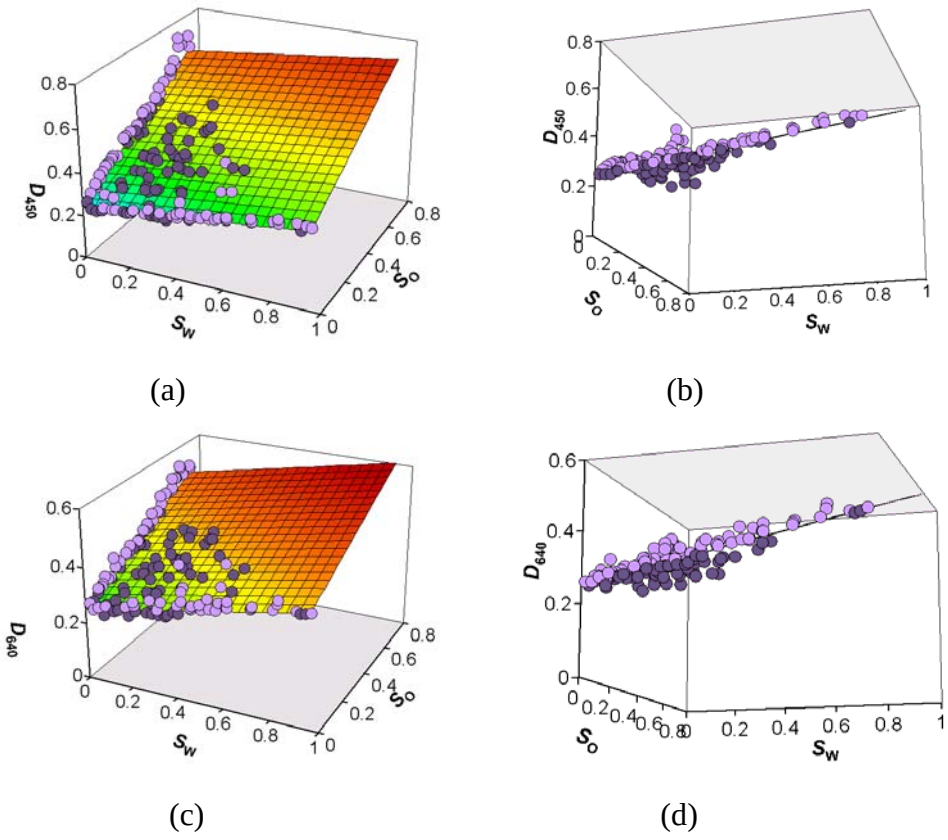

Figure 3.8 Additional test of Ottawa#3820 sand result, average optical density, diesel and water saturation relationship for each wavelength. (a) Optical density for λ =450 nm (D_{450}), Diesel saturation (S_o) and water saturation (S_w) relationship. (b) Orthogonal view to regression plane of D_{450}, S_o and S_w. (c) Optical density for λ =640

nm (D_{640}), Diesel saturation (S_o) and water saturation (S_w) relationship. (d) Orthogonal view to regression plane of D_{640}, S_o and S_w.

$$D_{450} = 0.242 + 0.127S_w + 0.528S_o \qquad (R^2 = 0.86)$$
$$D_{640} = 0.250 + 0.157S_w + 0.322S_o \qquad (R^2 = 0.78) \tag{3.5}$$

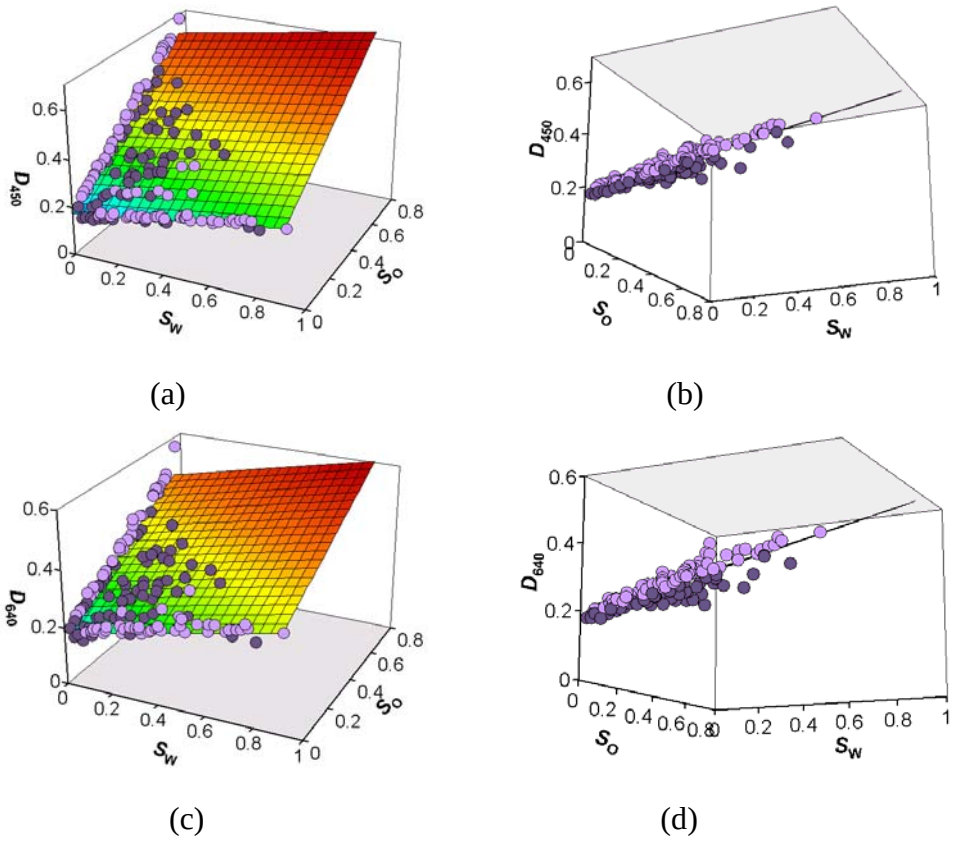

Figure 3.9 Additional test of Ottawa#3821 sand result, average optical density, diesel and water saturation relationship for each wavelength. (a) Optical density for λ =450 nm (D_{450}), Diesel saturation (S_o) and water saturation (S_w) relationship. (b) Orthogonal view to regression plane of D_{450}, S_o and S_w. (c) Optical density for λ =640 nm (D_{640}), Diesel saturation (S_o) and water saturation (S_w) relationship. (d) Orthogonal view to regression plane of D_{640}, S_o and S_w.

$$D_{450} = 0.176 + 0.145S_w + 0.590S_o \qquad (R^2 = 0.93)$$
$$D_{640} = 0.183 + 0.174S_w + 0.373S_o \qquad (R^2 = 0.83) \tag{3.6}$$

A linear relationship existed between optical density and saturations of Diesel and water in Ottawa#3820 sand and Ottawa#3821 sand. Their coefficients of correlation (R^2) are in ranges between 0.78 and 0.93 therefore the produced regression equations are acceptable.

There might have the questions that Simplified Image Analysis Method still applicable or not for mixture of two porous media that each one already proved that linear relationship existed. Ottawa#3820 sand and Ottawa#3821 sand were mixed (50:50 by weight) and hundred and thirty five samples were prepared and test following the same procedure with previous section. The result of mixed Ottawa sand saturation-optical density relationship test is presented in Figure 3.10

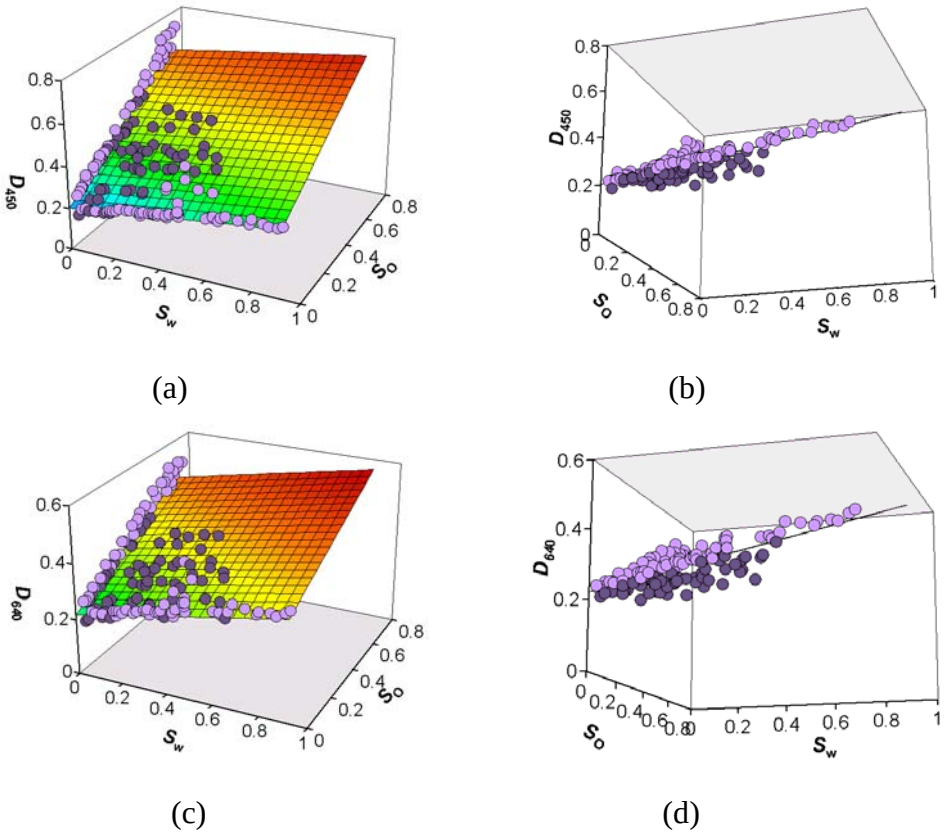

Figure 3.10 Mixed Ottawa sand optical density, diesel and water saturation relationship for each wavelength. (a) Optical density for λ =450 nm (D_{450}), Diesel saturation (S_o) and water saturation (S_w) relationship. (b) Orthogonal view to regression plane of D_{450}, S_o and S_w. (c) Optical density for λ =640 nm (D_{640}), Diesel

saturation (S_o) and water saturation (S_w) relationship. (d) Orthogonal view to regression plane of D_{640}, S_o and S_w.

$$\begin{aligned} D_{450} &= 0.202 + 0.137S_w - 0.594S_o \qquad (R^2 = 0.90) \\ D_{640} &= 0.220 + 0.157S_w - 0.335S_o \qquad (R^2 = 0.74) \end{aligned} \tag{3.7}$$

The results shown that linear relationship between saturation and optical density still existed in mixed Ottawa#3820 sand and Ottawa#3821 sand and regression equation of saturation-optical density of Mixed Ottawa sand can be predicted by the average value of regression equation for saturation-optical density of Ottawa#3820 (equation 3.6) and regression equation for saturation-optical density of Ottawa#3821 (equation 3.7). Predicted regression equation for saturation and optical density of mixed Ottawa sand can be written as

$$\begin{aligned} D_{450} &= 0.209 + 0.136S_w - 0.561S_o \\ D_{640} &= 0.216 + 0.166S_w - 0.348S_o \end{aligned} \tag{3.8}$$

Regression plane of predicted saturation-optical density of mixed Ottawa sand is shown in Figure 3.11

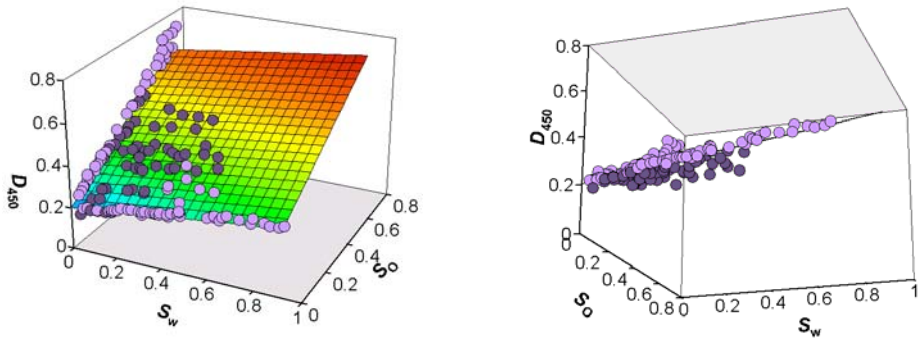

(a) (b)

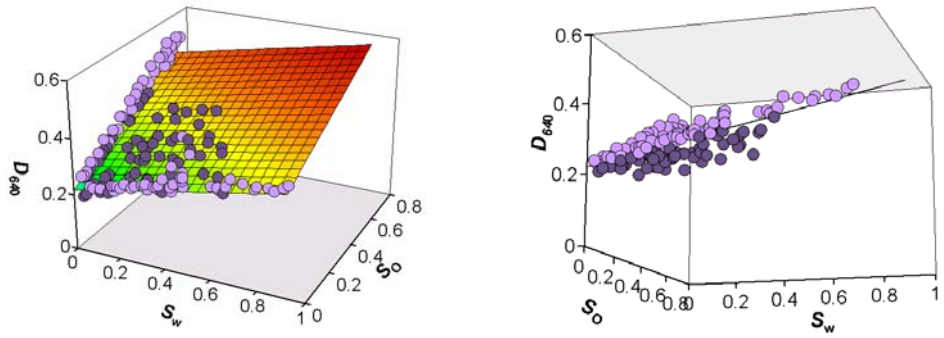

(c) (d)

Figure 3.11 Predicted mixed Ottawa sand optical density, diesel and water saturation relationship for each wavelength. (a) Optical density for λ =450 nm (D_{450}), Diesel saturation (S_o) and water saturation (S_w) relationship. (b) Orthogonal view to regression plane of D_{450}, S_o and S_w. (c) Optical density for λ =640 nm (D_{640}), Diesel saturation (S_o) and water saturation (S_w) relationship. (d) Orthogonal view to regression plane of D_{640}, S_o and S_w.

There was an average 6.64% different of predicted optical density at 450 nm (D_{450}) when compared with optical density obtained from Multispectral Image Analysis Method and 8.58% different in case of optical density at 640 nm (D_{640}). The results indicated that for the known ratio mixture of two porous media that each one already proved that linear relationship between saturation-optical density existed, calibration processes required by Multispectral Image Analysis Method can be neglected and regression equation of saturation-optical density can be predicted.

3.3 Two-phase column experiment

Water drainage test and diesel drainage test are conducted in Ottawa#3820 sand and Ottawa#3821 sand. Both tests are conducted in 110 cm height column fill with fully saturated water and diesel and let drain for 48 hours. Water saturation distribution and diesel saturation distribution are obtained by Simplified Image Analysis Method. Two-Phase column testing program is shown in Table 3.3

Table 3.3 Two-phase column testing program.

Test	Column	Medium	Wetting fluid
C-1	I	Ottawa#3820 sand	Water
C-1	II	Ottawa#3821 sand	Water
C-2	I	Ottawa#3820 sand	Diesel
C-2	II	Ottawa#3821 sand	Diesel

3.3.1 Materials

Ottawa#3820 sand and Ottawa#3821 sand were used as a porous media. Diesel (Specific gravity = 0.865 g/cm^3) was dyed red with Red Sudan III (1:10000 by weight) to enhance visual observation and increase their light absorbance properties. There is no noticeable change in the physical properties of water and diesel after being mixed with their respective dyes and the dyes do not migrate between water and diesel and are not absorbed by the soil particles.

3.2.2 Equipments

Two 3.5×3.5×110 cm one-dimensional acrylics column (Figure 3.12) were designed to study the soil-liquid characteristic in Ottawa#3820 and Ottawa#3821. Two cameras were used in this study, First cameras Nikon D90 cameras with the 450 nm band-pass filter installed was used to capture the picture of water drainage column test and second one Nikon D90 camera with 640 nm band-pass filter installed was used to capture the picture of diesel drainage column test. Both cameras were set to manual mode so that their aperture, shutter speed and white balance were kept constant. Both cameras were connected to a computer via USB cables and remotely controlled by Nikon Camera control Pro 2. X-Rite Gretagmacbeth ColorChecker white balance card was located next to the sample to provide a white and black reference. Two 120 W LED floodlights were used to illuminate the samples which were automatically turned on 30 seconds before the pictures were taken, and turned off 30 seconds later by in-house development timer control software. Black curtain was installed between column and both cameras to avoid reflections from column surface. Equipments set up is shown in Figure 3.13

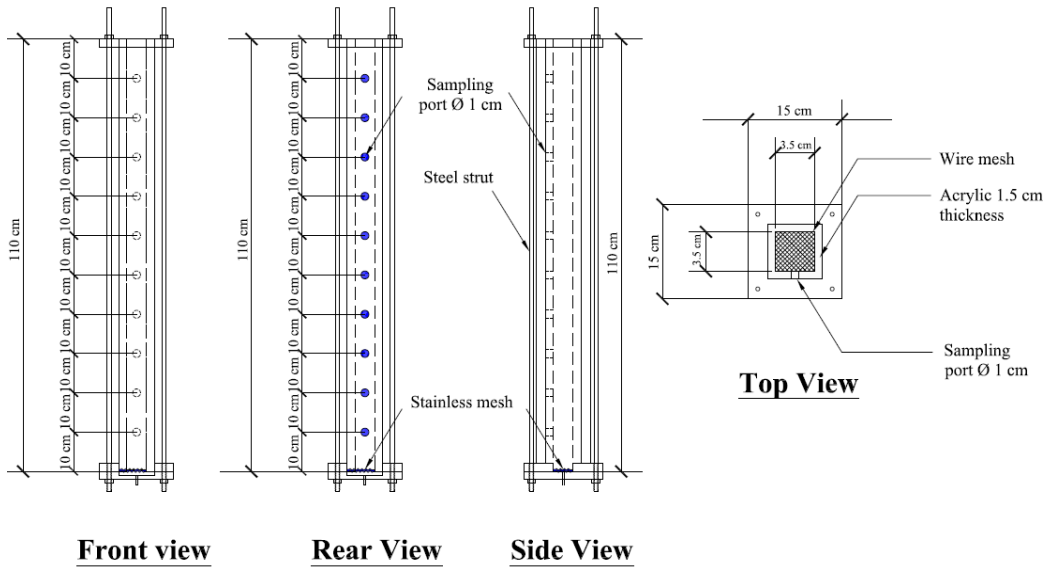

Figure 3.12 One-dimensional column designed

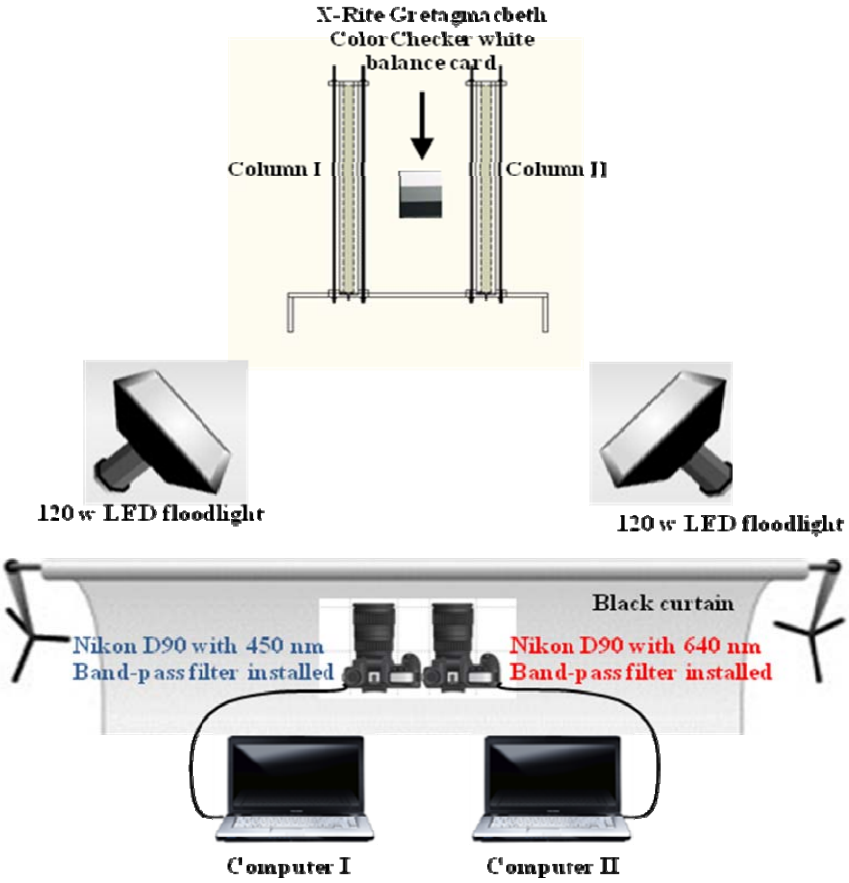

Figure 3.13 Two-phase column test equipment set up

3.2.3 Calibration

Two-phase column experiment required only two calibration photographs: the studied column filled with dry sand and the column filled with interested liquid (water or diesel) saturated sand. Calibration picture for two phase column is shown in Figure 3.14 and because water or diesel was used, we can focus on one side of the regression plane Hence, In case of water drainage column test Equation 2.13 can be reduced to:

$$\left[D_{450}\right]_{mn} = \left[\left(D_{450}^{10} - D_{450}^{00}\right).S_w + D_{450}^{00}\right]_{mn} \tag{3.9}$$

In case of diesel drainage column test regression equation is expressed as:

$$\left[D_{640}\right]_{mn} = \left[\left(D_{640}^{01} - D_{450}^{00}\right).S_o + D_{450}^{00}\right]_{mn} \tag{3.10}$$

(a) (b) (c)

Figure 3.14 Calibration pictures (a) Column filled with dry sand. (b) Column filled with fully saturated water and (c) Column filled with fully saturated diesel.

3.2.4 Experiments

Water drainage test and diesel drainage test are conducted in Ottawa#3820 sand and Ottawa#3821 sand. Column I (Figure 3.15) was initially filled with oven dried Ottawa#3820 sand and column II filled with oven dried Ottawa#3821 sand. Dry sand was filled up to 100 cm in both column and dry density of both sand was 1.76 g/cm^3. Digital pictures of dry sand were taken by the equipment that mentioned in section 3.2.3 and will be used as dry sand reference picture in the image analysis processes. Valve B was closed and valve A was opened to slowly saturated the sand from the bottom in both columns (Water used in Test-1 and diesel used in Test-2) (Table 3.2). Digital pictures of fully water saturated sand in Test-1 and fully diesel saturated sand in Test-2 were taken and will be used as liquid saturated sand reference picture. Valve A was closed and valve B was opened and liquid inside columns was drained for 48 hours in both column and to avoid producing a vacuum, the top of the column was open. Digital pictures were taken every half hour. The camera was set to manual mode, and the aperture, shutter speed, and white balance were defined and maintained constant throughout the experiment. The camera was remotely controlled (using Nikon Camera Control Pro 2 software) to avoid vibrations and camera displacement. The two 120 W LED floodlights were turned on 30 seconds prior to taking the pictures and turned off right after that to avoid fluctuations in the column's temperature. Room temperature was kept at 20 °C and humidity at 70%. Testing condition is summarized in Table 3.4

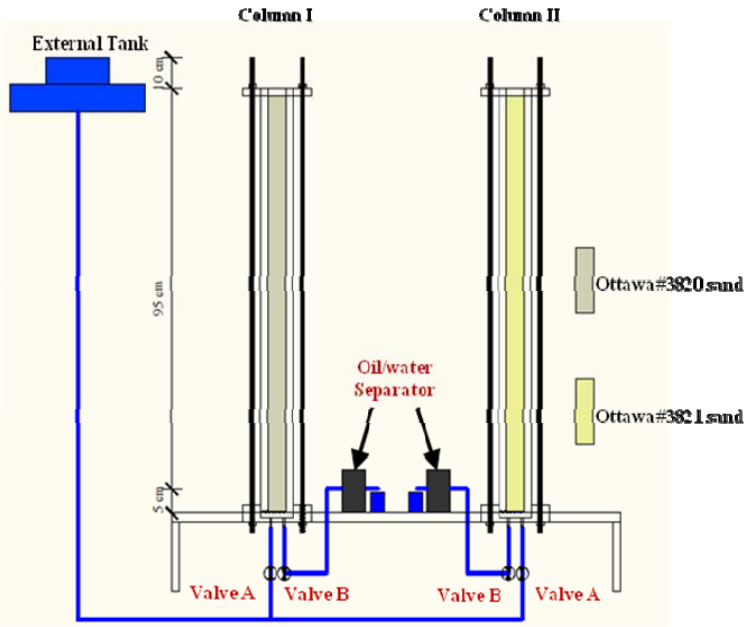

Figure 3.15 Two-phase column experiment set up

Table 3.4 Two-phase column testing condition

Test	Testing State	Time	Head	Comments
C-1	Initial Condition	0 hr	120 cm	Water saturated columns
	Drainage	0 hr - 48 hr	5 cm	
C-2	Initial Condition	0 hr	120 cm	Diesel saturated columns
	Drainage	0 hr - 48 hr	5 cm	

3.2.5 Computational analysis

All pictures were exported from the NEF format (Nikon proprietary RAW version files) to the TIFF format (Tagged Image File Format) using Nikon ViewNX 2.0 TIFF images were analyzed with an ad-hoc program in MATLAB 2007a written by Flores (2010). $[D_{450}]_{mn}$ for water drainage test and $[D_{640}]_{mn}$ for diesel drainage test are optical density matrices calculated from the two calibration picture and each pictures taken during the test so that water saturation matrices ($[S_w]_{mn}$) in test C-1 and diesel saturation matrices ($[S_o]_{mn}$) in test C-2 can be solved

3.2.6 Results and discussions

Water distribution in entire domain at the end of the test (t = 48 hr) and degree of water saturation vs. column height is presented in Figure 3.16.

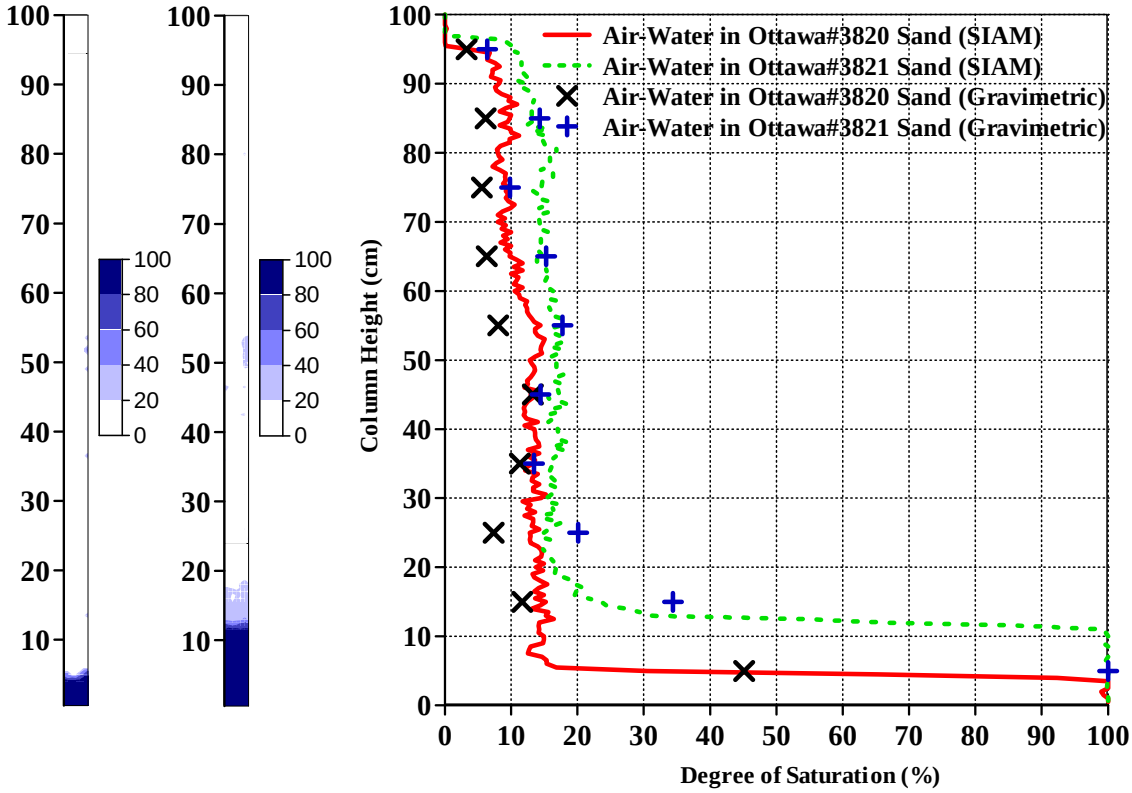

Figure 3.16 Test C-1 (a) Water saturation contour in Ottawa#3820 sand.
(b) Water saturation contour in Ottawa#3821 sand and
(c) Water saturation profiles at the end of the test (t=48 hr)

Diesel distribution in entire domain at the end of the test (t = 48 hr) and degree of diesel saturation vs. column height is presented in Figure 3.17. At the end of the tests, 10 soil samples from each test were collected from sampling ports (Figure 3.12). Degree of saturation of water and diesel were obtained from gravimetric method. The different of saturation values from simplified image analysis method and Gravimetric method vary from -10% to 10%. Degree of liquid saturation obtained from simplified image analysis method and gravimetric method are plot with column height is shown in Figure 3.18

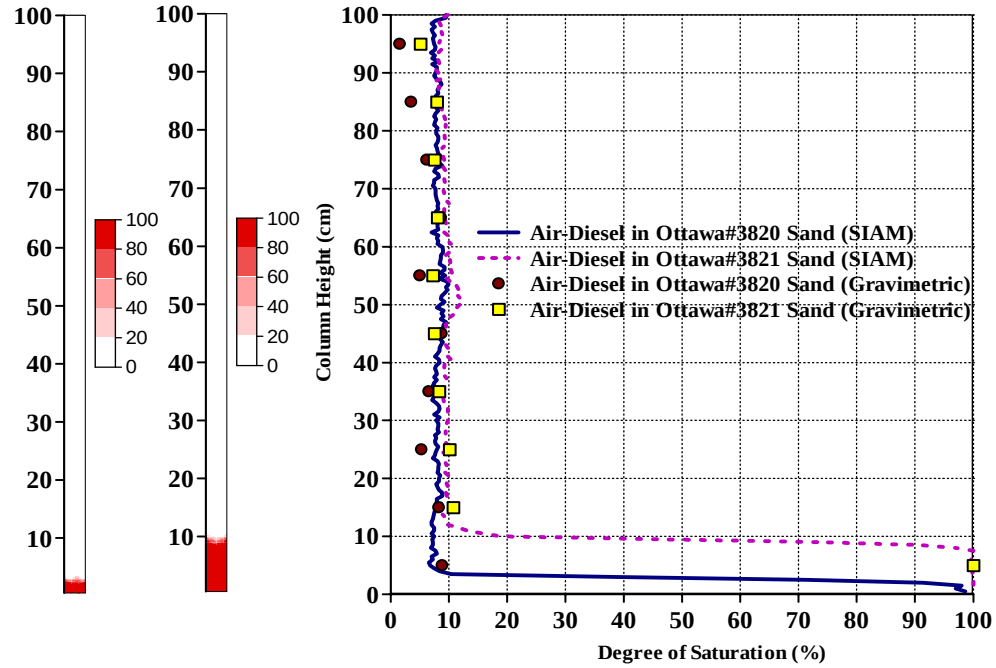

(a) (b) (c)

Figure 3.17 Test C-2 (a) Diesel saturation contour in Ottawa#3820 sand.
(b) Diesel saturation contour in Ottawa#3821 sand and
(c) Diesel saturation profiles at the end of the test (t=48 hr)

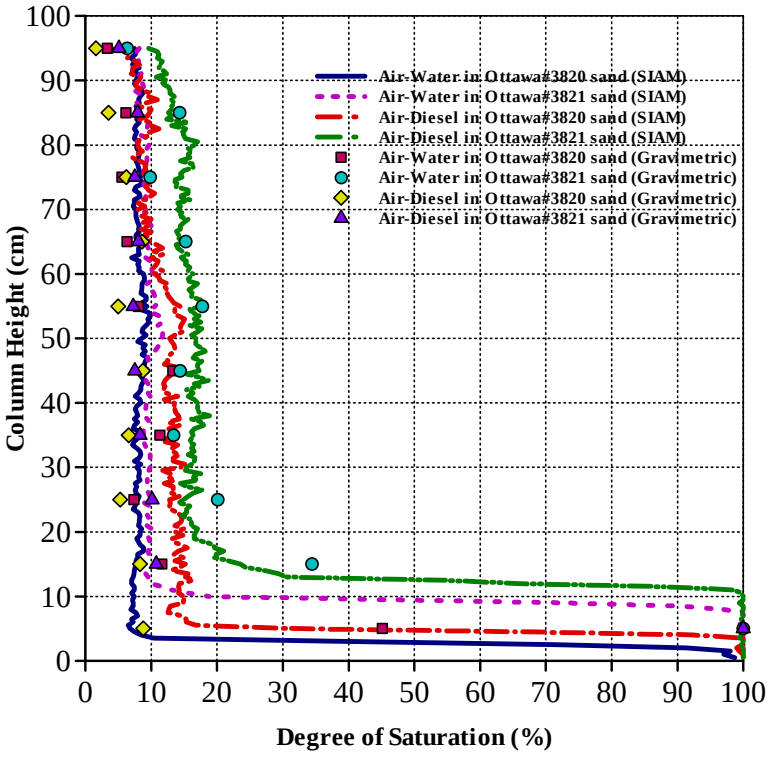

Figure 3.18 Degree of liquid saturation profiles at the end of test (t=48 hr)

3.4 Three-phase column experiment

One-dimensional column tests with water drainage following with diesel and air infiltration were conducted to investigate the effects of fluctuating water table on diesel migration behavior in both homogeneous porous media and heterogeneous . porous media. Three-Phase column experiment testing program is presented in Table 3.5

Table 3.5 Three-Phase column testing program.

Test	Column	Medium	Testing condition
C-3	I	Ottawa#3820 sand	Drainage/Imbibition
C-3	II	Ottawa#3821 sand	Drainage/Imbibition
C-4	I	Ottawa#3820 sand/Ottawa#3821 sand	Drainage/Imbibition
C-4	II	Ottawa#3821 sand/Ottawa#3820 sand	Drainage/Imbibition

3.4.1 Equipments and materials

The same one-dimensional column designed in section 3.3 as well as similar equipments set up (Figure 3.13) were used. Ottawa#3820 sand and Ottawa#3821 sand were used as a porous media. Diesel was dyed red with Red Sudan III (1:10000 by weight). Experimental set up in homogeneous porous media cases and heterogeneous porous media cases is shown in Figure 3.19

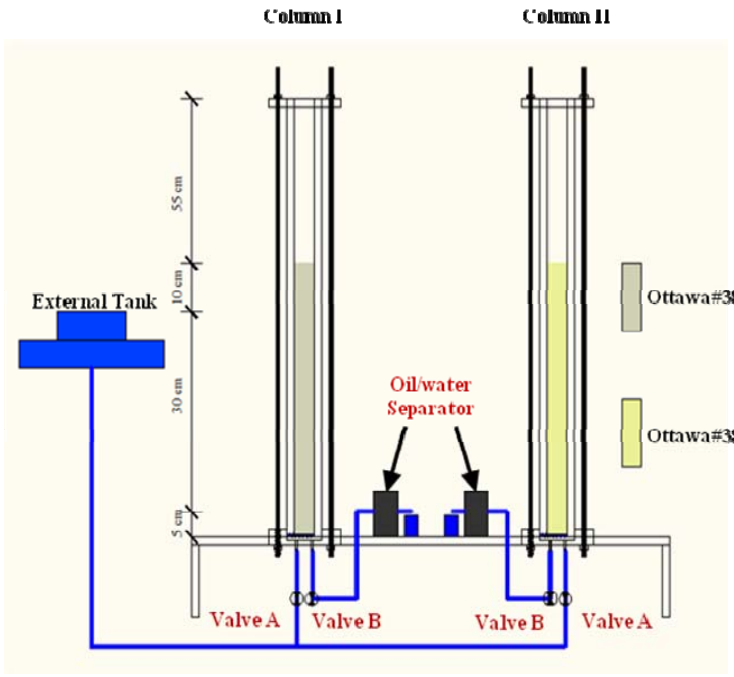

(a)

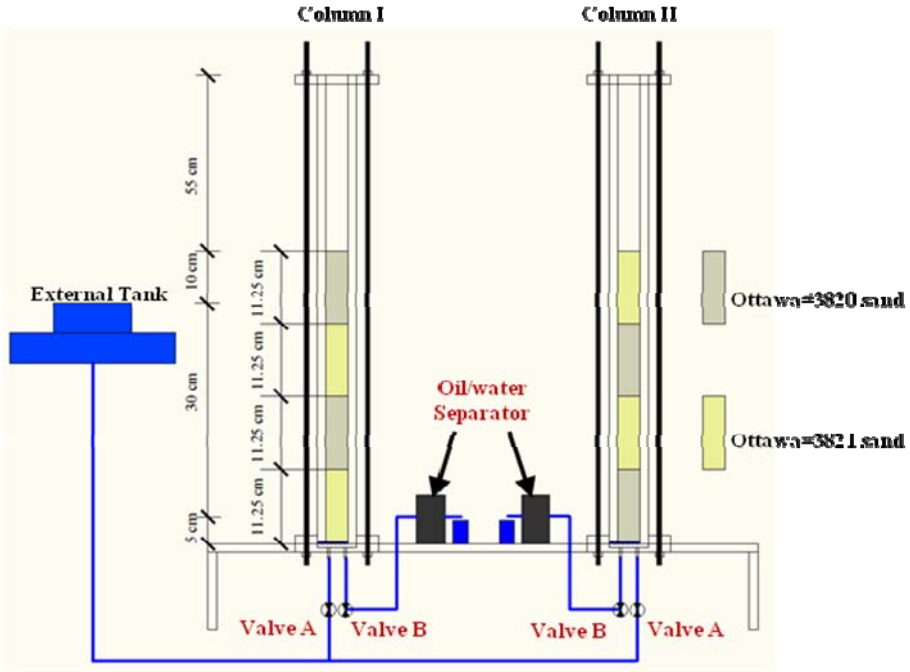

(b)

Figure 3.19 One-dimensional column set up (a) Homogeneous porous media (b) Heterogeneous porous media.

3.4.2 Calibration

Three-phase column experiment required three pictures with each camera. Each camera took a picture of the column fill with dry sand, water saturated sand and diesel saturated sand. Diesel saturated sand pictures in section 3.2 were used as reference picture in image analysis processes From Equation 2.16, these six pictures correspond to $[D_{450}{}^{00}]_{mn,}$ $[D_{450}{}^{10}]_{mn}$, $[D_{450}{}^{01}]_{mn,}$ $[D_{640}{}^{00}]_{mn,}$ $[D_{640}{}^{10}]_{mn}$ and $[D_{640}{}^{01}]_{mn}$.

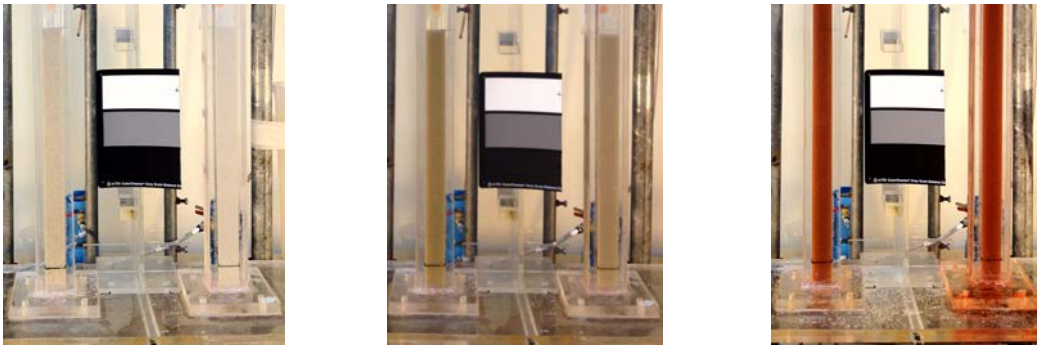

(a) (b) (c)

Figure 3.20 Homogeneous porous media calibration pictures (a) Column filled with dry sand. (b) Column filled with fully saturated water and (c) Column filled with fully saturated diesel.

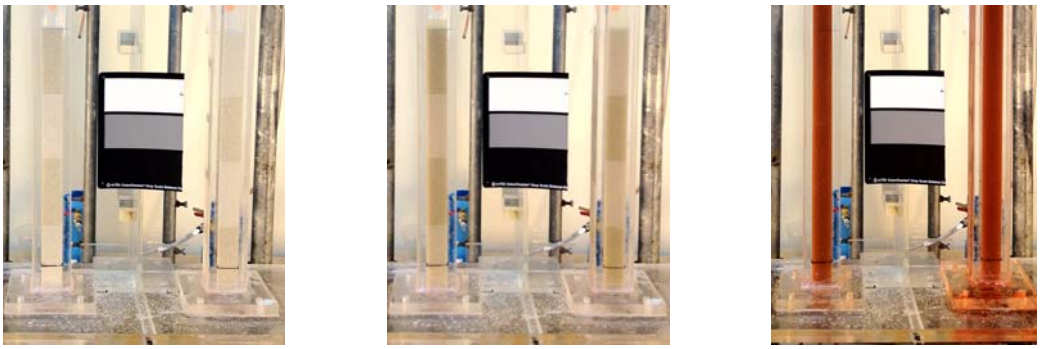

(a) (b) (c)

Figure 3.21 Heterogeneous porous media calibration pictures (a) Column filled with dry sand. (b) Column filled with fully saturated water and (c) Column filled with fully saturated diesel.

3.4.3 Experiments

One-dimensional column tests with water drainage following with diesel and air infiltration were conducted in Ottawa#3820 sand and Ottawa#3821 sand. Oven dried sand was filled up to 45 cm in one-dimensional column and dry density was 1.76 g/cm^3. Digital pictures of dry sand were taken by the equipment that mentioned in section 3.4.2 and were used as dry sand reference picture in the image analysis processes. External tank (Figure 3.19) was placed at 55 cm from the bottom of column. Valve B was closed and valve A was opened to slowly saturate the sand from the bottom in both columns. Digital pictures of fully water saturated sand were taken and were used as reference picture. The test was divided into four stages: first drainage (t = 0 to 18 hr), first imbibition (t = 18 to 30 hr), second drainage (t = 30 to 42 hr) and second imbibitions (t = 42 to 54 hr)

First Drainage: Valve A (Figure 3.19) was closed and valve B was opened and water inside columns was allowed to drain and after 6 hours of water drainage 15 g of diesel infiltrated from the top of column and air was also allowed to freely infiltrate into the column. This stage took 18 hours.

First Imbibition: Valve B was closed and valve A was opened. The water table inside the column moved up and Diesel that infiltrated into the column during the drainage process was displaced by the water. This stage took 12 hours.

Second Drainage: Valve A was closed and valve B was opened again. Water and diesel inside the column were allowed to drain. No additional diesel was infiltrated into the column and this stage took 12 hours.

Second Imbibition: The water table inside the column moved up again following the same procedure as the First imbibition and this stage took 12 hour.

Two digital pictures were taken every half hour from two cameras. The camera was set to manual mode, and the aperture, shutter speed, and white balance were defined and maintained constant throughout the experiment. The camera was remotely controlled (using Nikon Camera Control Pro 2 software) to avoid vibrations

and camera displacement. The two 120 W LED floodlights were turned on 30 seconds prior to taking the pictures and turned off right after that to avoid fluctuations in the column's temperature. Room temperature was kept at 20 °C and humidity at 70%. Testing condition is summarized in Table 3.6

Table 3.6 Three-phase column testing condition

Test Stage	Time	Water Head	Comments
Initial Condition	0 hr	45 cm	
First Drainage	0 hr - 18 hr	5 cm	15 g Diesel infiltrated at t = 6 hr
First Imbibition	18 hr - 30 hr	30 cm	
Second Drainage	30 hr - 42 hr	5 cm	
Second Imbibition	42 hr - 54 hr	30 cm	

3.4.4 Computational analysis

Similar to the previous test, all pictures were exported from the NEF format (Nikon proprietary RAW version files) to the TIFF format (Tagged Image File Format) using Nikon ViewNX 2.0 TIFF images were analyzed with an ad-hoc program in MATLAB 2007a written by Flores (2010) Using the six calibration pictures, the average optical density matrices $[D_{450}{}^{00}]_{mn,}$ $[D_{450}{}^{10}]_{mn}$, $[D_{450}{}^{01}]_{mn,}$ $[D_{640}{}^{00}]_{mn,}$ $[D_{640}{}^{10}]_{mn}$ and $[D_{640}{}^{01}]_{mn}$ were calculated. The following matrix of correlation equations was obtained:

$$\begin{bmatrix} D_{450} \\ D_{640} \end{bmatrix}_{mn} = \begin{bmatrix} \left(D_{450}^{10} - D_{450}^{00}\right).S_w + \left(D_{450}^{01} - D_{450}^{00}\right).S_o + D_{450}^{00} \\ \left(D_{640}^{10} - D_{640}^{00}\right).S_w + \left(D_{640}^{01} - D_{640}^{00}\right).S_o + D_{640}^{00} \end{bmatrix}_{mn} \quad (3.11)$$

$[D_{450}]_{mn}$ and $[D_{640}]_{mn}$ were calculated for each picture taken during the test, and the water saturation matrices ($[S_w]_{mn}$) and diesel saturation matrices ($[S_o]_{mn}$) were solved.

3.4.5 Results

Water distribution and diesel distribution in entire domain at the end of each test stage for both homogeneous cases and heterogeneous cases are presented from Figure 3.22 to Figure 3.25 and degree of saturation profile vs. column height for

all cases are shown from Figure 3.26 to Figure 3.29. Dynamic behavior of both diesel saturation and water saturation in column were analyzed by plot degree of water saturation at 10 cm, 30 cm, 50 cm, 70 cm and 90 cm from the bottom of column with time. The results are presented in Figure 3.30 - Figure 3.33

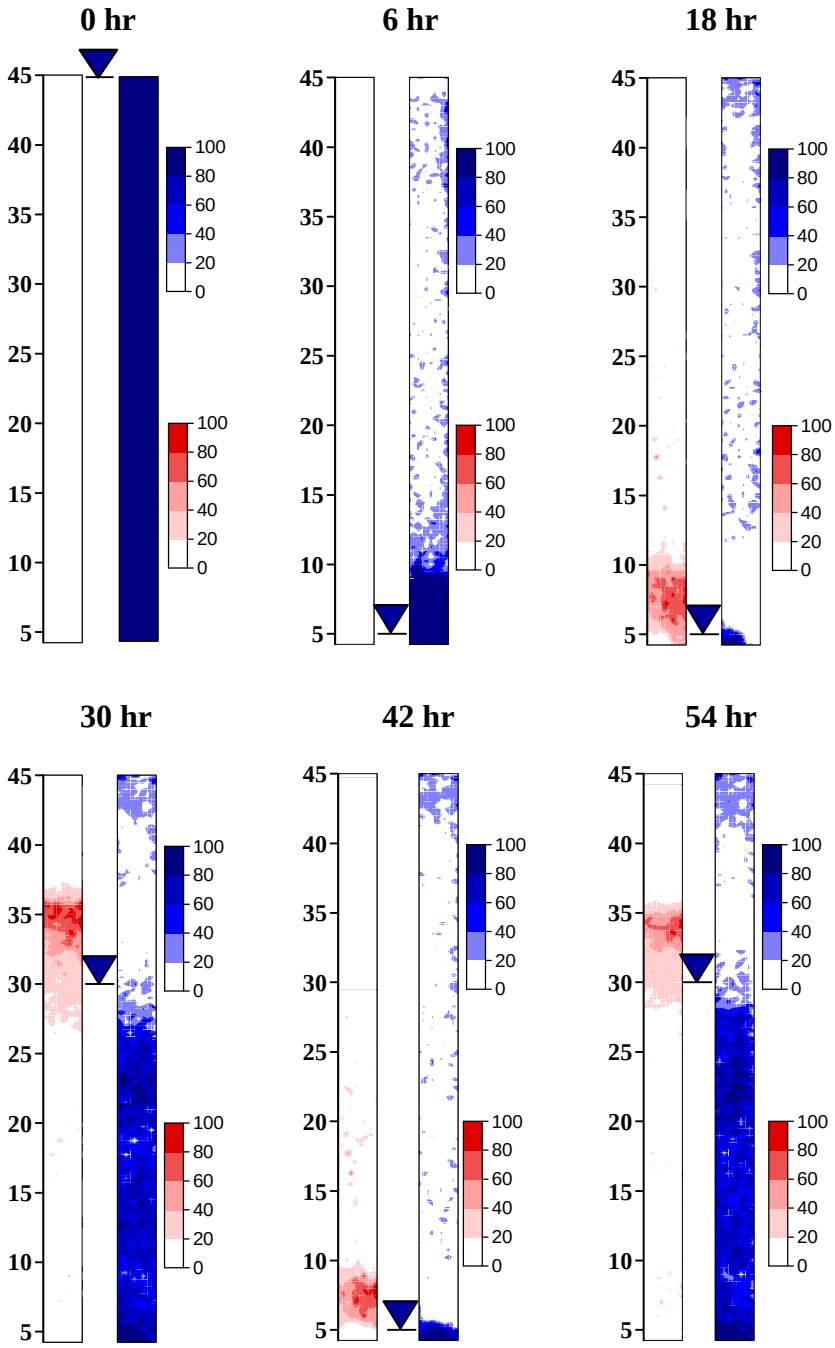

Figure 3.22 Diesel saturation contour (red plots) and Water saturation contour (blue plots) in Test C-3 Column I.

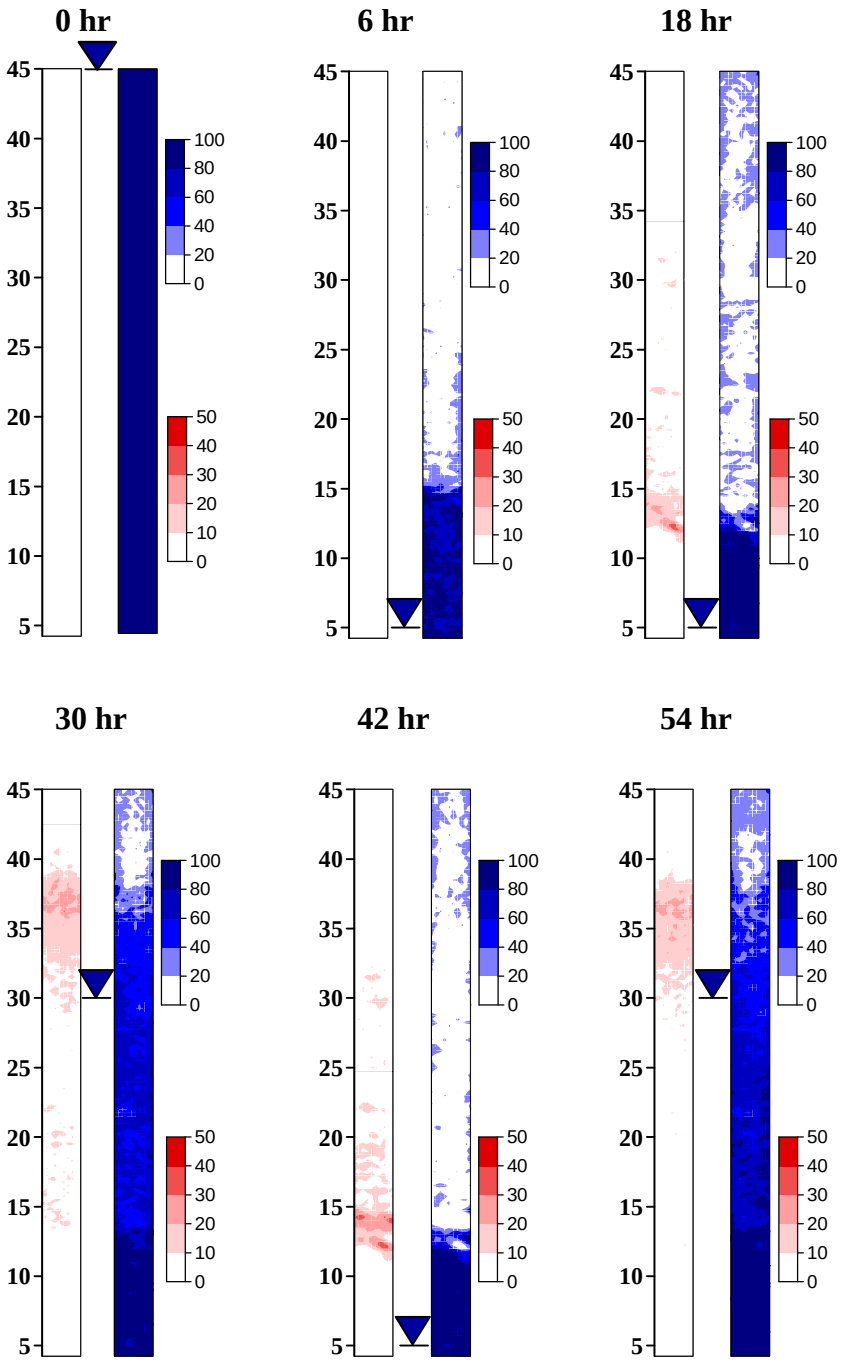

Figure 3.23 Diesel saturation contour (red plots) and Water saturation contour (blue plots) in Test-C3 Column II

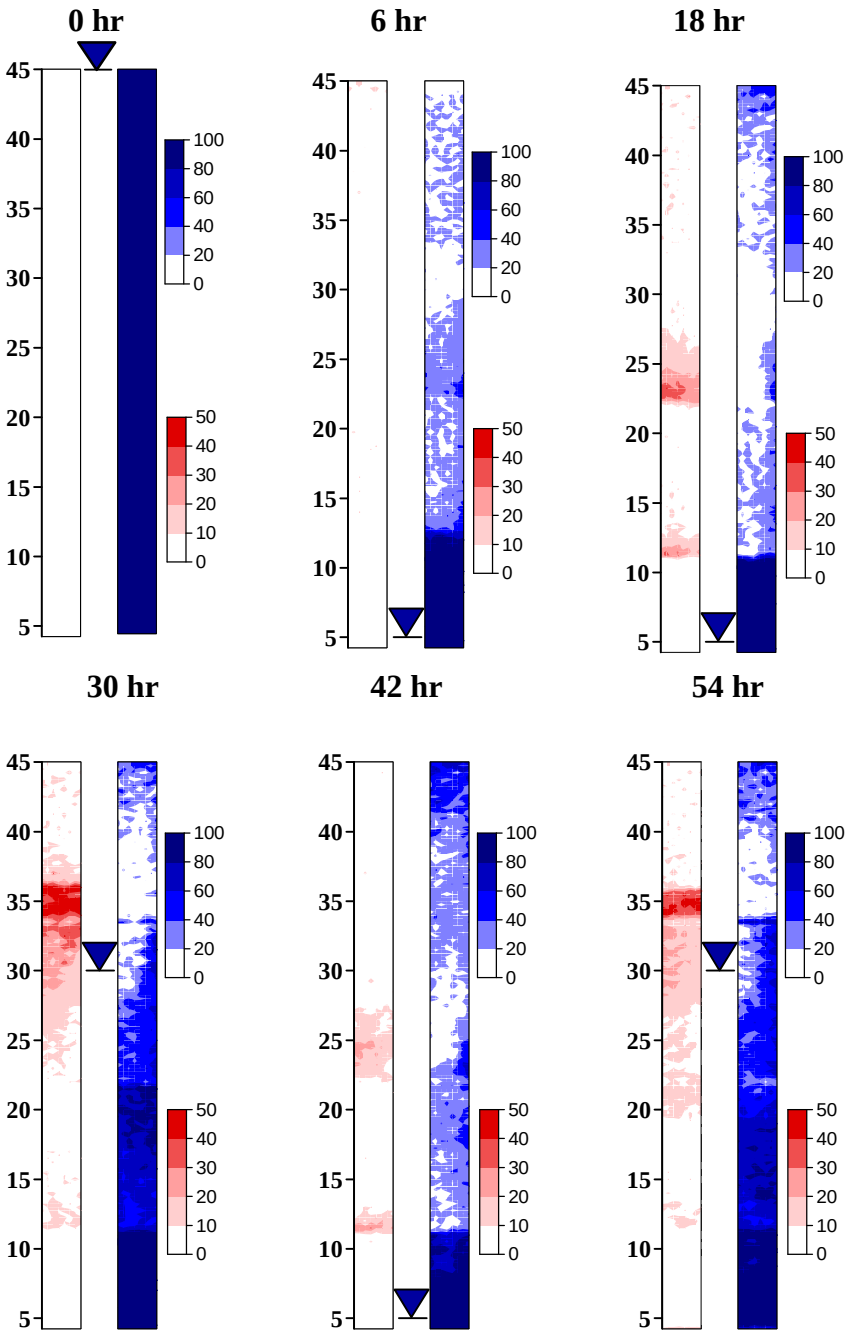

Figure 3.24 Diesel saturation contour (red plots) and Water saturation contour (blue plots) in Test C-4 Column I

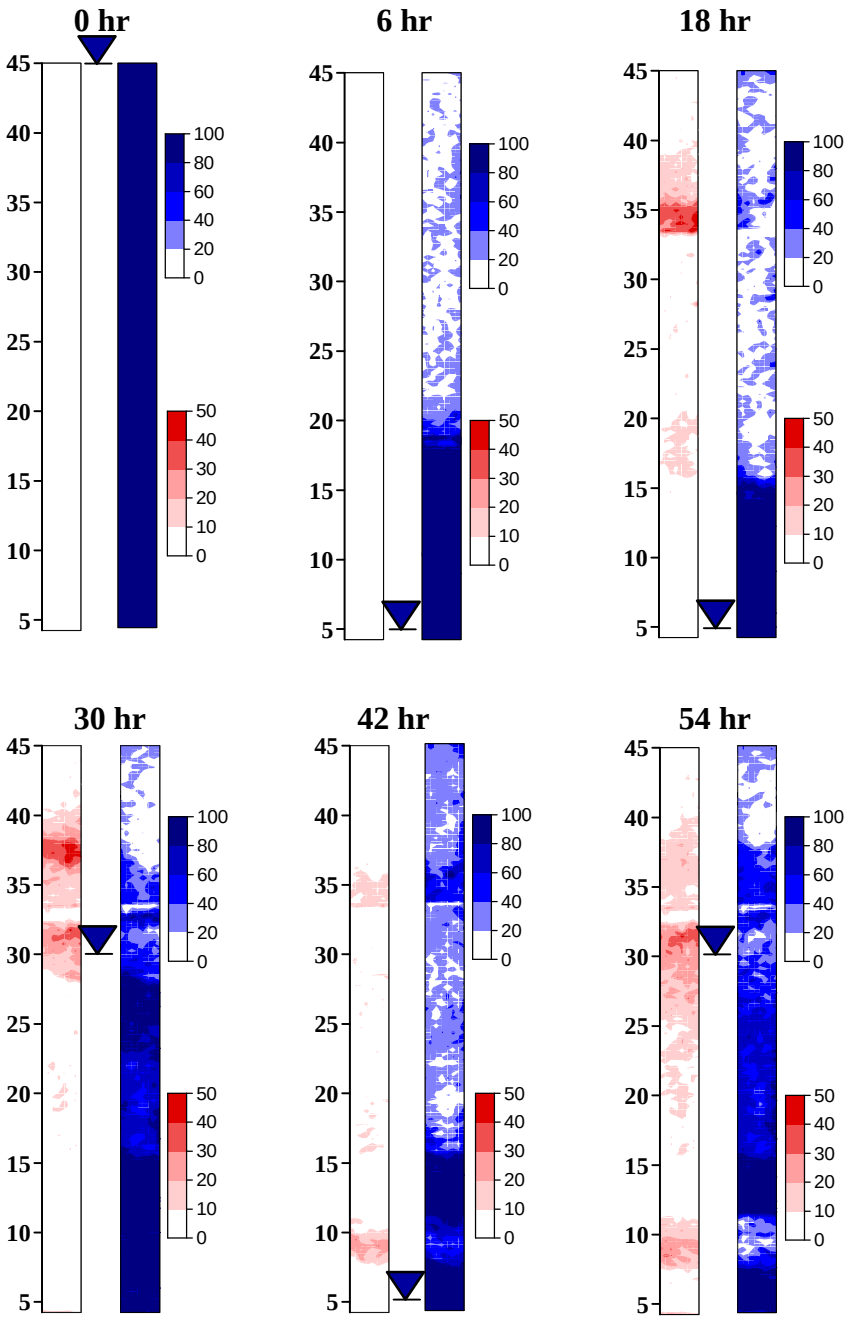

Figure 3.25 Diesel saturation contour (red plots) and Water saturation contour (blue plots) in test C-4 Column II

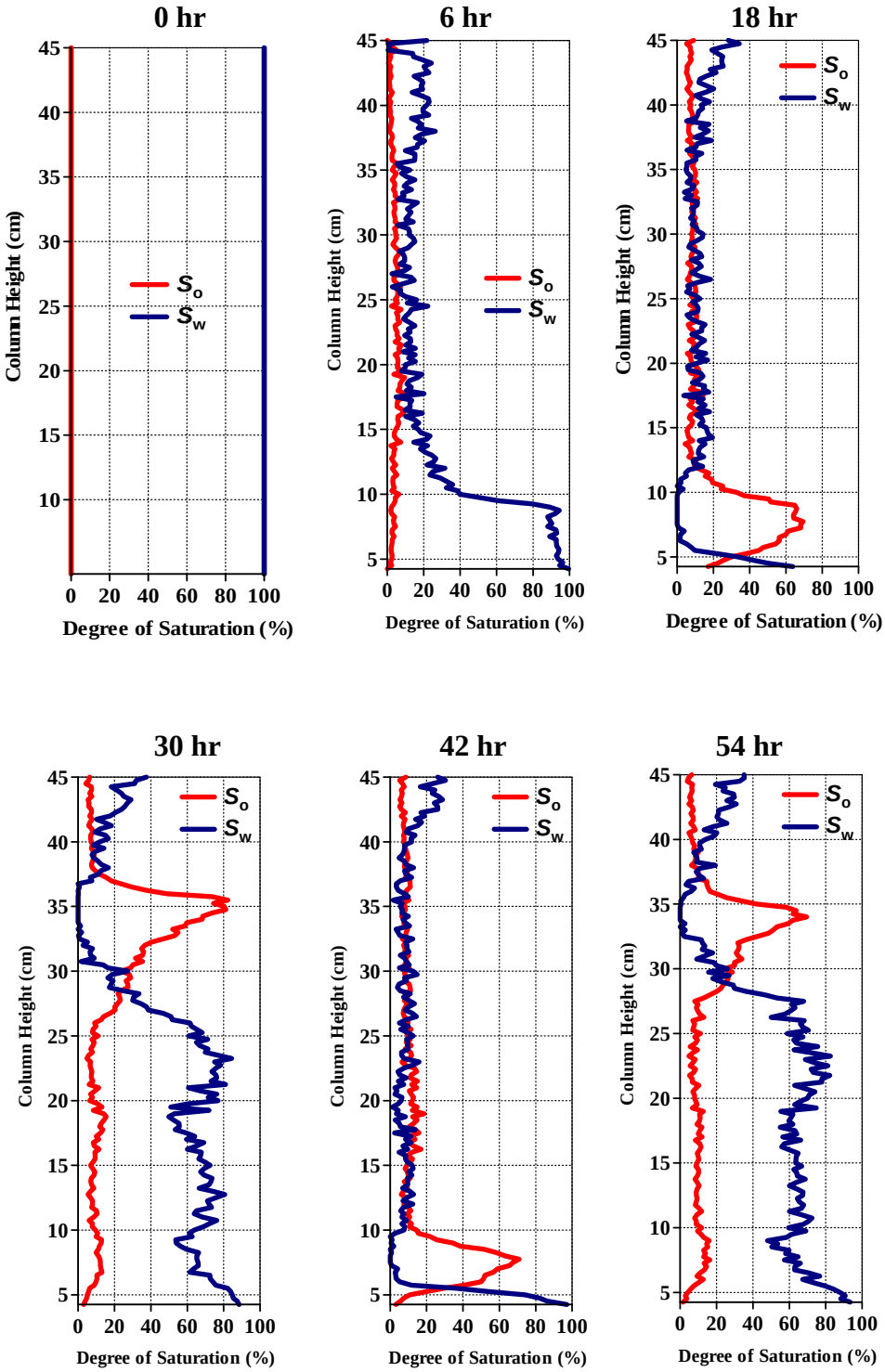

Figure 3.26 Diesel saturation profiles (red plots) and Water saturation profiles (blue plots) in Test C-3 Column I

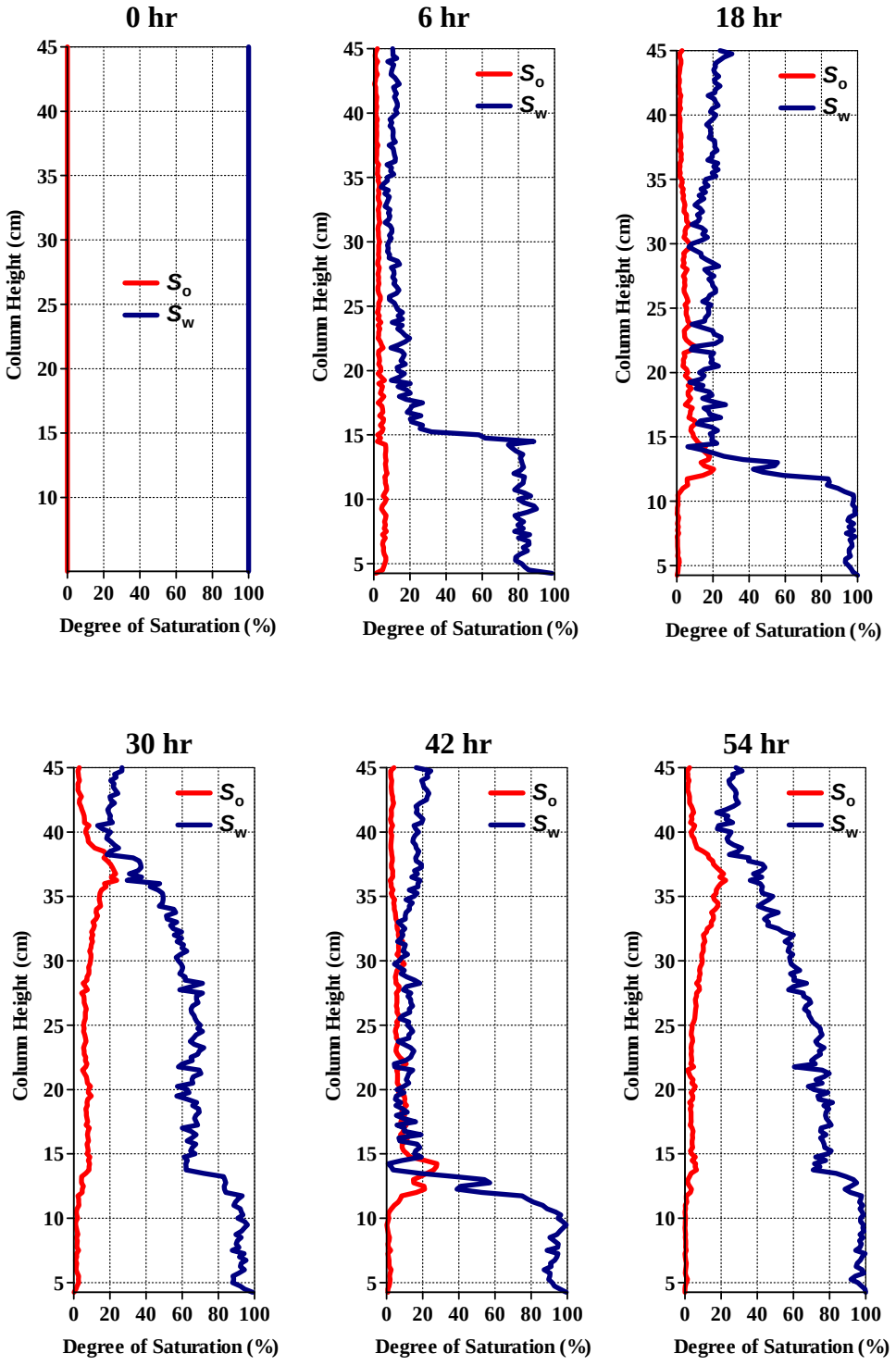

Figure 3.27 Diesel saturation profiles (red plots) and Water saturation profiles (blue plots) in test C-3 Column II

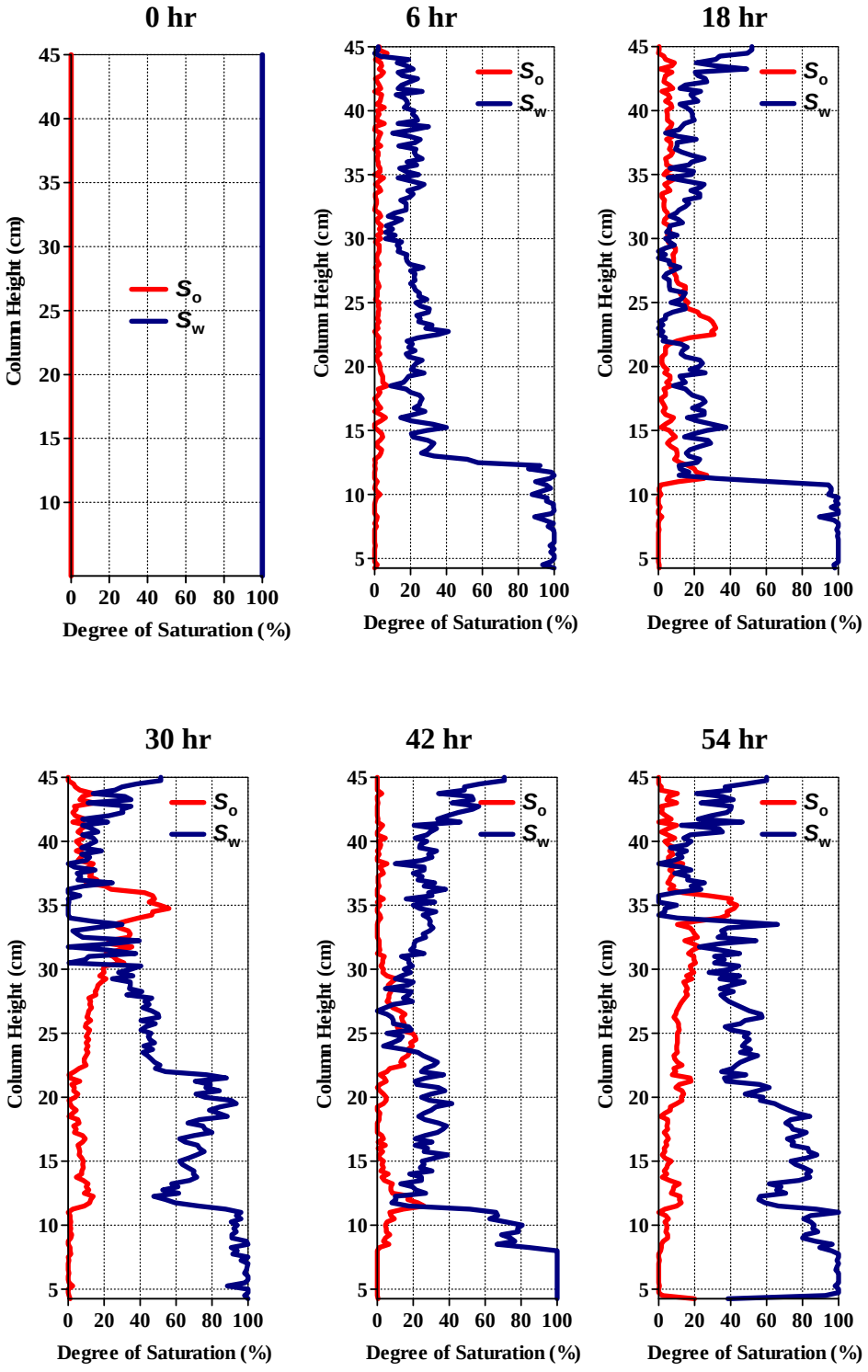

Figure 3.28 Diesel saturation (red plots) profiles and Water saturation profiles (blue plots) in test C-4 Column I

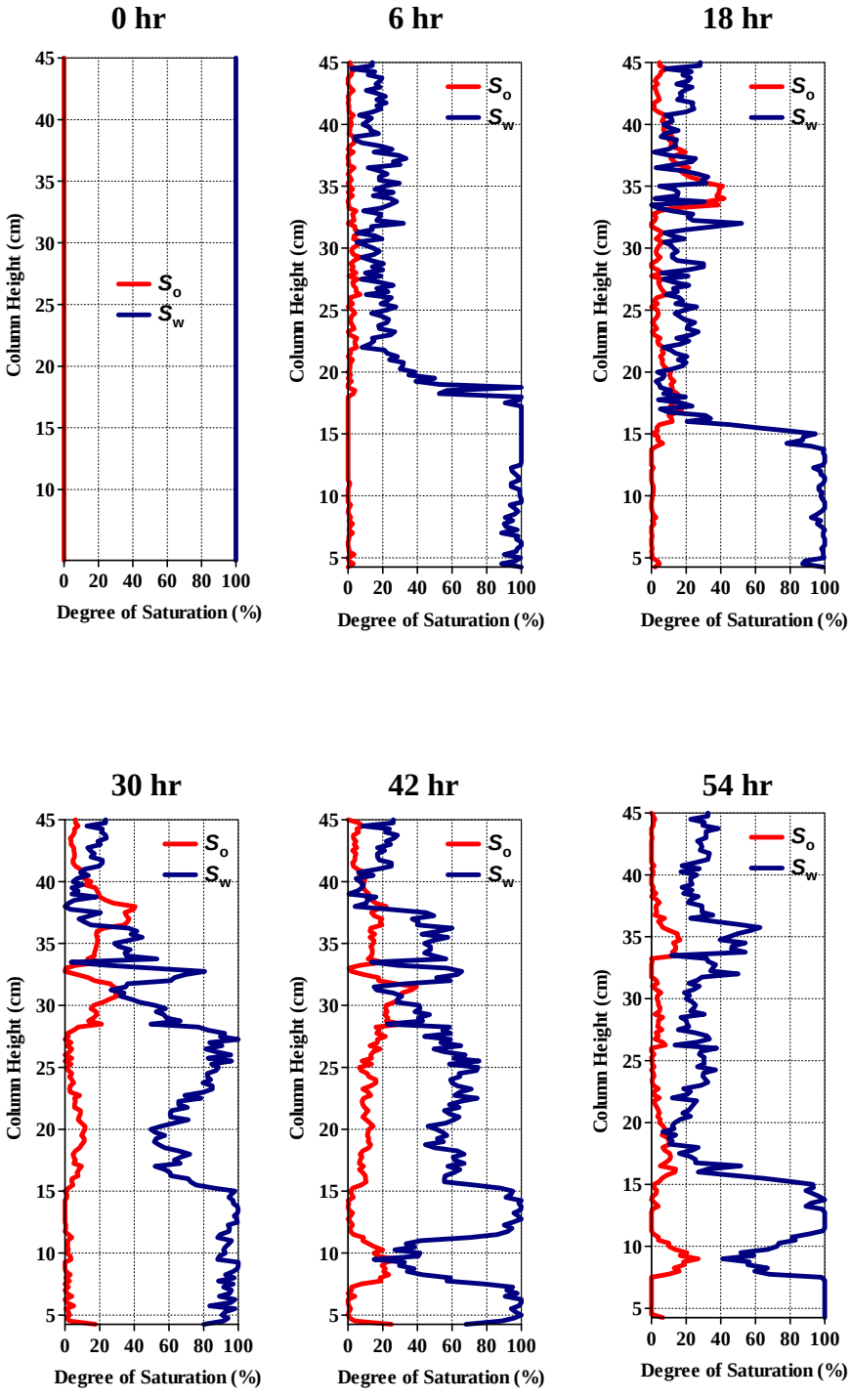

Figure 3.29 Diesel saturation (red plots) profiles and Water saturation profile (blue plots) in test C-4 Column II

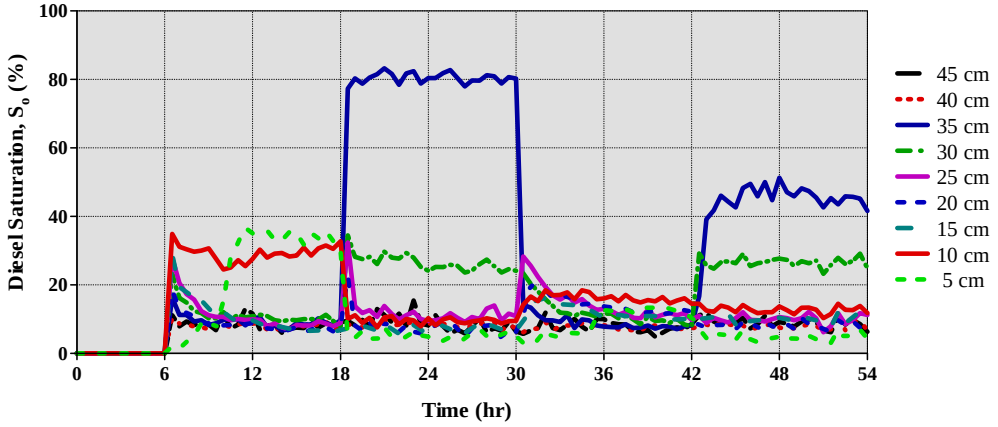

(a)

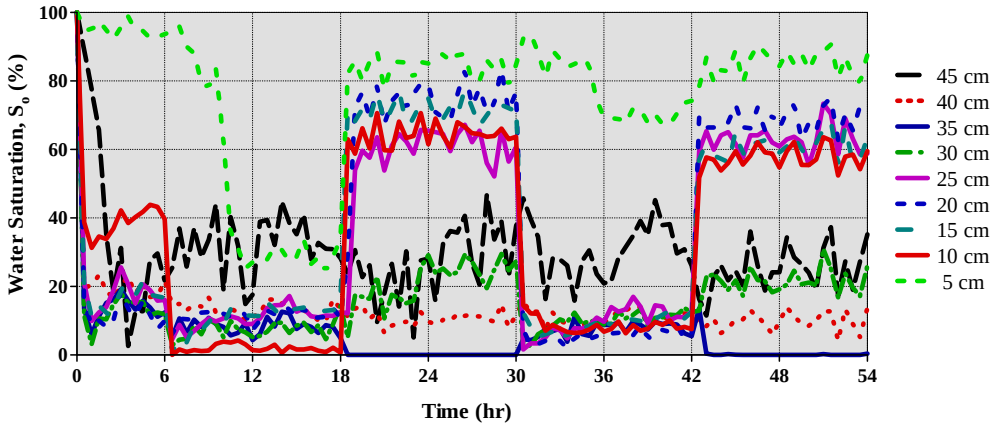

(b)

Figure 3.30 Test C-3 Column I (a) Diesel saturation profiles vs. Time (b) Water saturation profile vs. Time

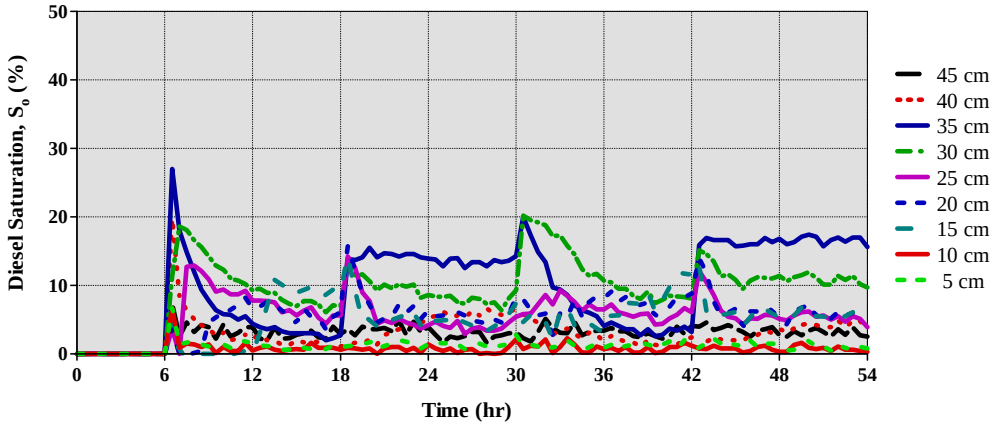

(a)

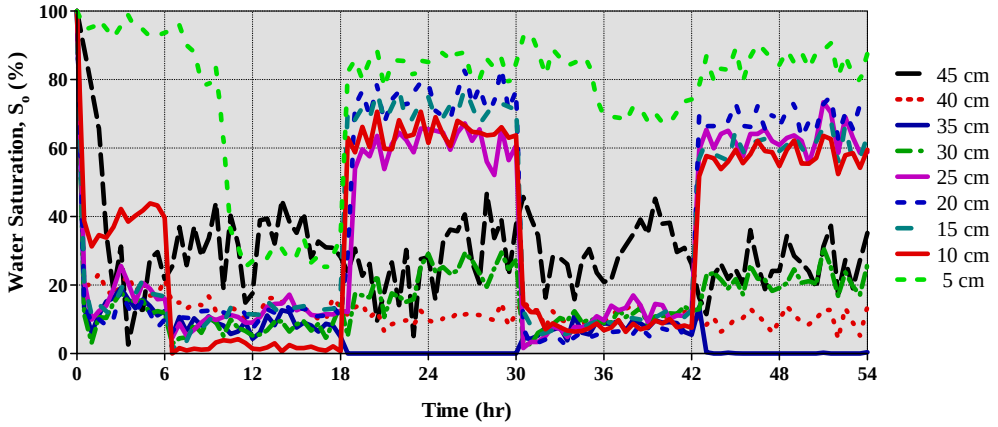

(b)

Figure 3.31 Test C-3 Column II (a) Diesel saturation profiles vs. Time (b) Water saturation profiles vs. Time

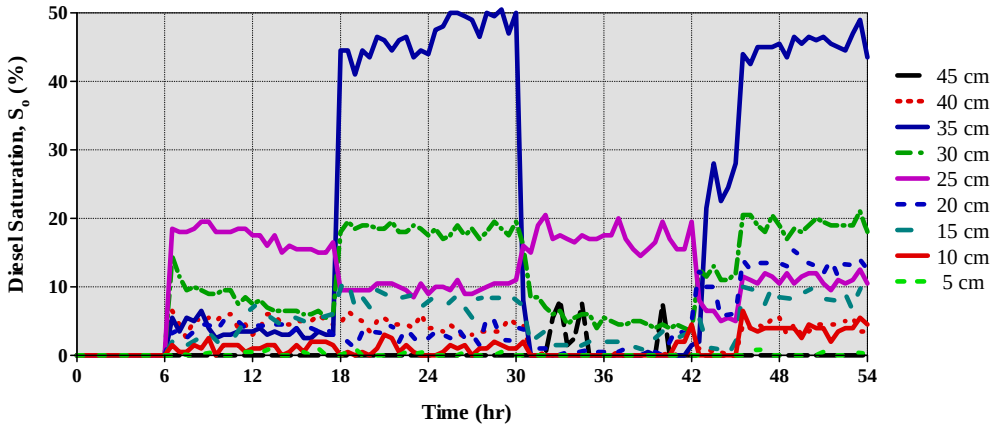

(a)

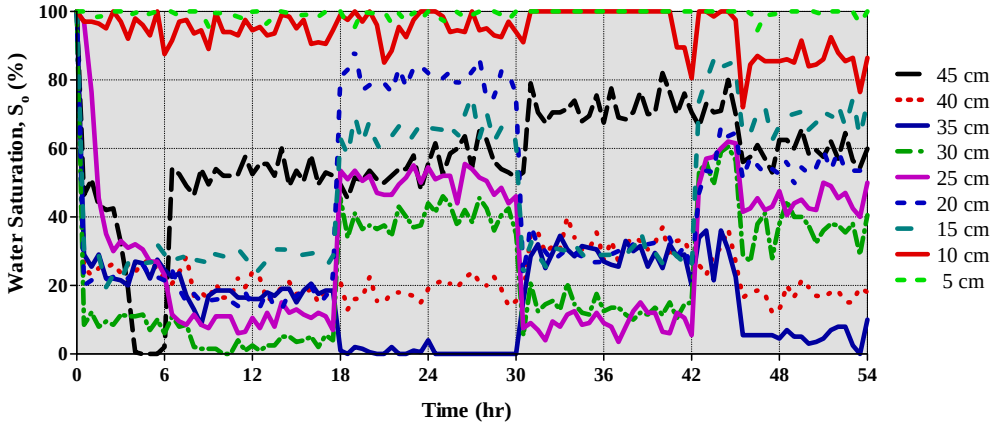

(b)

Figure 3.32 Test C-4 Column I (a) Diesel saturation profiles vs. Time (b) Water saturation profiles vs. Time

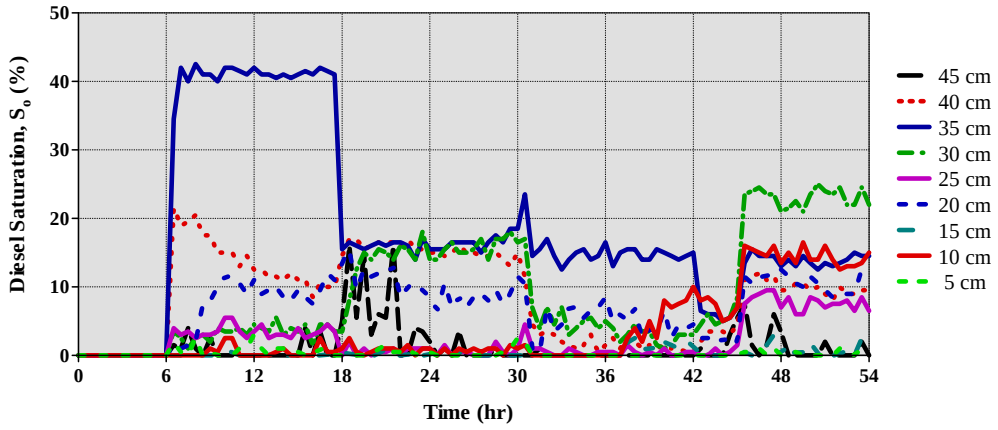

(a)

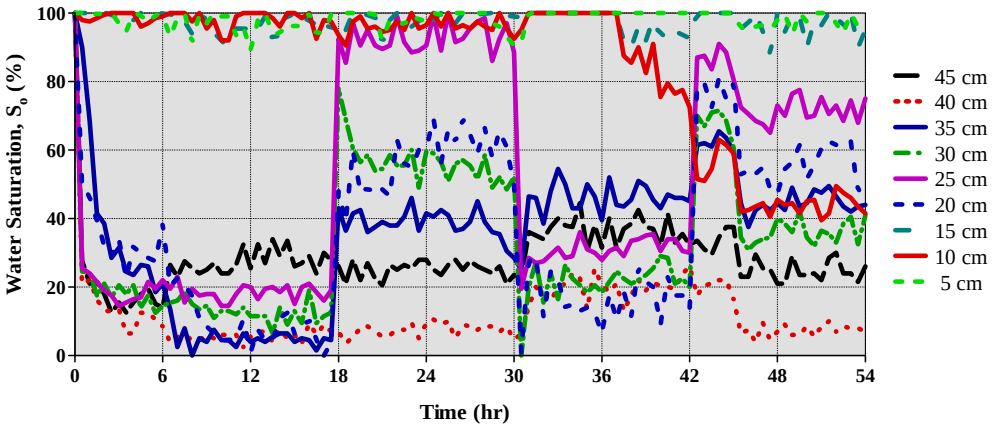

(b)

Figure 3.33 Test C-4 Column II (a) Diesel saturation profiles vs. Time (b) Water saturation profiles vs. Time

3.4.6 Discussions

Behaviors of diesel migration in homogeneous porous media were observed in Figure 3.22, Figure 3.23, Figure 3.26, Figure 3.27, Figure 3.30 and Figure 3.31. Diesel shows a typical LNAPL behaviour under water table fluctuating condition. During 1st drainage, it migrates downward following the water drainage until it reaches equilibrium. In Test C-3 Column I (Ottawa#3820 sand) Diesel penetrated to 5 cm from the bottom of column deeper than in Test C-3 Column II (Ottawa#3821 sand) which diesel presented at 13 cm from the bottom of column.

Similar behaviour were observed in Ottawa#3820 sand and Ottawa#3821 sand by Sudsaeng *et al.* (2011b). During 1st imbibition, the rise of water table displaces part of the diesel, but some diesel is entrapped and becomes immobile as discontinuous blob and ganglia, occluded by water (Fagerlund *et al*., 2007) even though it should float over the water table because of its lower density. The 2nd drainage and imbibition cycles also re-exhibits this behavior similar results also observed in toyoura sand and silica sand by Sudsaeng *et al*. (2010)

Diesel migration behaviors in heterogeneous porous media were presented in Figure 3.24, Figure 3.25, Figure 3.28, Figure 3.29, Figure 3.32 and Figure 3.33. During the 1st drainage in Test C-4 Column I, Diesel penetrated downward through the first layer following the lowering of water table and pass through 2nd layer and reached the 3nd layer, at 3rd layer immobilized diesel was presents at the interface of Layer-3 (Ottawa#3821) and Layer-4 (Ottawa#3820). Same behavior was observed in Test C-4 Column-II at the interface of 1st Layer (Ottawa#3821) and 2nd Layer-(Ottawa#3820). This behavior can be explained by pore size of Ottawa#3821 sand is smaller than that of Ottawa#3820 sand therefore more diesel was retained in Ottawa#3821 sand layer and was not move downward to Ottawa#3820 sand layer. However there was approximately 20% of diesel in both columns can pass through this interface during the 1st drainage. In 2nd drainage stage there was diesel observed at 8 cm from bottom part of Test C-4 Column I compared to 1st drainage stage diesel presented at 15 cm from bottom of column this can be explained by the saturation hysteresis effect from water table fluctuating. (Figure 3.29) but there was less effect from water fluctuating in Test C-4 Column II (Figure 3.30) Diesel presented at 11 cm from the bottom of column, exactly above the capillary fringe in both drainage stage. During imbibitions processes water was displaced diesel and air and from the experiment we observed that more trapped diesel were presented under the water table in 2nd drainage stage than in 1st drainage stage.

3.5 Conclusions

In this chapter we have proven that there is a linear relationship existed between Average Optical Density and degree of diesel saturation and degree of water

saturation in different porous media so that Simplified Image Analysis Method can be applied as a non-intrusive and non-destructive technique to measure temporal and spatial distribution of fluid saturations in a whole domain in the dynamic behavior of diesel migrating in porous media under water table fluctuating conditions.

Ottawa#3820 sand and Ottawa#3821 sand were selected to use as porous media in this study. Two-phase (air-water and air-diesel) experiment was conducted in both Ottawa#3820 sand and Ottawa#3821 sand.

Three-phase (air-water-diesel) experiment was conducted in both homogeneous and heterogeneous porous media. In homogeneous porous media case, Diesel shown a typical LNAPL behavior under the water fluctuating condition It migrated downward following the lowering of water table during the drainage stage until it reach equilibrium and during the imbibition stage it float over the water table however some trapped diesel were observed during the experiment. In heterogeneous porous media case, Immobilized diesel was observed at the interface of finer sand (Ottawa#3821) and coarse sand (Ottawa#3820).

Diesel presents quite different flow pattern and distribution in different porous media indicating the difficulty in studying LNAPL movement in subsurface also engineering properties and configuration of porous media play a significant role in LNAPL distribution in heterogeneous porous media.

CHAPTER IV

TWO-DIMENSIONAL TANK TEST

4.1 Introduction

Two-dimensional tank were conducted to investigate the effects of water table fluctuation and horizontal groundwater flow on the migration of diesel in homogeneous and heterogeneous porous media. Simplified Image Analysis Method was used to obtain the degree of water saturation and degree of diesel saturation distribution in the system. Totally 12 tank tests with different condition will be discussed in this chapter.

4.2 Three-phase in homogeneous porous media experiment

Two-dimensional tank tests with water drainage following with diesel and air infiltration were conducted to investigate the effects of fluctuating water table and horizontal groundwater flow on diesel migration behavior in homogeneous porous media. Three-Phase tank testing program is presented in Table 4.1

Table 4.1 Three-phase in homogeneous porous media testing program.

Test	Medium	Hydraulics gradient (i)	Water Table Fluctuating
T-1	Ottawa#3820 sand	0	Yes
T-2	Ottawa#3820 sand	0.1	Yes
T-3	Ottawa#3820 sand	0.2	Yes
T-4	Ottawa#3821 sand	0	Yes
T-5	Ottawa#3821 sand	0.1	Yes
T-6	Ottawa#3821 sand	0.2	Yes

4.2.1 Equipments and materials

Ottawa#3820 sand and Ottawa#3821 sand were used as a porous media. Diesel was dyed red with Red Sudan III (1:10000 by weight). 50×60×3.5 cm (inside dimension) acrylics tank (Figure 4.1) was designed to use in this study. Similar as

previous chapter, two cameras were used. First cameras Nikon D90 with the 450 nm band-pass filter installed and second one Nikon D90 with 640 nm band-pass filter installed. Both cameras were set to manual mode so that their aperture, shutter speed and white balance were kept constant and cameras were connected to a computer via USB cables and remotely controlled by Nikon Camera control Pro 2. X-Rite Gretagmacbeth ColorChecker white balance card was located next to the sample to provide a white and black reference. Two 120 W LED floodlights were used to illuminate the samples which were automatically turned on 30 seconds before the pictures were taken, and turned off 30 seconds later by in-house development timer control software. Black curtain was installed between tank and both cameras to avoid reflections from tank surface. Equipments set up is shown in Figure 4.2

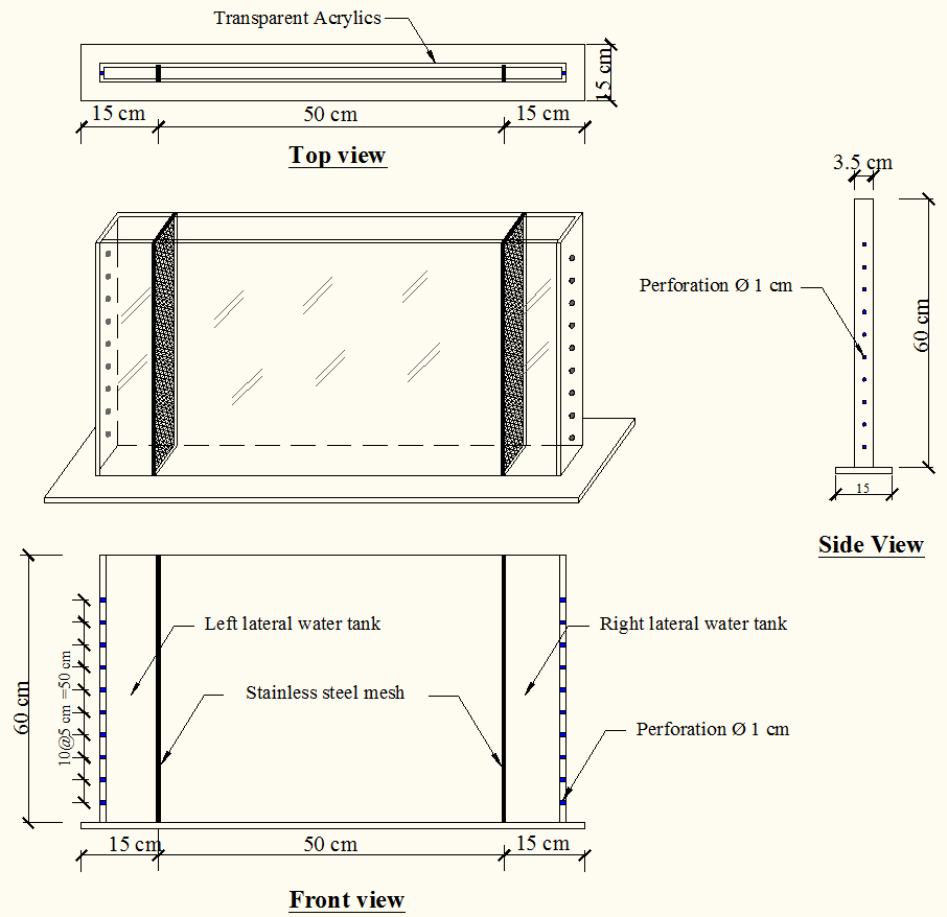

Figure 4.1 Two-dimensional tank designed.

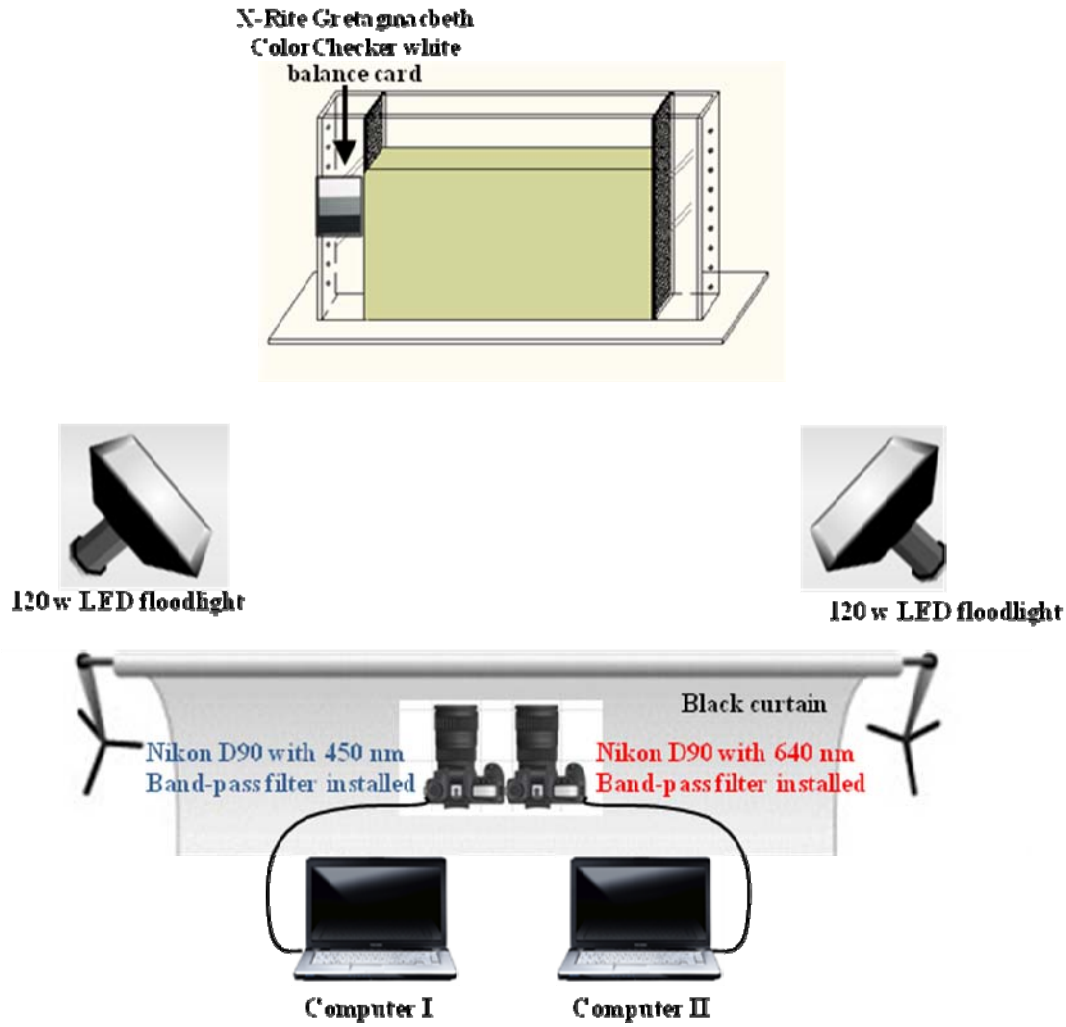

Figure 4.2 Three-phase in homogeneous porous media equipments set up

4.2.2 Calibration

Three-phase tank experiment required three pictures with each camera. Each camera took a picture of the tank fill with dry sand, water saturated sand and diesel saturated sand. From Equation 2.16, these six pictures correspond to $[D_{450}{}^{00}]_{mn,}$ $[D_{450}{}^{10}]_{mn}$, $[D_{450}{}^{01}]_{mn,}$ $[D_{640}{}^{00}]_{mn,}$ $[D_{640}{}^{10}]_{mn}$ and $[D_{640}{}^{01}]_{mn}$. Calibration pictures for Ottawa#3820 sand and Ottawa#3821 sand are presented in Figure 4.3 and Figure 4.4 respectively.

(a) (b) (c)

Figure 4.3 Calibration pictures for test T-1, T-2 and T-3 (a) Tank filled with dry sand. (b) Tank filled with fully saturated water and (c) Tank filled with fully saturated diesel.

(a) (b) (c)

Figure 4.4 Calibration pictures for test T-4, T-5 and T-6 (a) Tank filled with dry sand. (b) Tank filled with fully saturated water and (c) Tank filled with fully saturated diesel.

4.2.3 Experiments

Two-dimensional tank tests with water drainage following with diesel and air infiltration were conducted in Ottawa#3820 sand and Ottawa#3821 sand. Oven dried sand was filled up to 50 cm in two-dimensional tank and dry density was 1.76 g/cm^3. Digital pictures of dry sand were taken by the equipment that mentioned in section 4.2.1 and were used as dry sand reference picture in the image analysis processes. Right lateral tank and left lateral tank (Figure 4.1) were slowly filled with water to saturate the sand inside the tank and digital pictures of fully water saturated sand were taken and used as fully saturated water reference picture. Similar with the

one-dimensional column test, the test was divided into four stages: first drainage (t = 0 to 18 hr), first imbibition (t = 18 to 30 hr), second drainage (t = 30 to 42 hr) and second imbibitions (t = 42 to 54 hr) and hydraulics gradient for each test controlled by lateral tanks (h1 and h2) (Figure 4.5) and water level in lateral tank in each stage is shown in Table 4.2.

First Drainage: Water inside the tank was allowed to drain and after 6 hours of water drainage, 100 g of diesel infiltrated from diesel infiltration point (Test T-1 and Test T-4, X=25 cm, Test T-2, T-3, T-5 and T-6, X = 15 cm) (Figure 4.5). Diesel was allowed to freely infiltrate into the tank for 12 hours. This stage took 18 hours.

First Imbibition: Water inside the tank was slowly raised up 30 cm from previous stage by filled the water in both lateral tank and diesel that infiltrated into the tank during the drainage process was displaced by the water. This stage took 12 hours.

Second Drainage: Water and diesel inside the tank were allowed to drain again by lowering the water level inside the lateral tank to desired level as show in Table 4.2. No additional diesel was infiltrated into the tank. This stage took 12 hours.

Second Imbibition: The water table inside the tank raised up again following the same procedure as the First imbibition and this stage took 12 hour.

Two digital pictures were taken every half hour from two cameras. The camera was set to manual mode, and the aperture, shutter speed, and white balance were defined and maintained constant throughout the experiment. The camera was remotely controlled (using Nikon Camera Control Pro 2 software) to avoid vibrations and camera displacement. The two 120 W LED floodlights were turned on 30 seconds prior to taking the pictures and turned off right after that to avoid fluctuations in the column’s temperature. Room temperature was kept at 20 °C and humidity at 70%. Testing condition is summarized in Table 4.2

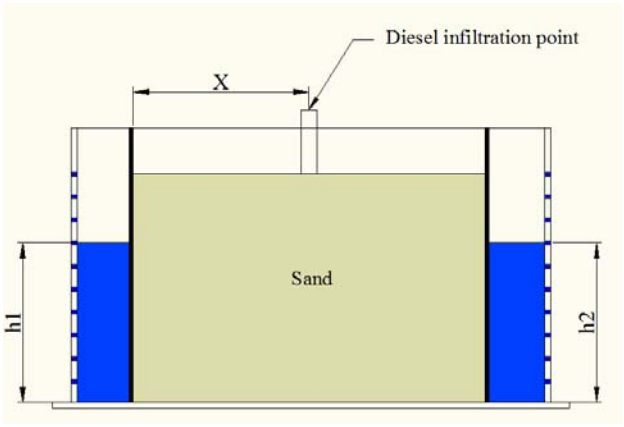

Figure 4.5 Homogeneous porous media in two-dimensional tank.

Table 4.2 Three-phase in homogeneous porous media testing condition

Test Stage	**Time**	**Water Head**						
		i = 0		**i = 0.1**		**i = 0.2**		**Comments**
		h1	h2	h1	h2	h1	h2	
Initial Condition	0 hr	50 cm	50 cm	50 cm	50 cm	50 cm	50 cm	
First Drainage	0 hr - 18 hr	5 cm	5 cm	10 cm	5 cm	15 cm	5 cm	100 g Diesel infiltrated at t = 6 hr
First Imbibition	18 hr - 30 hr	35 cm	35 cm	40 cm	35 cm	45 cm	35 cm	
Second Drainage	30 hr - 42 hr	5 cm	5 cm	10 cm	5 cm	15 cm	5 cm	
Second Imbibition	42 hr - 54 hr	35 cm	35 cm	40 cm	35 cm	45 cm	35 cm	

4.2.4 Computational analysis

Similar to the previous column test in chapter 3, all pictures were exported from the NEF format (Nikon proprietary RAW version files) to the TIFF format (Tagged Image File Format) using Nikon ViewNX 2.0 TIFF images were analyzed with an ad-hoc program in MATLAB 2007a written by Flores (2010) Using the six calibration pictures, the average optical density matrices $[D_{450}{}^{00}]_{mn,}$ $[D_{450}{}^{10}]_{mn}$, $[D_{450}{}^{01}]_{mn,}$ $[D_{640}{}^{00}]_{mn,}$ $[D_{640}{}^{10}]_{mn}$ and $[D_{640}{}^{01}]_{mn}$ were calculated. $[D_{450}]_{mn}$ and $[D_{640}]_{mn}$ were calculated for each picture taken during the test, and the water saturation matrices ($[S_w]_{mn}$) and diesel saturation matrices ($[S_o]_{mn}$) were solved.

4.2.5 Results

Diesel saturation contour, water saturation contour, Diesel and water saturation profiles together with diesel and water saturation profiles plot at the center line of diesel spill point with time for six tank tests are shown in Figure 4.6-Figure 4.17

Test T-1: Ottawa#3820, i = 0

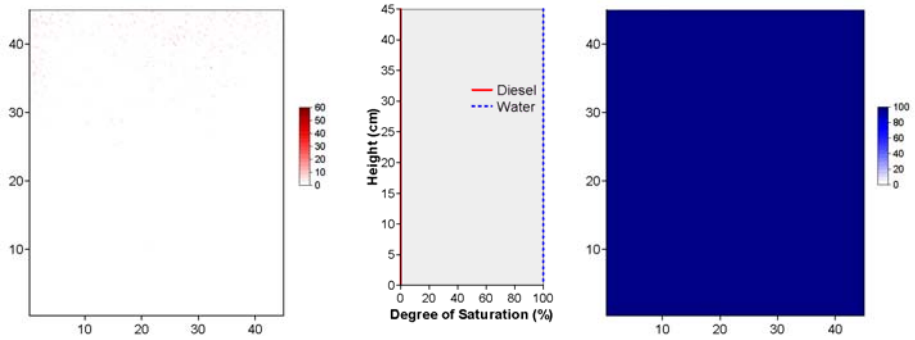

(a) t = 0 hour

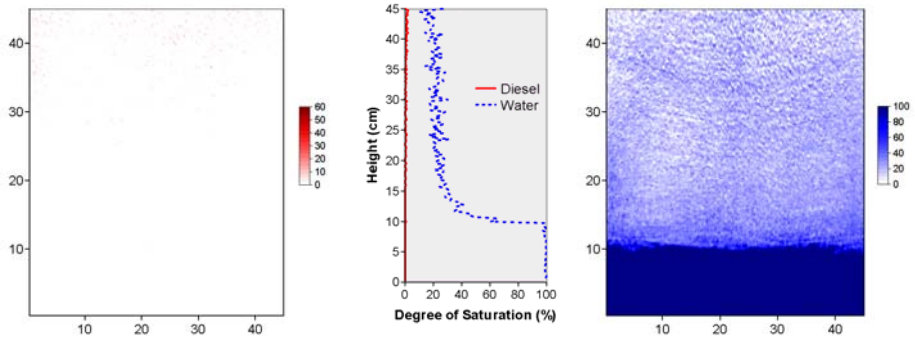

(b) t = 6 hours

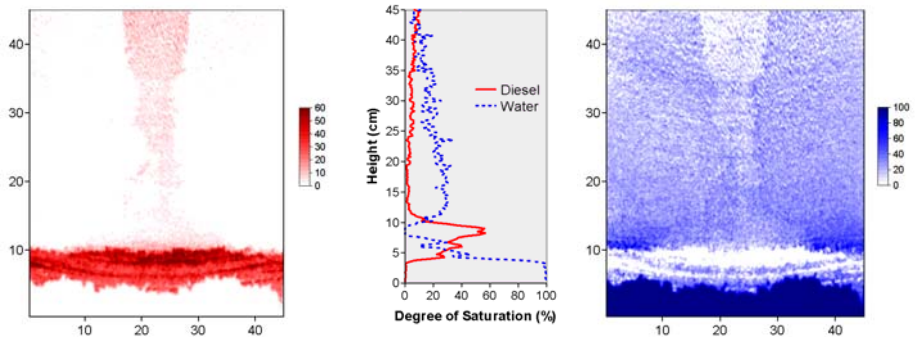

(c) t = 18 hours

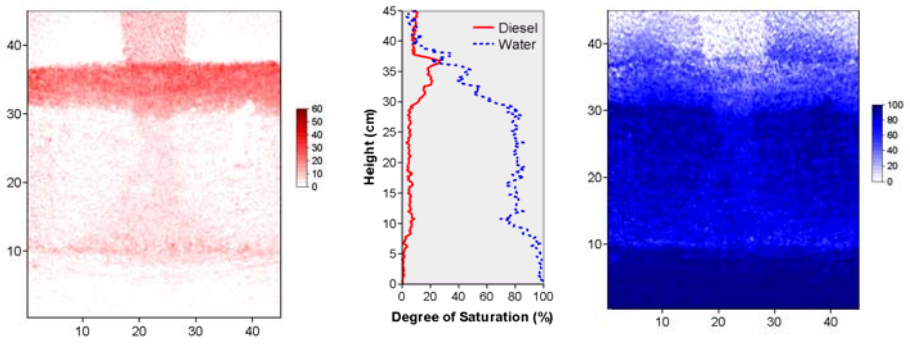

(d) t = 30 hours

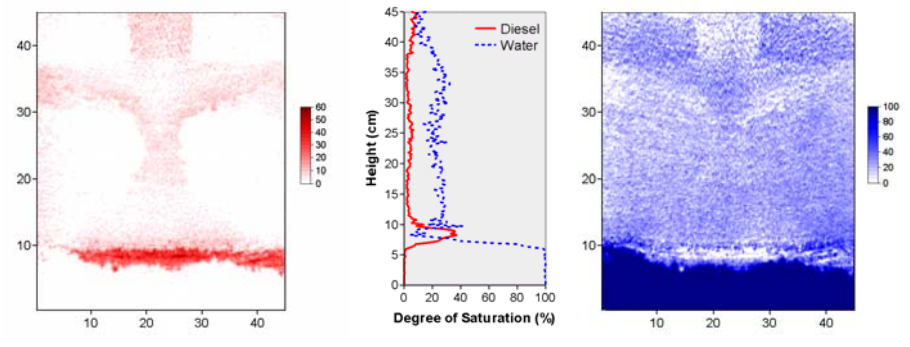

(e) t = 42 hours

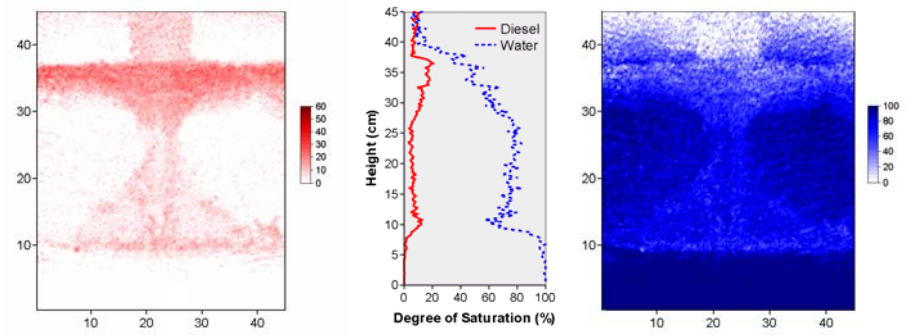

(f) t = 54 hours

Figure 4.6 Diesel saturation contour (left), diesel and water saturation profiles (center) and water saturation contour (right) for test T-1 (i = 0)

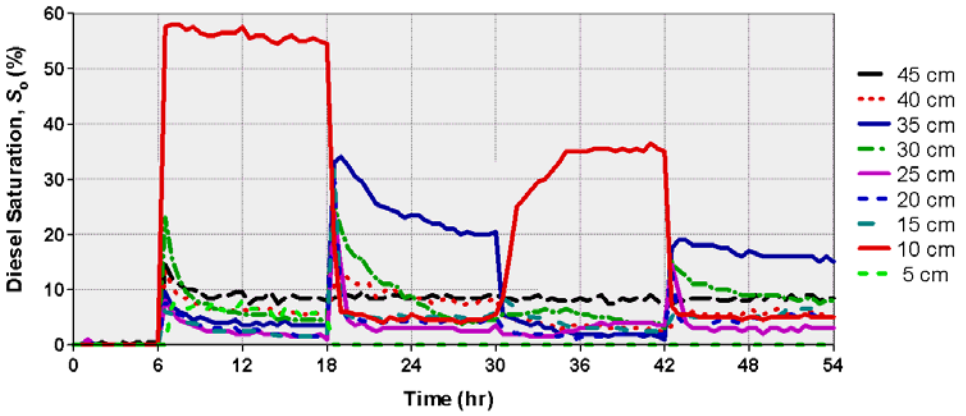

(a)

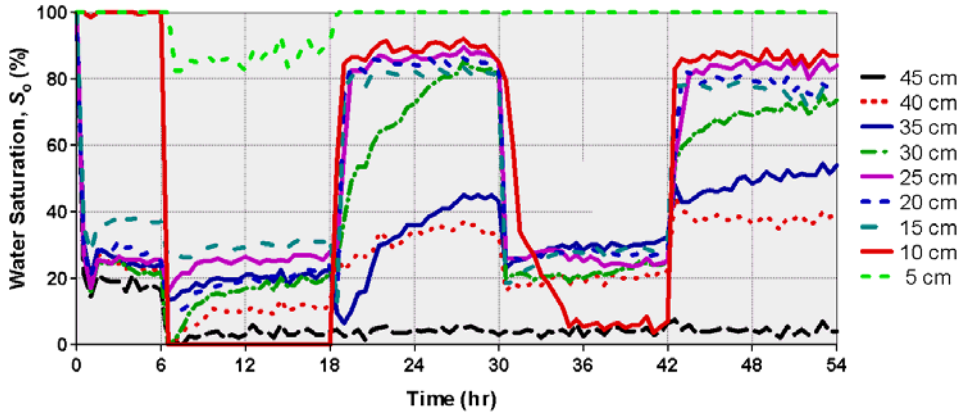

(b)

Figure 4.7 (a) Diesel saturation profiles vs. time for test T-1 and (b) Water saturation profiles vs time for test T-1

Test T-2: Ottawa#3820 sand, i = 0.1

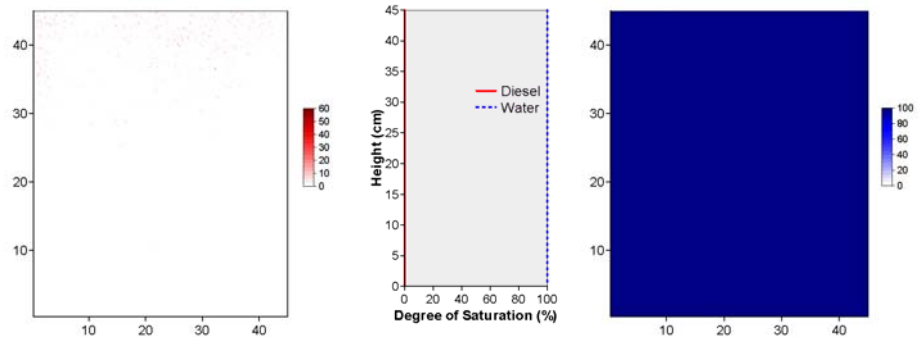

(a) t = 0 hour

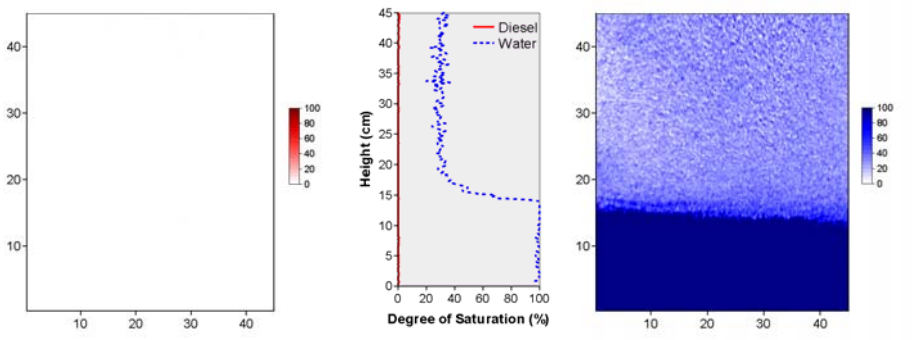

(b) t = 6 hour

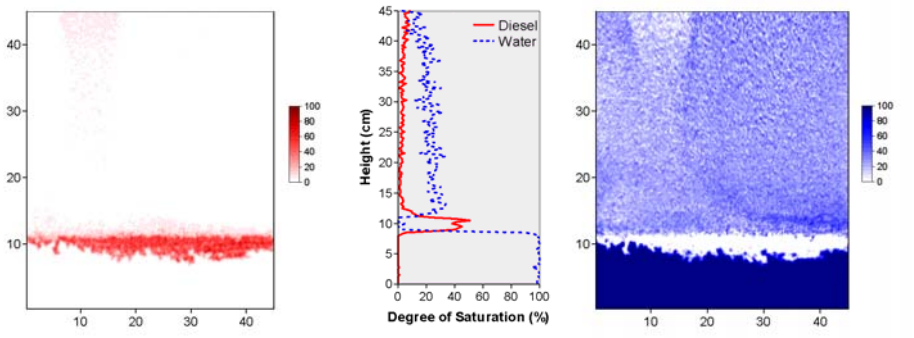

(c) t = 18 hour

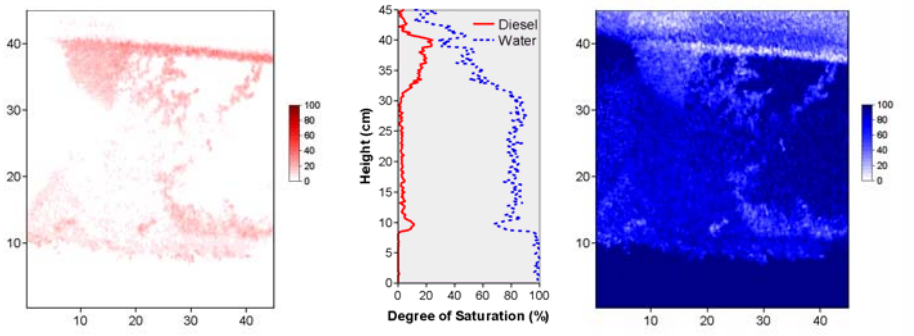

(d) t = 30 hour

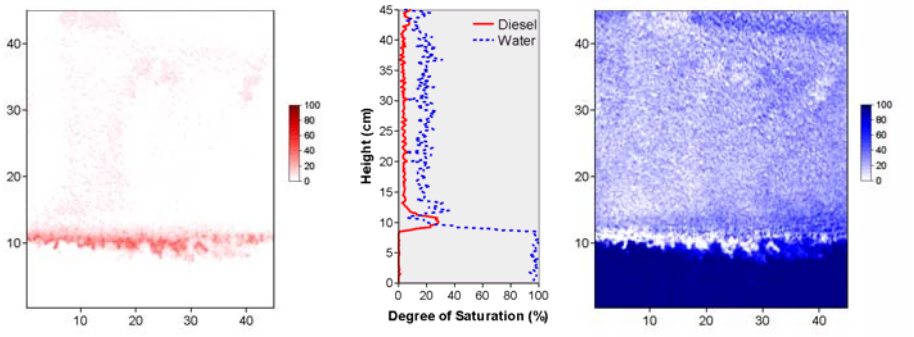

(e) t = 42 hour

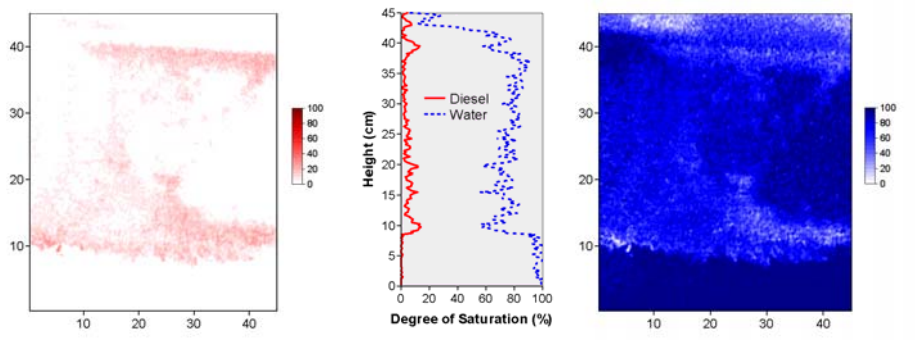

(f) t = 54 hour

Figure 4.8 Diesel saturation contour (left), Diesel and water saturation profiles (center) and water saturation contour (right) for test T-2 (i = 0.1)

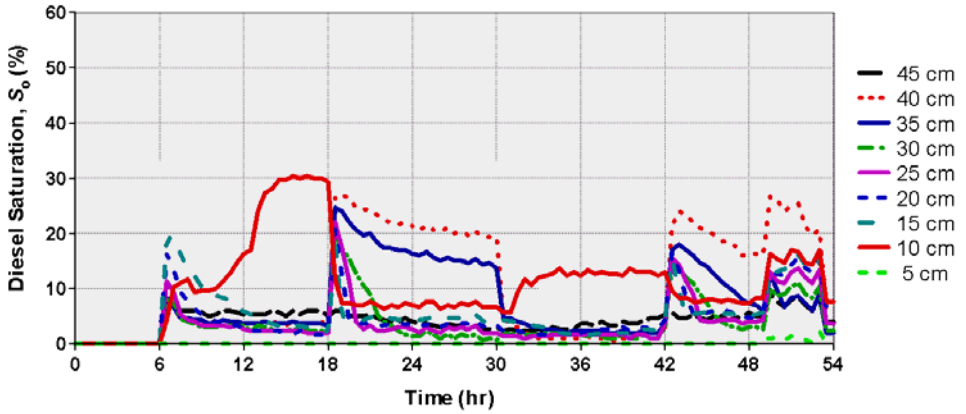

(a)

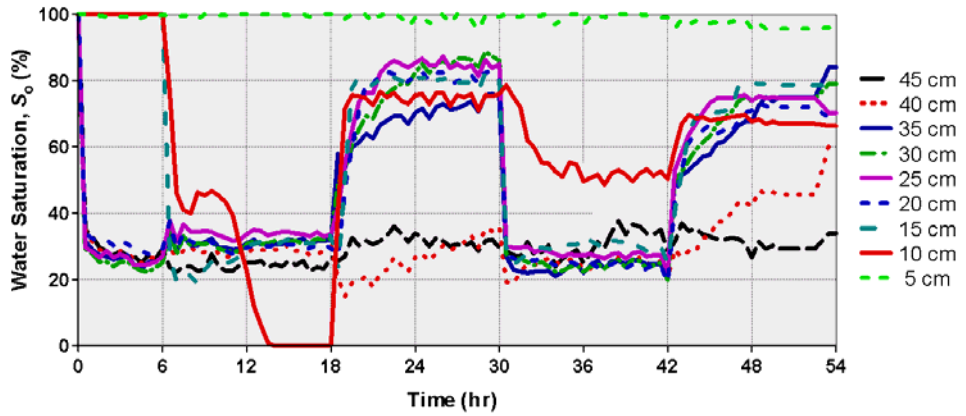

(b)

Figure 4.9 (a) Diesel saturation profiles vs. time for test T-2 and (b) Water saturation profiles vs time for test T-2

Test T-3: Ottawa#3820 sand, i = 0.2

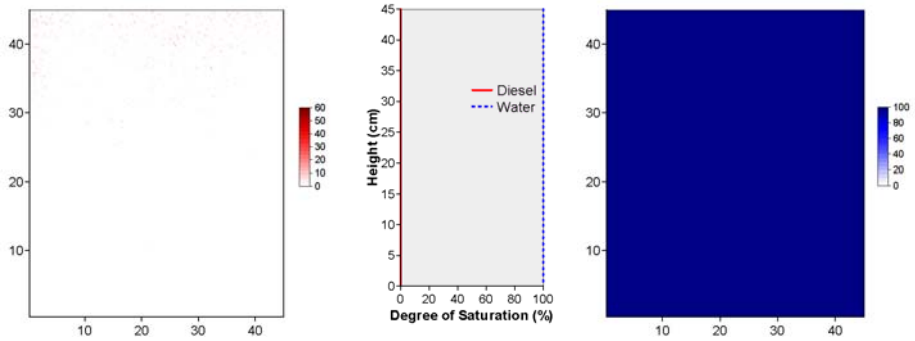

(a) t = 0 hour

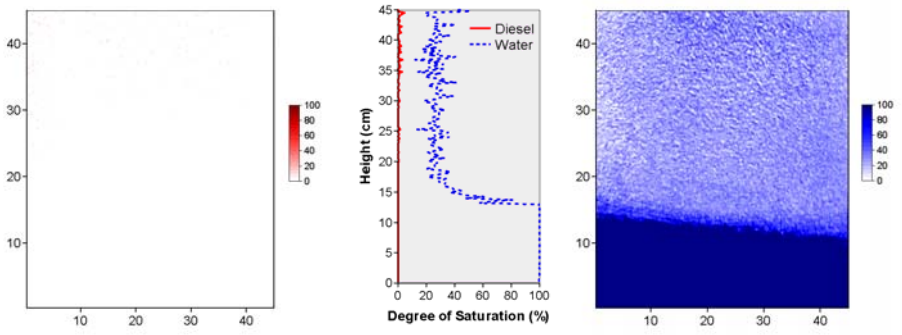

(b) t = 6 hour

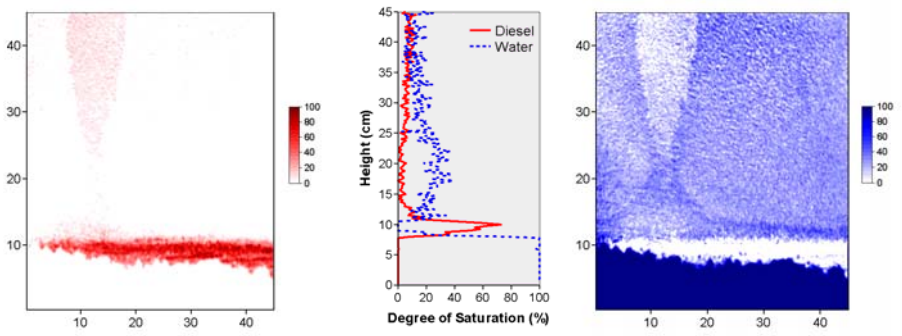

(c) t = 18 hour

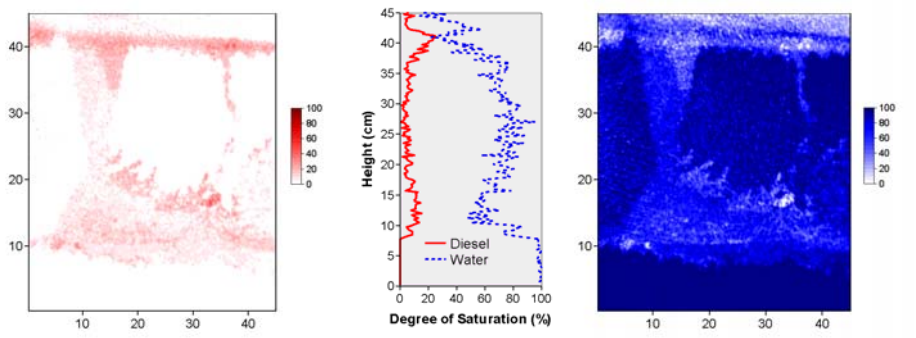

(d) t = 30 hour

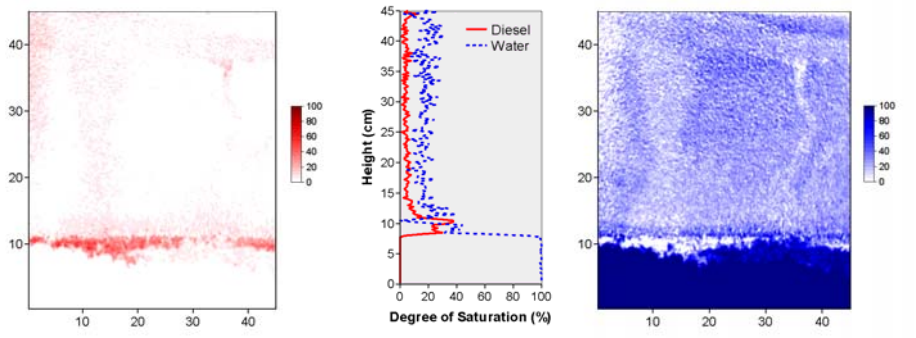

(e) t = 42 hour

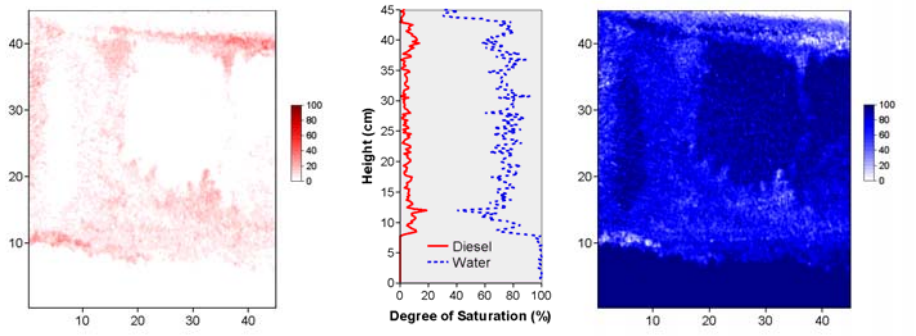

(f) t =542 hour

Figure 4.10 Diesel saturation contour (left), diesel and water saturation profiles (center) and water saturation contour (right) for test T-3 (i = 0.2)

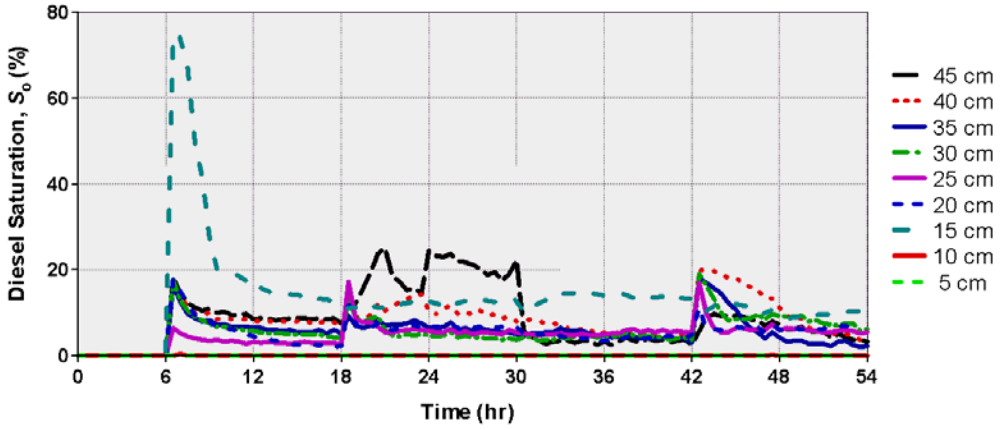

(a)

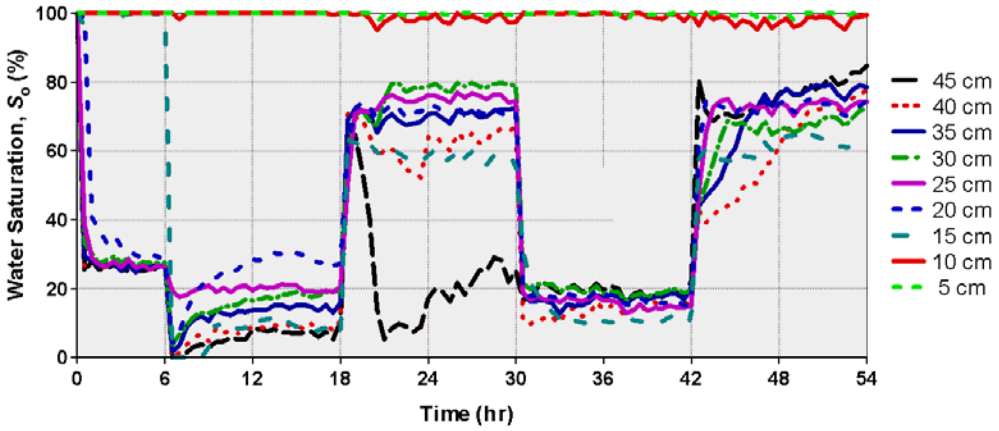

(b)

Figure 4.11 (a) Diesel saturation profiles vs. time for test T-3 and (b) Water saturation profiles vs time for test T-3

Test T-4: Ottawa#3821 sand, i = 0

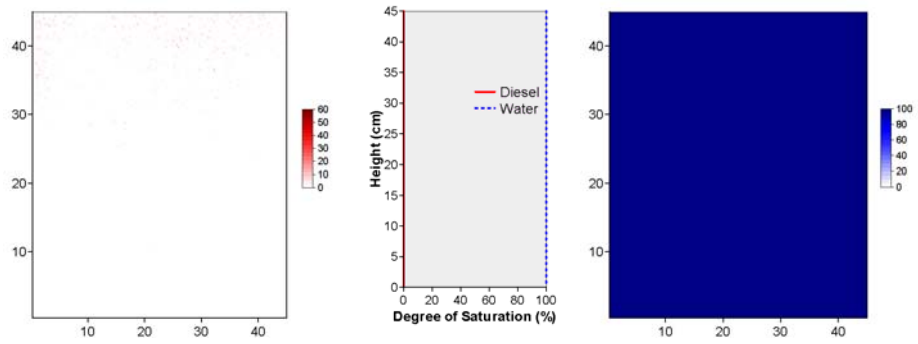

(a) t = 0 hour

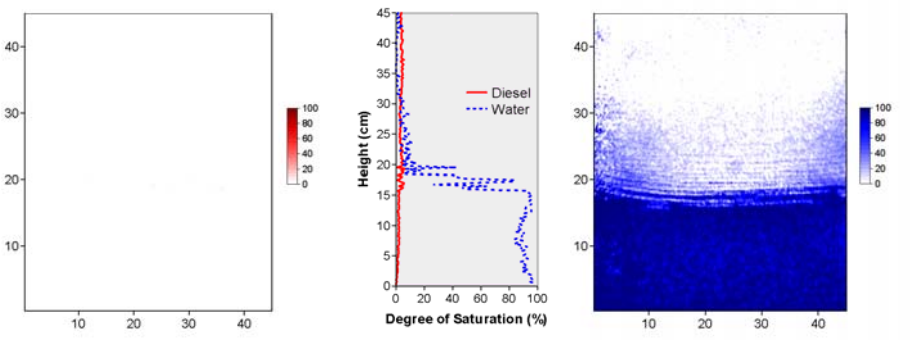

(b) t = 6 hour

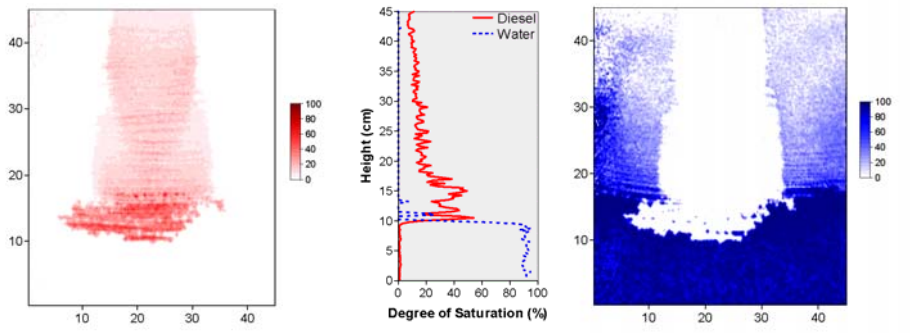

(c) t = 18 hour

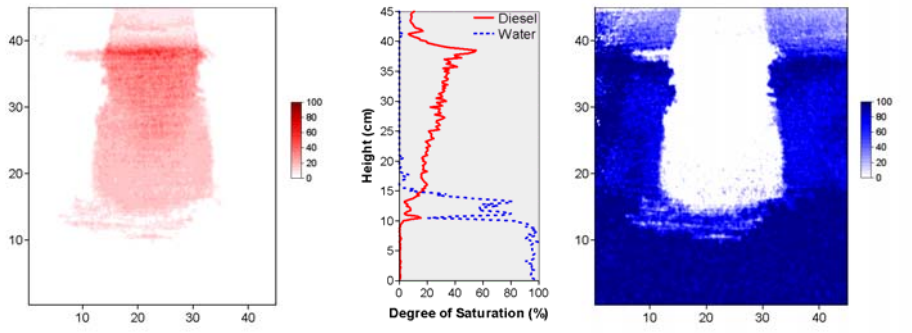

(d) t = 30 hour

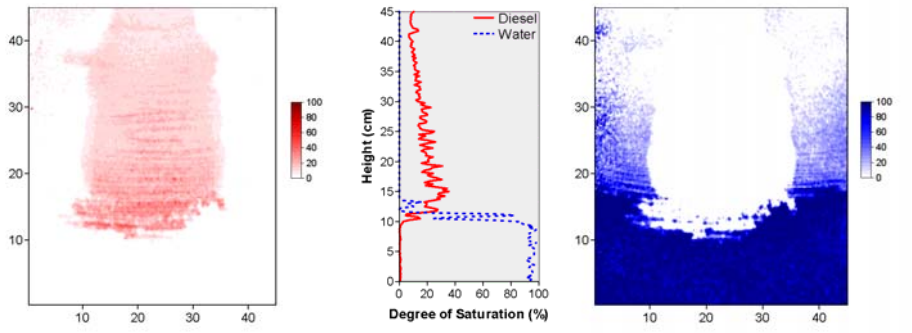

(e) t = 42 hour

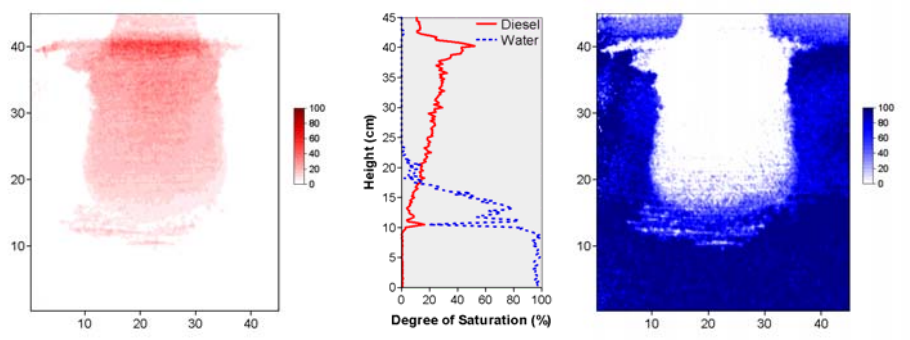

(f) t = 54 hour

Figure 4.12 Diesel saturation contour (left), diesel and water saturation profiles (center) and water saturation contour (right) for test T-4 (i = 0)

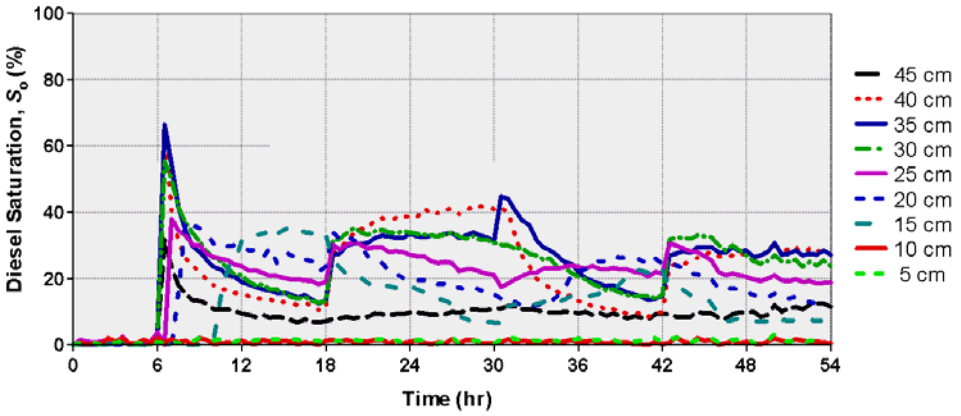

(a)

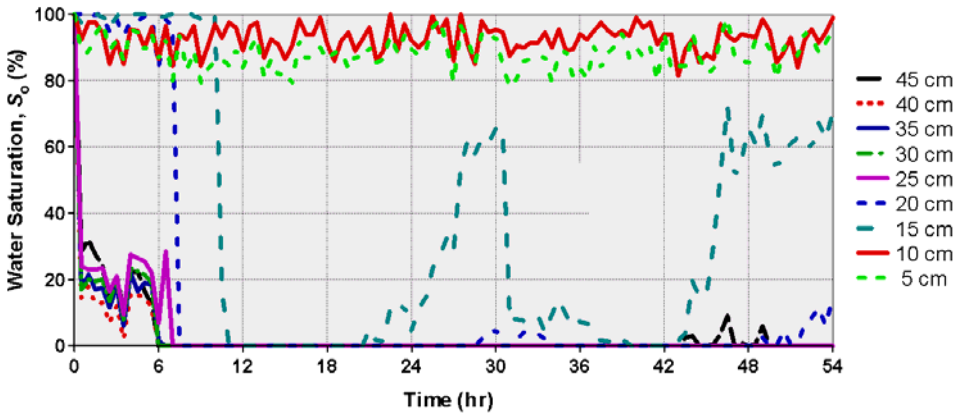

(b)

Figure 4.13 (a) Diesel saturation profiles vs. time for test T-4 and (b) Water saturation profiles vs time for test T-4

Test T-5: Ottawa#3821 sand, i = 0.1

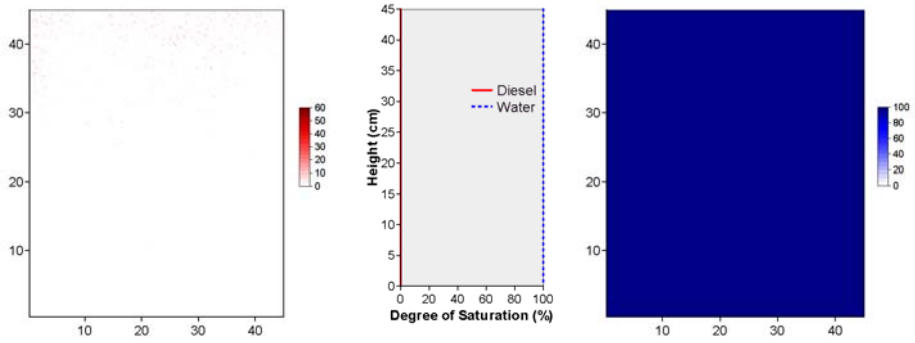

(a) t = 0 hour

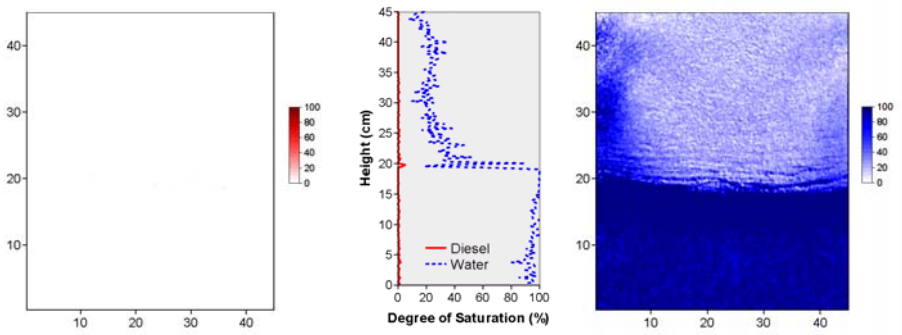

(b) t = 6 hour

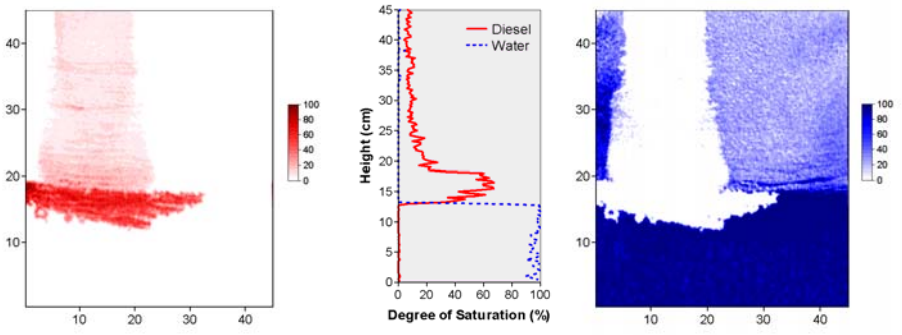

(c) t = 18 hour

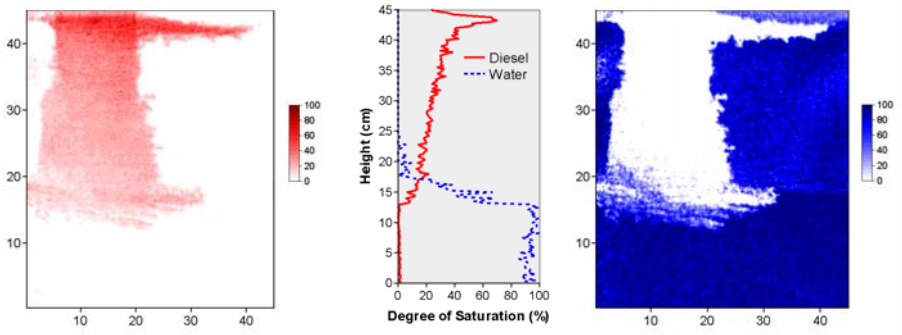

(d) t = 30 hour

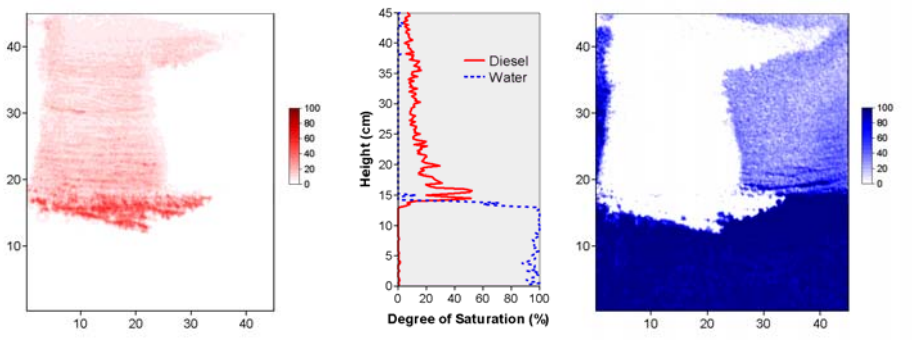

(e) t = 42 hour

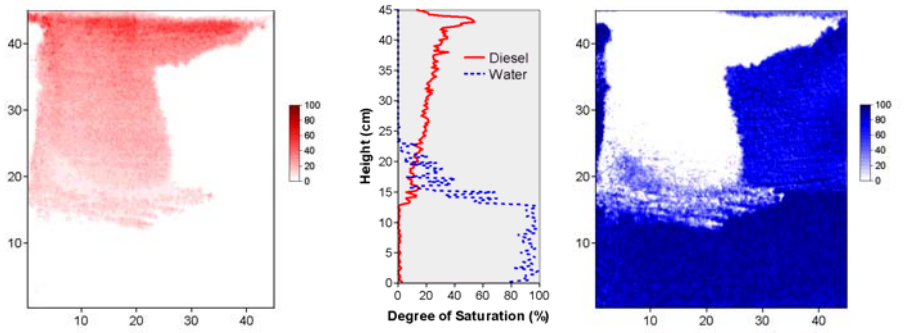

(f) t = 54 hour

Figure 4.14 Diesel saturation contour (left), diesel and water saturation profiles (center) and water saturation contour (right) for test T-5 (i = 0.1)

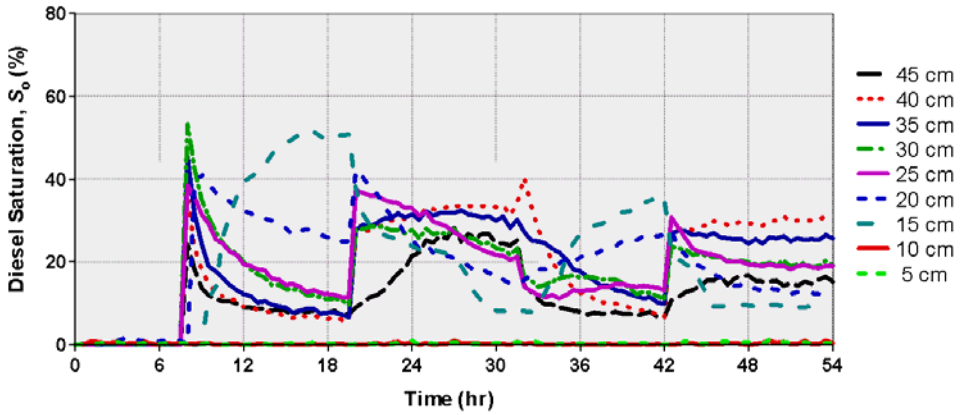

(a)

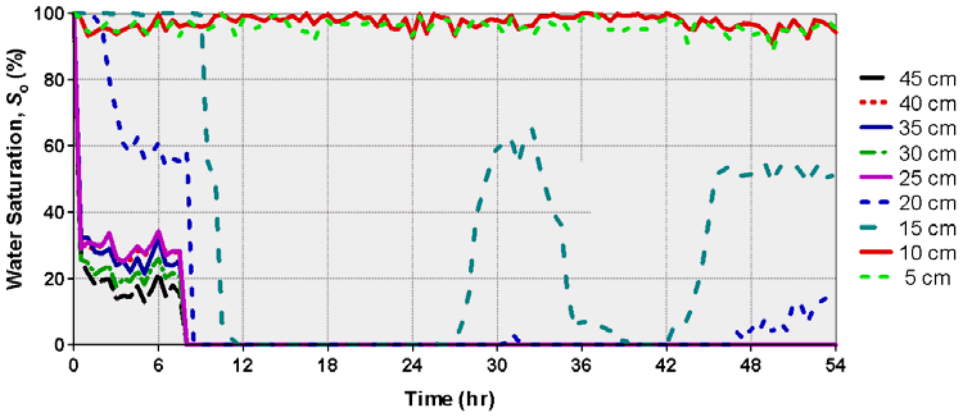

(b)

Figure 4.15 (a) Diesel saturation profiles vs. time for test T-5 and (b) Water saturation profiles vs time for test T-5

Test T-6: Ottawa#3821 sand, i = 0.2

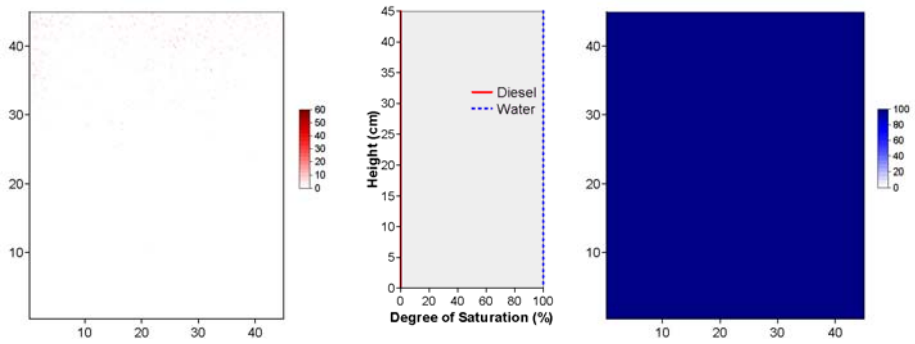

(a) t = 0 hour

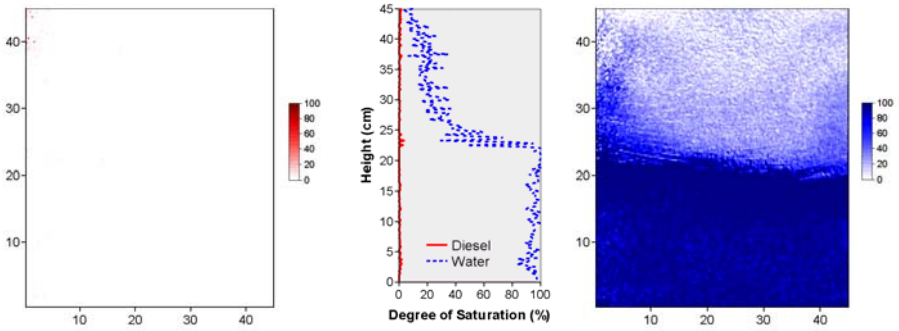

(b) t = 6 hour

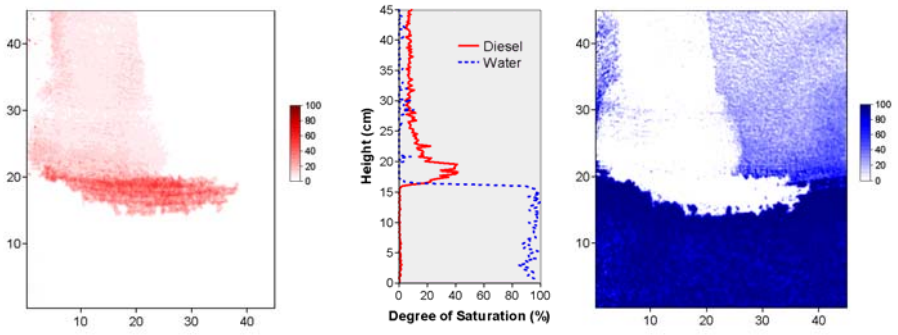

(c) t = 18 hour

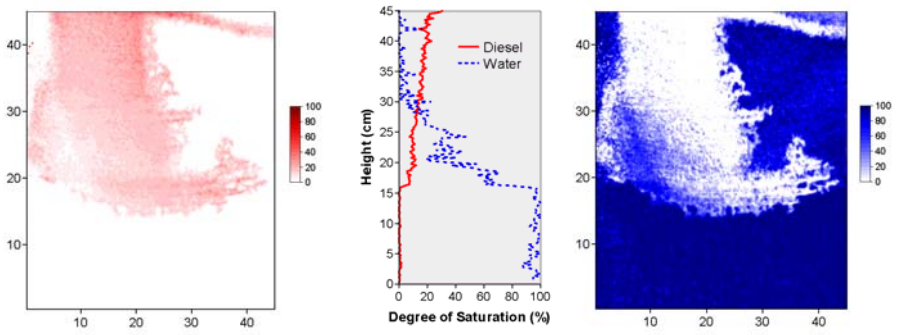

(d) t = 30 hour

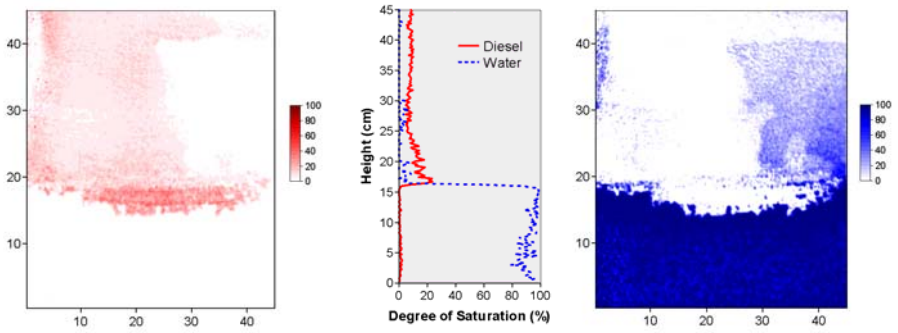

(e) t = 42 hour

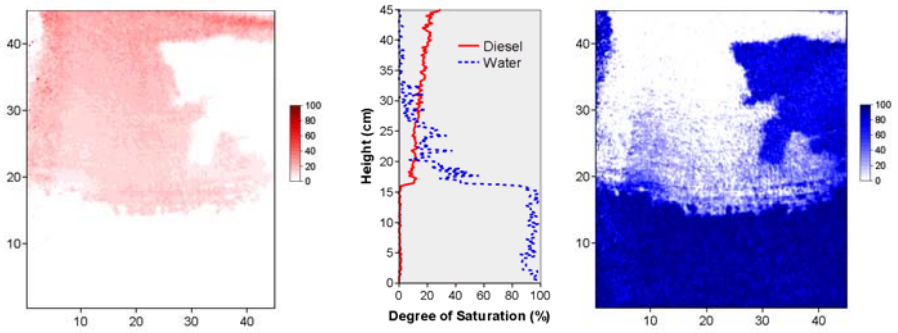

(f) t = 54 hour

Figure 4.16 Diesel saturation contour (left), diesel and water saturation profiles (center) and water saturation contour (right) for test T-6 (i = 0.2)

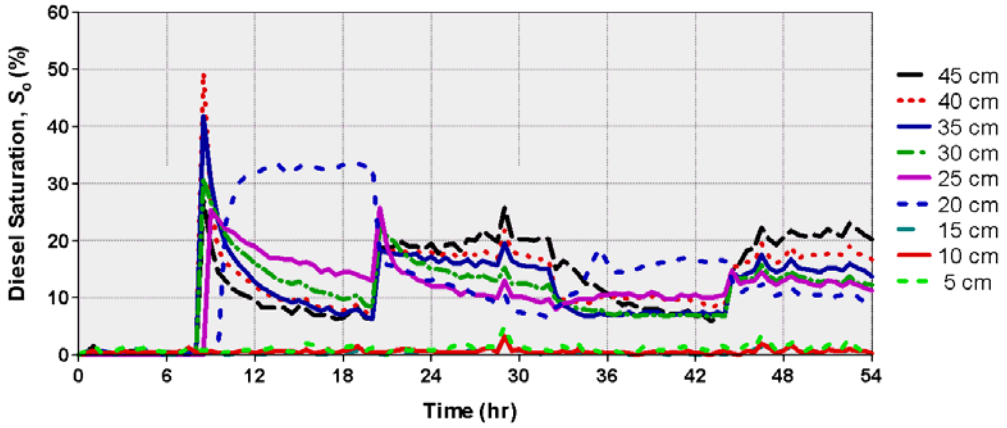

(a)

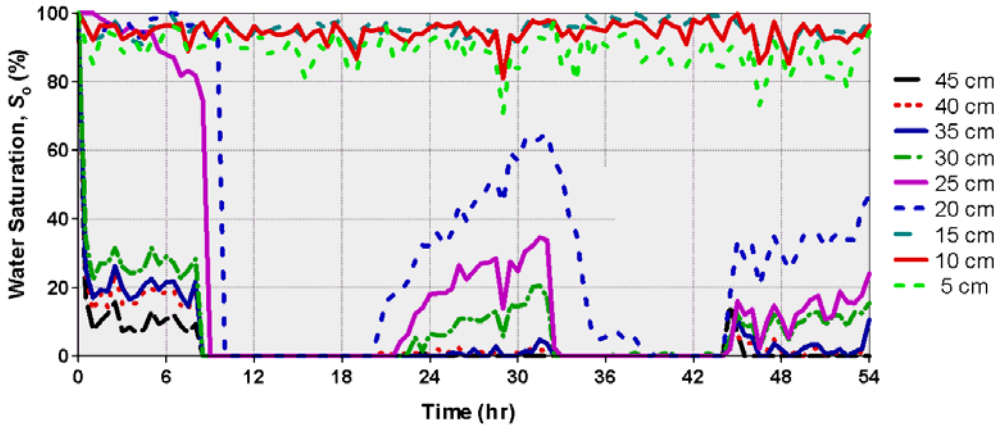

(b)

Figure 4.17 (a) Diesel saturation profiles vs. time for test T-6 and (b) Water saturation profiles vs time for test T-6

4.2.6 Discussions

From three-phase in homogeneous porous media experiment we found that, Diesel shown typical behavior of LANPL. Diesel move vertically downward under the gravity force and it migrate through the partially water saturated zone toward capillary fringe and water table. Some of diesel retains above the groundwater table. As diesel approach the water table, a large amount of diesel accumulates above the water table and resulted in collapse of the capillary fringe and it migrates laterally and lateral migration is controlled by diesel head distribution.

Symmetry lateral movement of diesel was observed in Test T-1and T-4 because there was no horizontal water flow. In Test T-2 (i = 0.1), Test T-3 (i=0.2), Test T-5 (i = 0.1), and Test T-6 (i = 0.2), lateral migration following the direction of groundwater flow were observed. Mobile diesel that floating above the water table at the end of 1st drainage stage (Figure 4.6 c. 4.8 c, 4.10 c. 4.12 c, 4.14 c and 4.16 c) moves vertically as the water table rise up in 1st imbibition stage. Redistribution of diesel was observed during the 2nd drainage, it again migrate downward follow the lowering of water table until it reach the capillary fringe and water table and move laterally following horizontal ground water flow. During the 2nd imbibition mobile diesel was move up follow the same behavior with the 1st imbibition. From the experiments it shows that the higher horizontal groundwater flow rate renders the larger diesel-contaminated area comparing with lower flow rate.

4.3 Three-phase in heterogeneous porous media experiment

Six tank tests were conducted to study the behavior of diesel migration in heterogeneous porous media with the coupling effect of water table fluctuating condition and horizontal groundwater flow. Water saturation distribution and diesel saturation distribution are obtained by Simplified Image Analysis Method. Testing program is shown in Table 4.3

Table 4.3 Three-phase in heterogeneous porous media testing program.

Test	Medium		Hydraulics gradient, i	Water Table Fluctuating
	Layer-1 and Layer-3	Layer-2 and Layer-4		
T-7	Ottawa#3821	Ottawa#3820	0	Yes
T-8	Ottawa#3821	Ottawa#3820	0.1	Yes
T-9	Ottawa#3821	Ottawa#3820	0.2	Yes
T-10	Ottawa#3820	Ottawa#3821	0	Yes
T-11	Ottawa#3820	Ottawa#3821	0.1	Yes
T-12	Ottawa#3820	Ottawa#3821	0.2	Yes

4.3.1 Equipments and materials

Similar with the experiment in section 4.2, Ottawa#3820 sand and Ottawa#3821 sand were used as a porous media. Dyed Diesel was used as LNAPL. Equipment set up is shown in Figure 4.2

4.3.2 Calibration

Three-phase column experiment required three pictures with each camera. Each camera took a picture of the column fill with dry sand, water saturated sand and diesel saturated sand. Diesel saturated sand pictures in section 4.2 were used as reference picture in image analysis processes From Equation 2.16, these six pictures correspond to $[D_{450}{}^{00}]_{mn,}$ $[D_{450}{}^{10}]_{mn}$, $[D_{450}{}^{01}]_{mn,}$ $[D_{640}{}^{00}]_{mn,}$ $[D_{640}{}^{10}]_{mn}$ and $[D_{640}{}^{01}]_{mn}$. Calibration pictures for three-phase heterogeneous porous media experiment are presented in Figure 4.18 and Figure 4.19

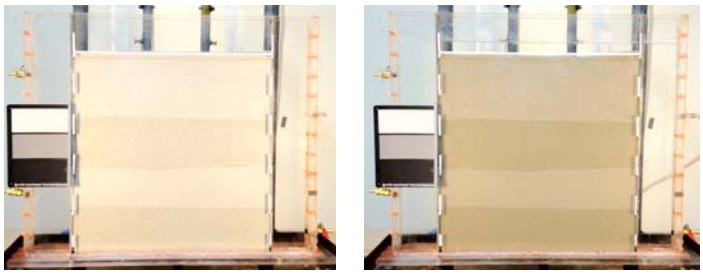

(a) (b)

Figure 4.18 Calibration pictures for test T-7, T-8 and T-9 (a) Tank filled with dry sand. (b) Tank filled with fully saturated water.

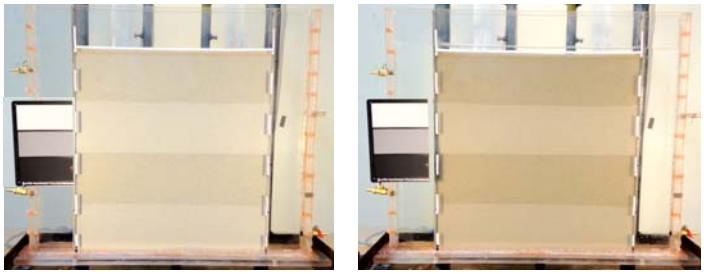

(a) (b)

Figure 4.19 Calibration pictures for test T-10, T-11 and T-12 (a) Tank filled with dry sand. (b) Tank filled with fully saturated water.

4.3.3 Experiments

Two-dimensional tank tests with water drainage following with diesel and air infiltration were conducted in four layered sand (Figure 4.20). Each layer was 12.5 cm height and dry density was 1.76 g/cm^3. The order of sand layer is presented in

Table 4.3. Digital pictures of dry sand were taken by the equipment that mentioned in section 4.2.1 and were used as dry sand reference picture in the image analysis processes. Right lateral tank and left lateral tank (Figure 4.1) were slowly filled with water to saturate the sand inside the tank and digital pictures of fully water saturated sand were taken and used as fully saturated water reference picture. Similar with the previous two-dimensional tank test in section 4.2, the test was divided into four stages: first drainage (t = 0 to 18 hr), first imbibition (t = 18 to 30 hr), second drainage (t = 30 to 42 hr) and second imbibitions (t = 42 to 54 hr) and hydraulics gradient for each test controlled by lateral tanks (h1 and h2) (Figure 4.21) and water level in lateral tank in each stage is shown in Table 4.2

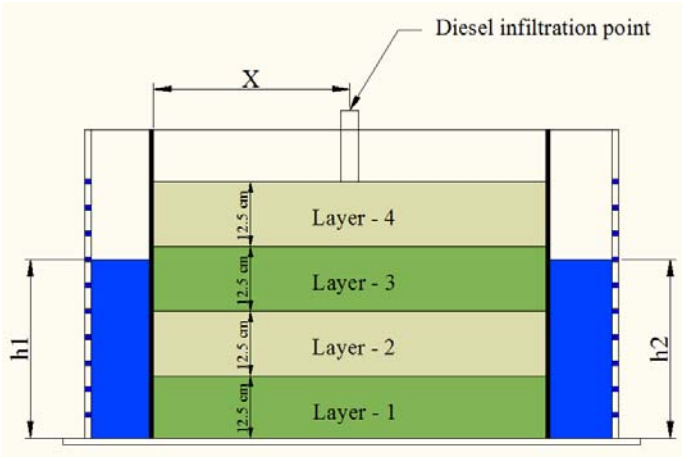

Figure 4.20 Heterogeneous porous media in two-dimensional tank

4.3.4 Computational analysis

Similar to the previous test in section 4.2, all pictures were exported from the NEF format (Nikon proprietary RAW version files) to the TIFF format (Tagged Image File Format) using Nikon ViewNX 2.0 TIFF images were analyzed with an ad-hoc program in MATLAB 2007a written by Flores (2010) Using the six calibration pictures, the average optical density matrices $[D_{450}{}^{00}]_{mn,}$ $[D_{450}{}^{10}]_{mn}$, $[D_{450}{}^{01}]_{mn,}$ $[D_{640}{}^{00}]_{mn,}$ $[D_{640}{}^{10}]_{mn}$ and $[D_{640}{}^{01}]_{mn}$ were calculated. $[D_{450}]_{mn}$ and $[D_{640}]_{mn}$ were calculated for each picture taken during the test, and the water saturation matrices ($[S_w]_{mn}$) and diesel saturation matrices ($[S_o]_{mn}$) were solved.

4.3.5 Results

Diesel saturation contour, water saturation contour, Diesel and water saturation profiles together with diesel and water saturation profiles plot with time for six tank tests are shown in Figure 4.21-Figure 4.32

Test T-7: Ottawa#3820 sand/Ottawa#3821 sand, i = 0

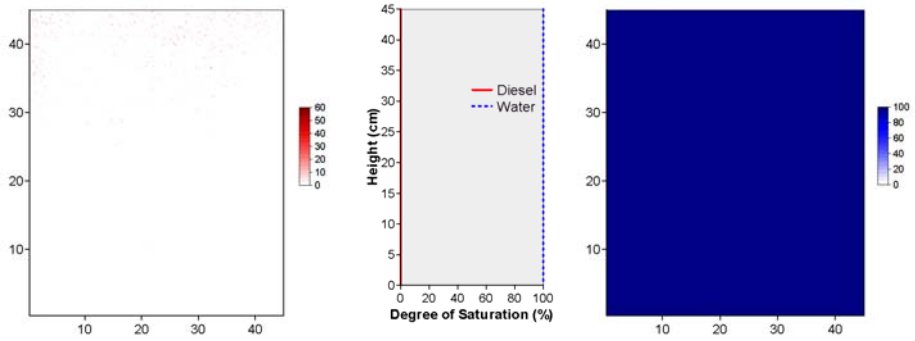

(a) t = 0 hour

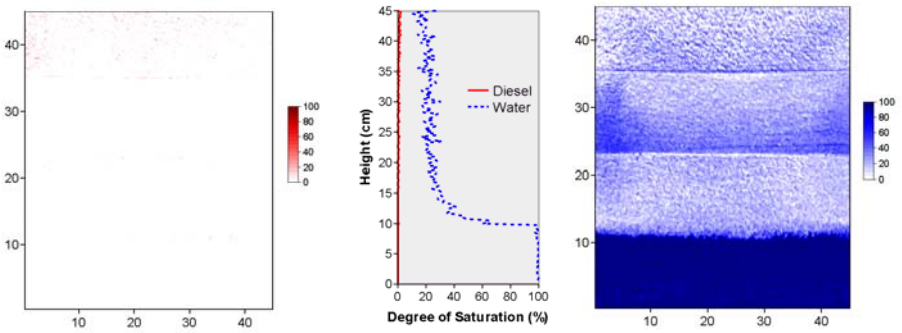

(b) t = 6 hour

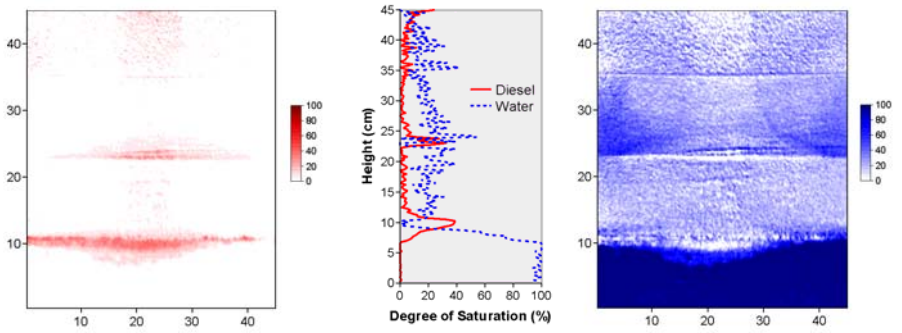

(c) t = 18 hour

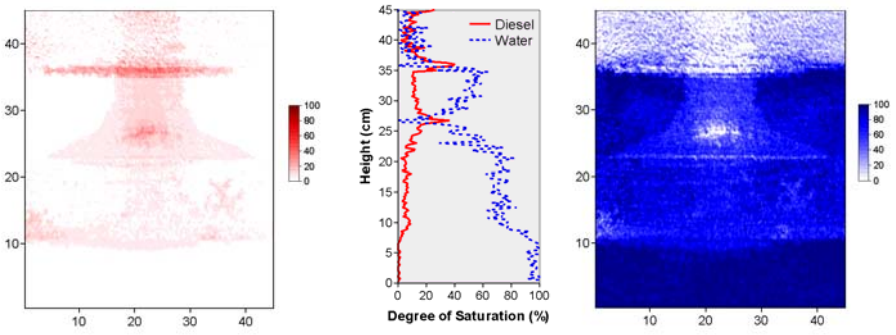

(d) t = 30 hour

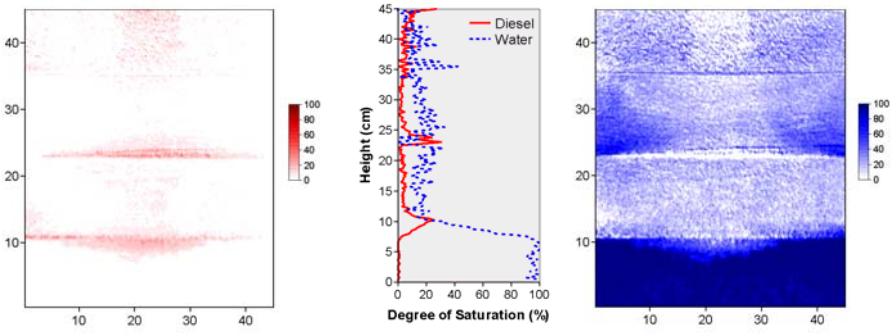

(e) t = 42 hour

(f)

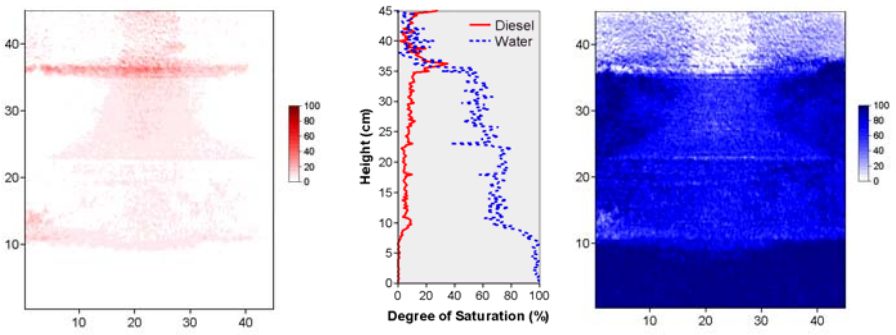

(g) t = 54 hour

Figure 4.21 Diesel saturation contour (left), diesel and water saturation profiles (center) and water saturation contour (right) for test T-7 (i = 0)

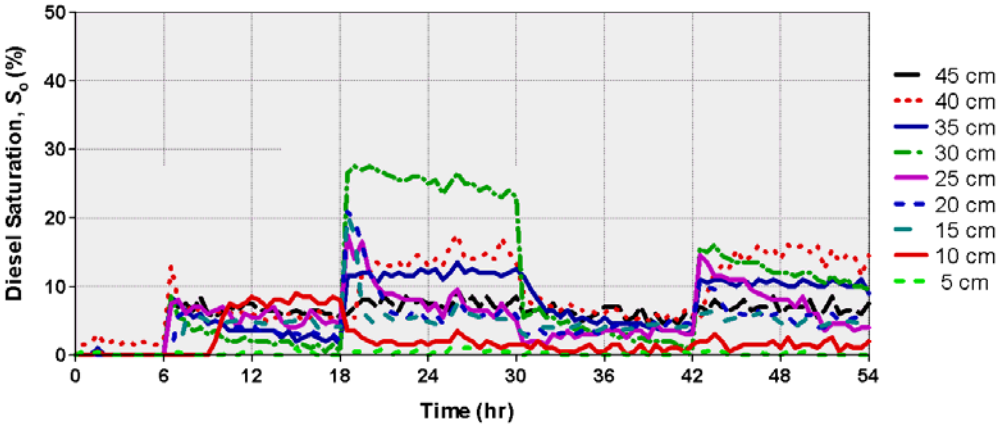

(a)

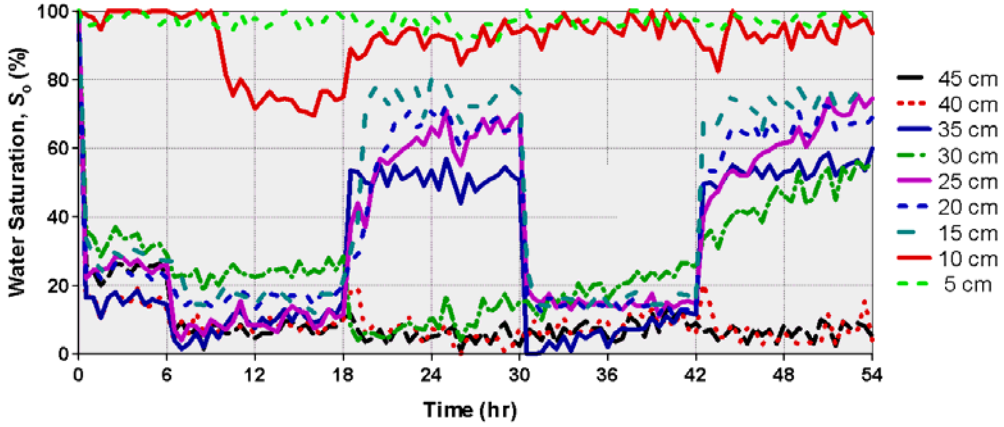

(b)

Figure 4.22 (a) Diesel saturation profiles vs. time for test T-7 and (b) Water saturation profiles vs time for test T-7

Test T-8: Ottawa#3820 sand/Ottawa#3821 sand, i = 0.1

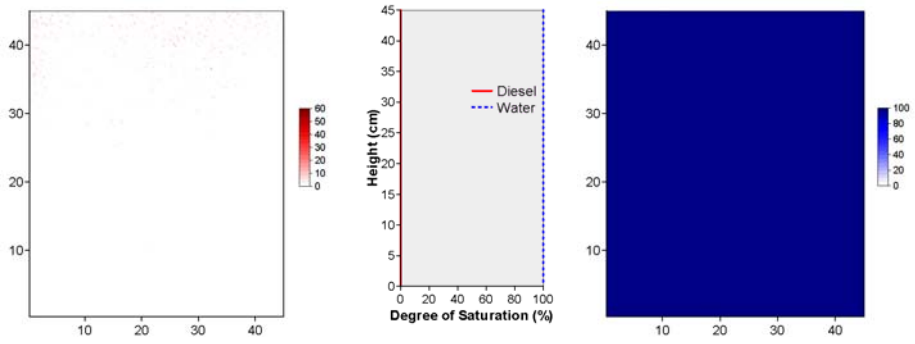

(a) t = 0 hour

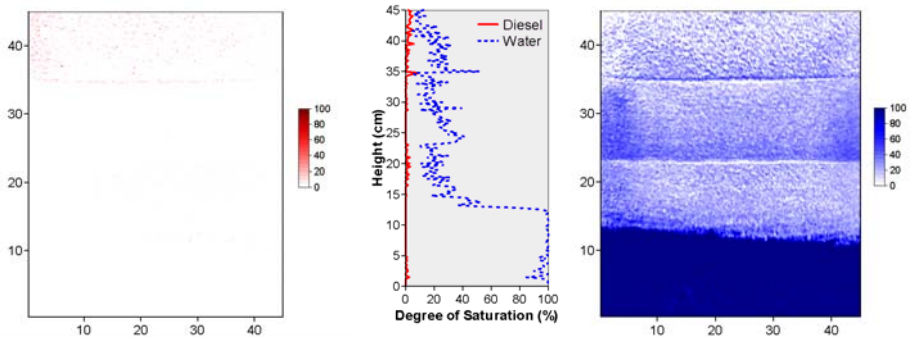

(b) t = 6 hour

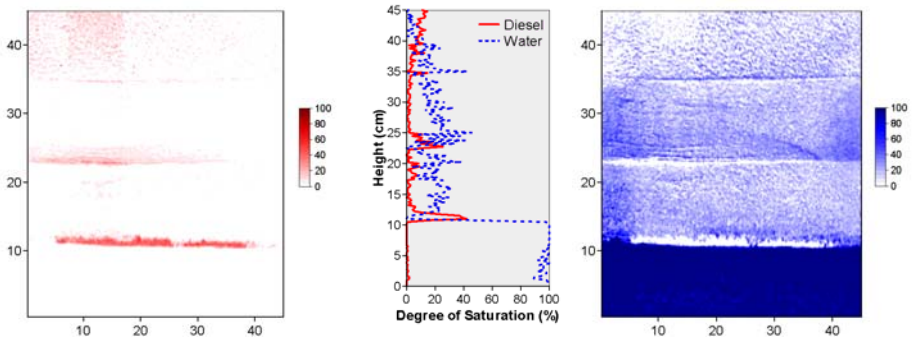

(c) t = 18 hour

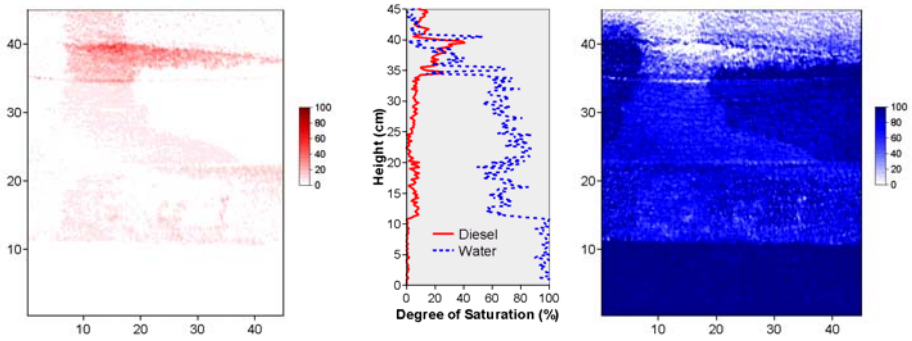

(d) t = 30 hour

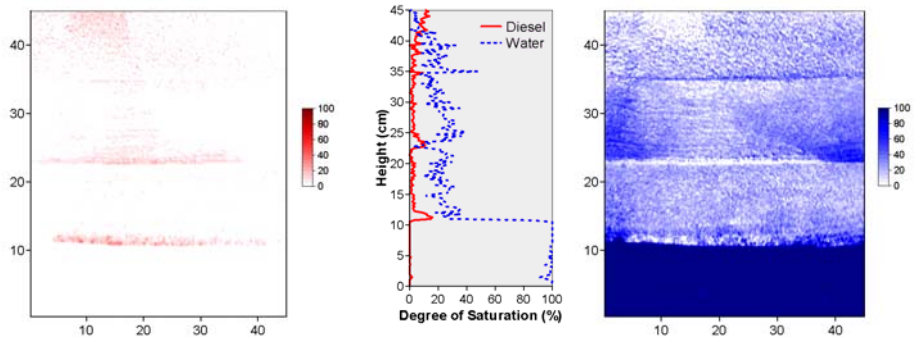

(e) t = 42 hour

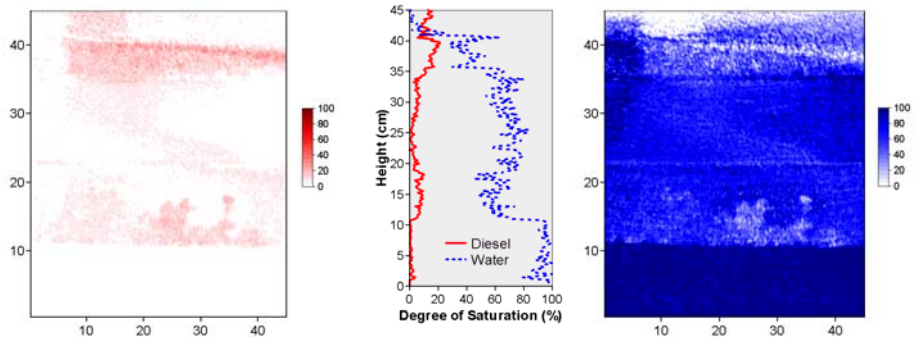

(f) t = 54 hour

Figure 4.23 Diesel saturation contour (left), diesel and water saturation profiles (center) and water saturation contour (right) for test T-8 (i = 0.1)

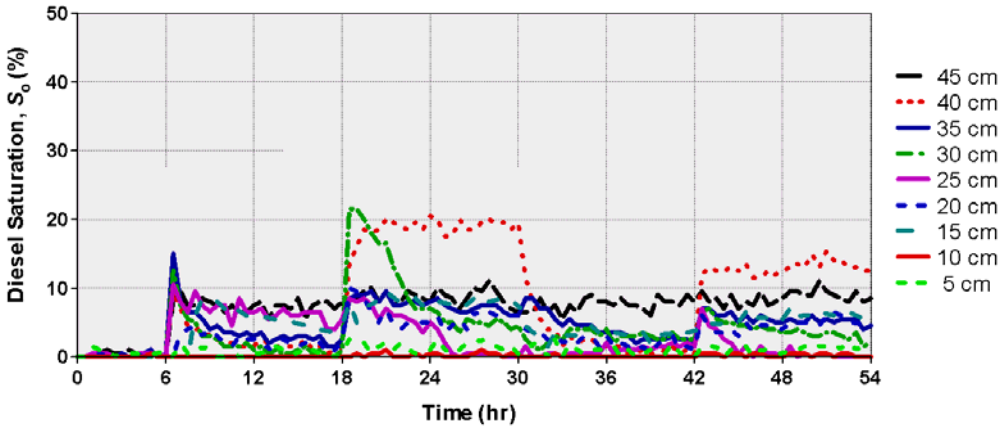

(a)

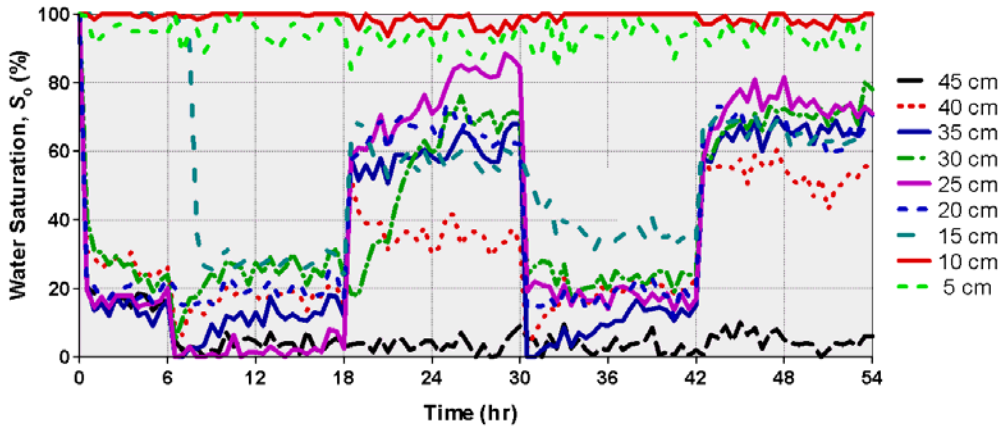

(b)

Figure 4.24 (a) Diesel saturation profiles vs. time for test T-8 and (b) Water saturation profiles vs time for test T-8

Test T-9: Ottawa#3820 sand/Ottawa#3821 sand, i = 0.2

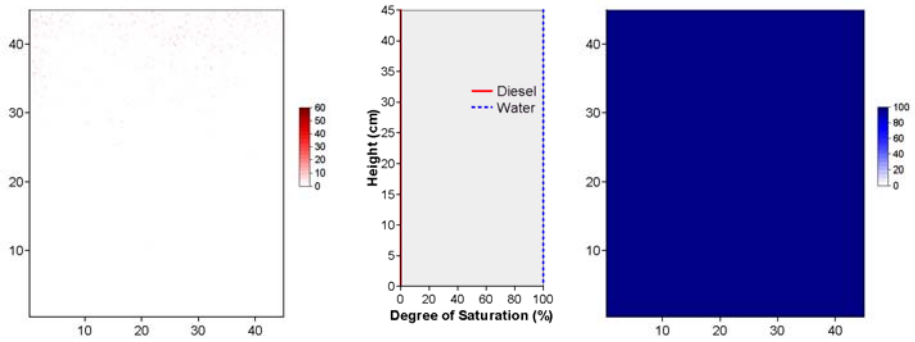

(a) t = 0 hour

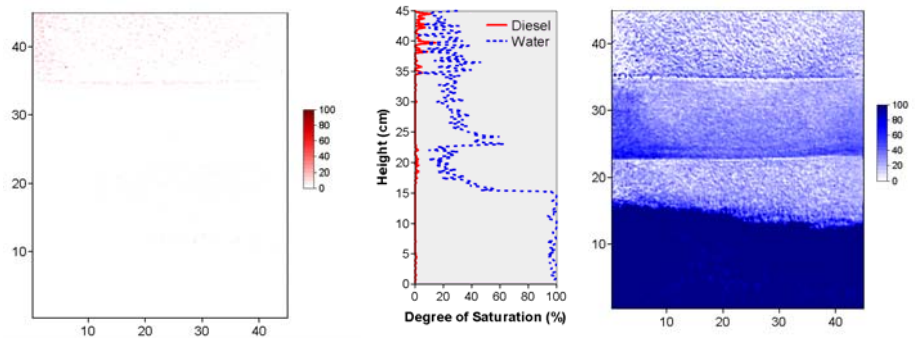

(b) t = 6 hour

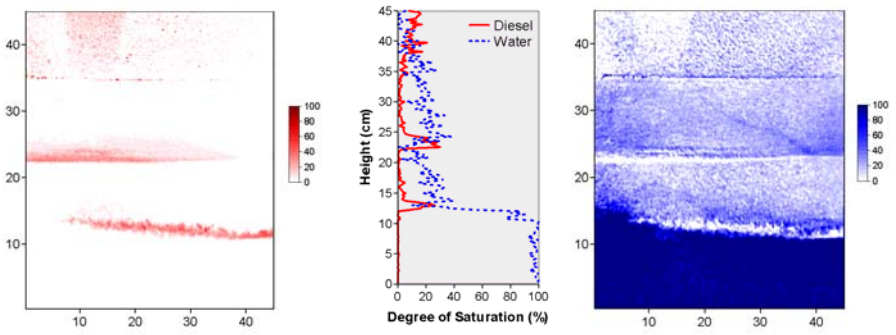

(c) t = 18 hour

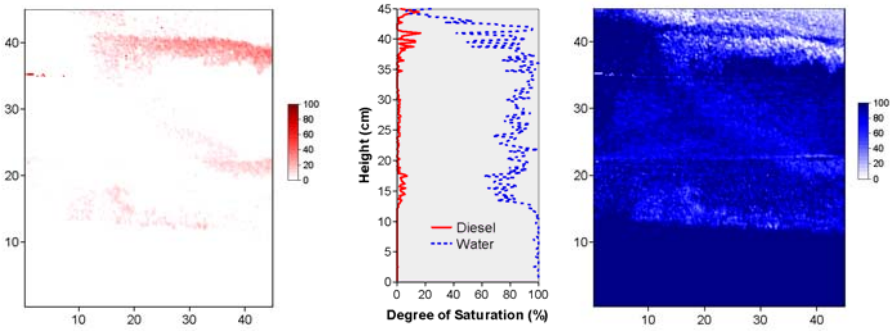

(d) t = 30 hour

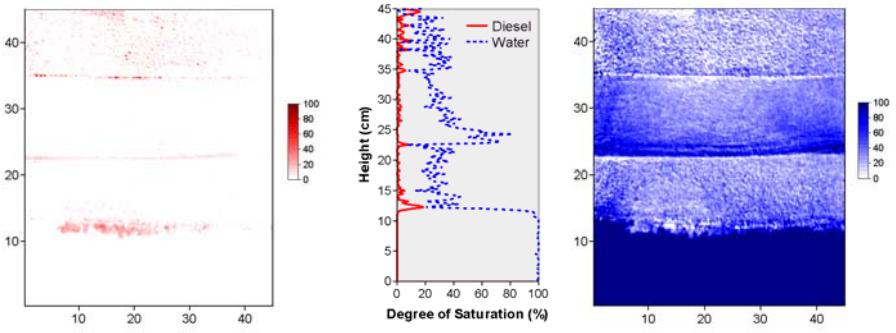

(e) t = 42 hour

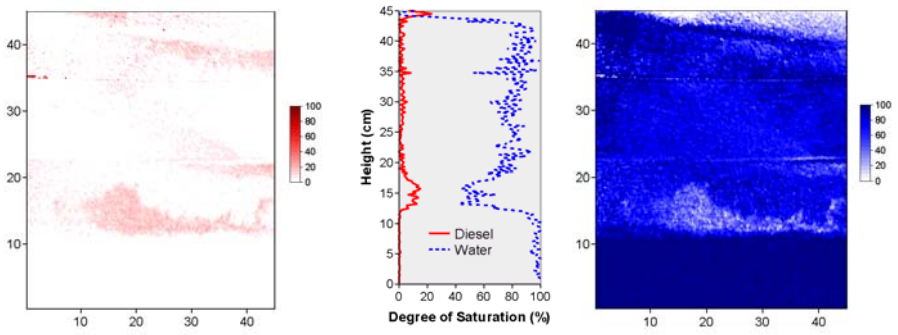

(f) t = 54 hour

Figure 4.25 Diesel saturation contour (left), diesel and water saturation profiles (center) and water saturation contour (right) for test T-9 (i = 0.2)

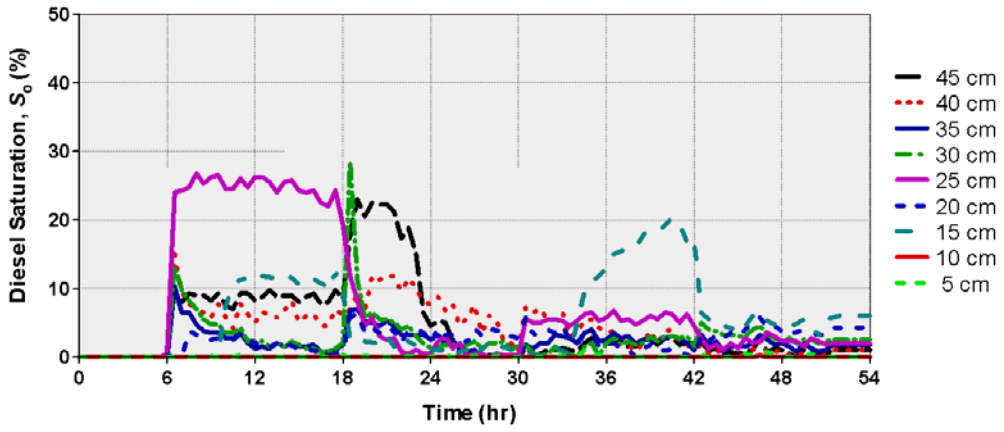

(a)

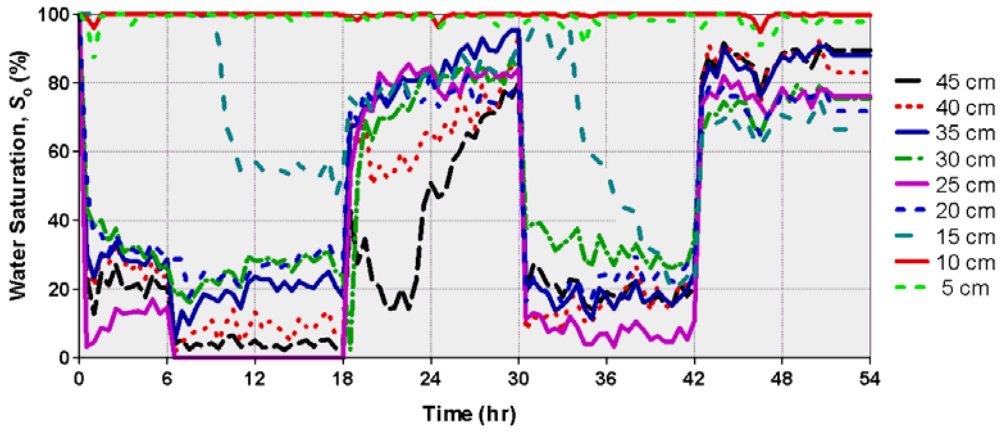

(b)

Figure 4.26 (a) Diesel saturation profiles vs. time for test T-9 and (b) Water saturation profiles vs time for test T-9

Test T-10: Ottawa#3821sand/Ottawa#3820 sand, i = 0

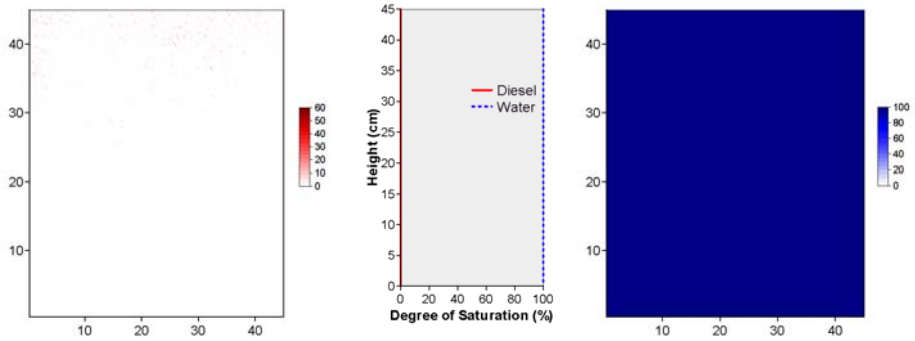

(a) t = 0 hour

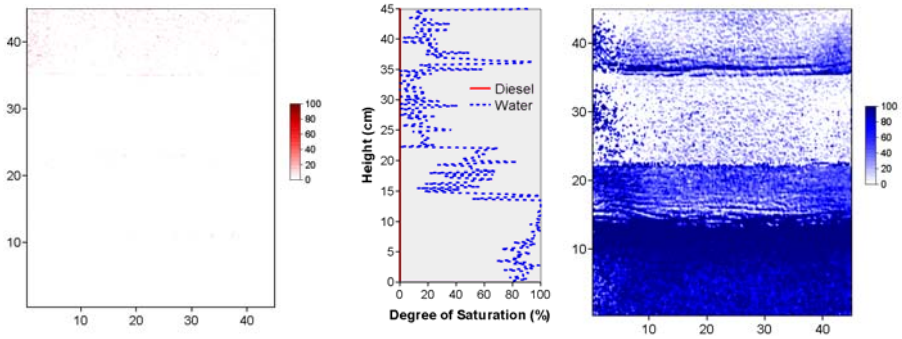

(b) t = 6 hour

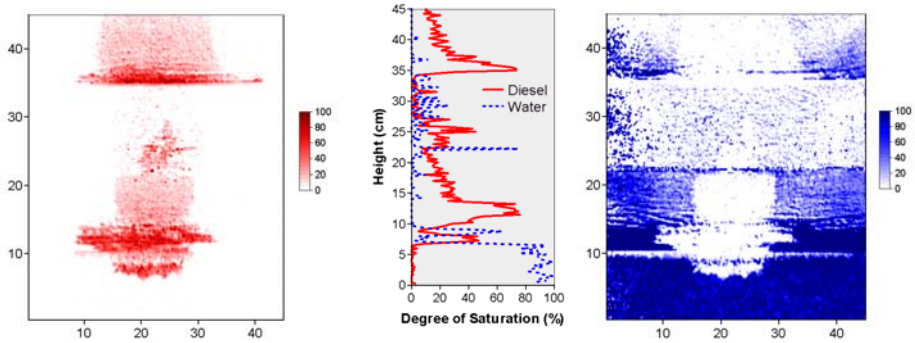

(c) t = 18 hour

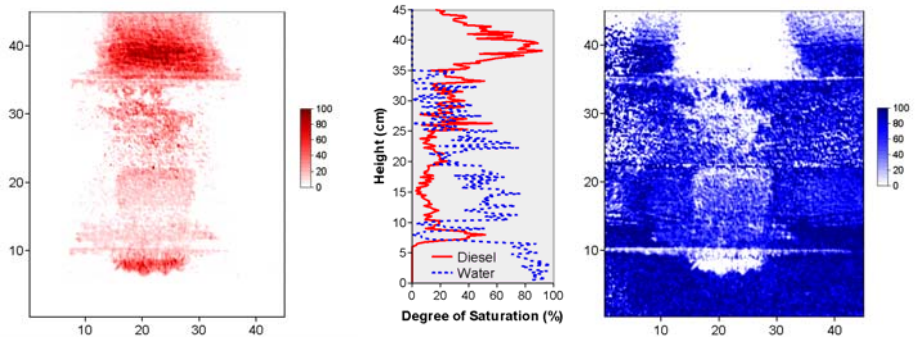

(d) t = 30 hour

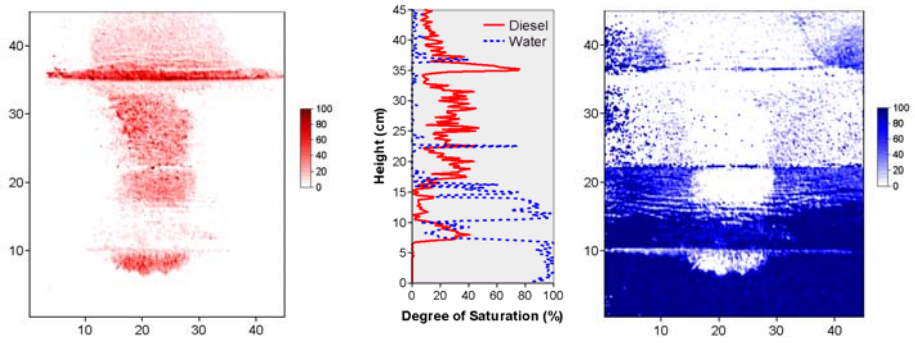

(e) t = 42 hour

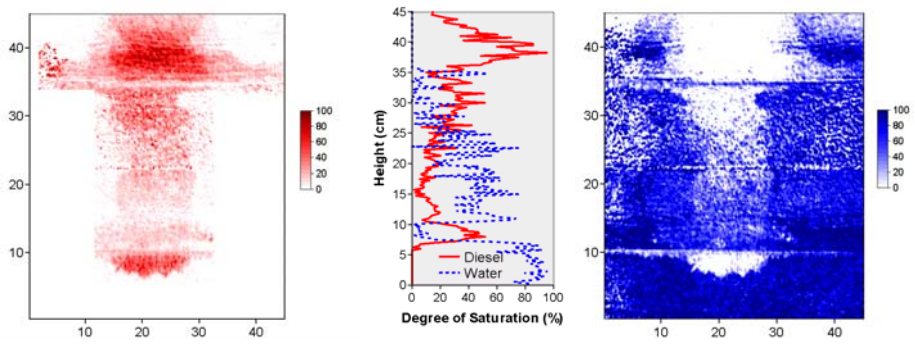

(f) t = 54 hour

Figure 4.27 Diesel saturation contour (left), diesel and water saturation profiles (center) and water saturation contour (right) for test T-10 (i = 0)

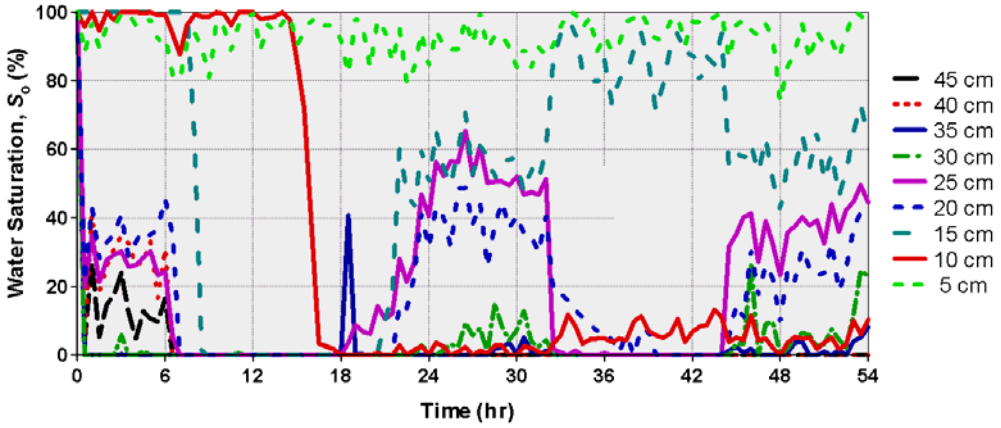

(a)

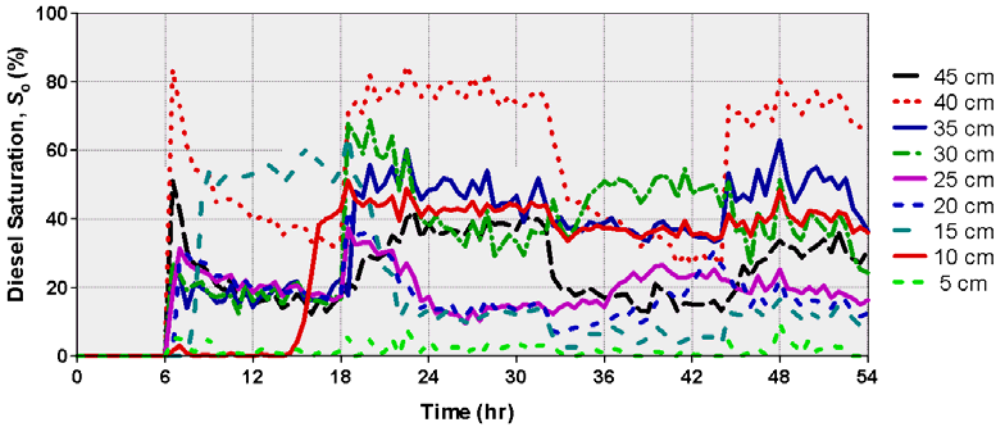

(b)

Figure 4.28 (a) Diesel saturation profiles vs. time for test T-10 and (b) Water saturation profiles vs time for test T-10

Test T-11: Ottawa#3821sand/Ottawa#3820 sand, i = 0.1

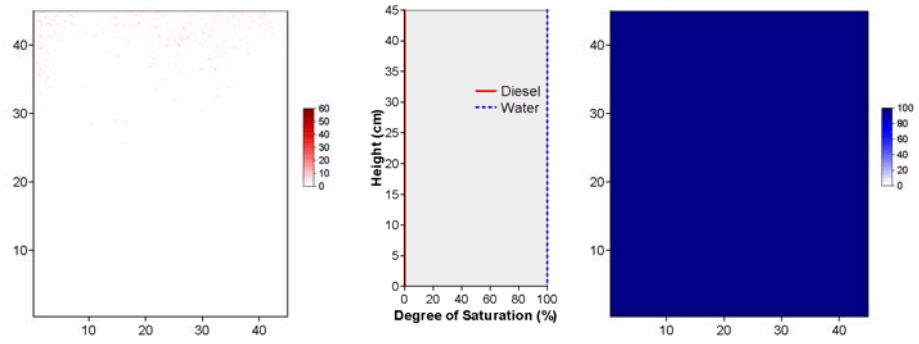

(a) t = 0 hour

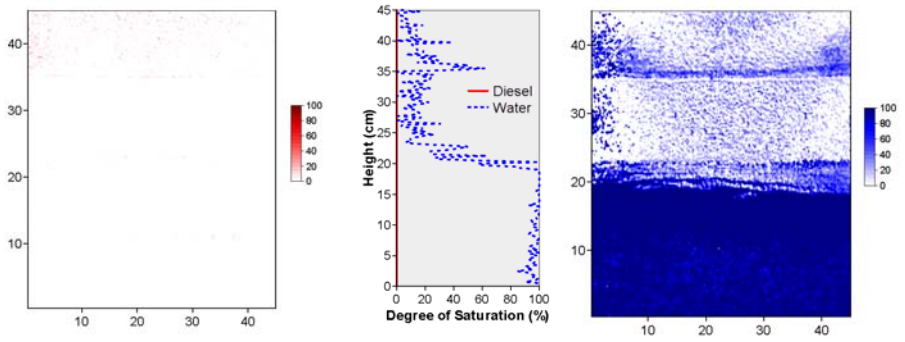

(b) t = 6 hour

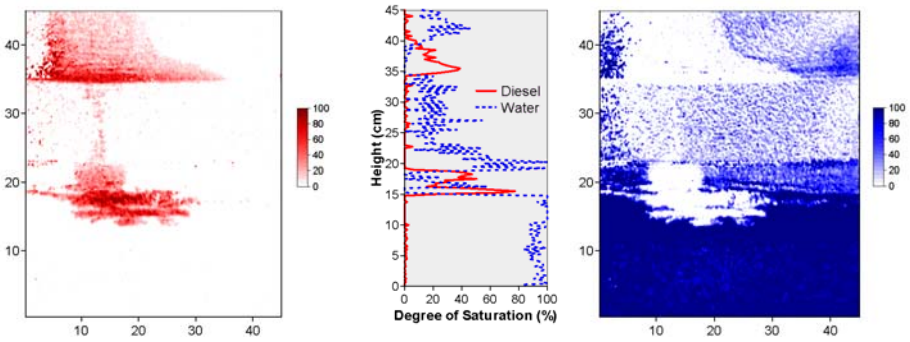

(c) t = 18 hour

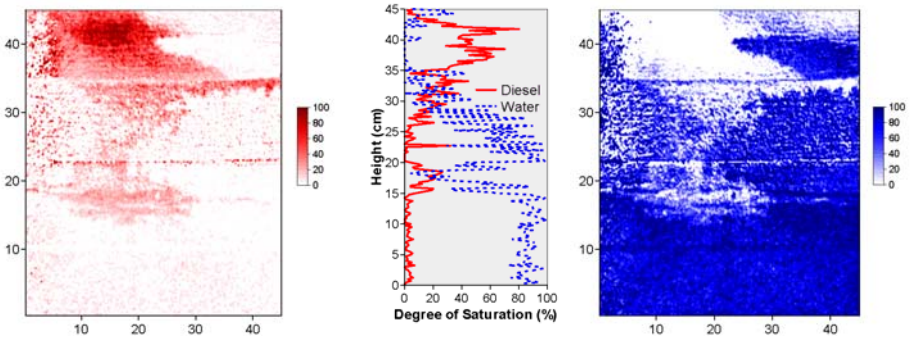

(d) t = 30 hour

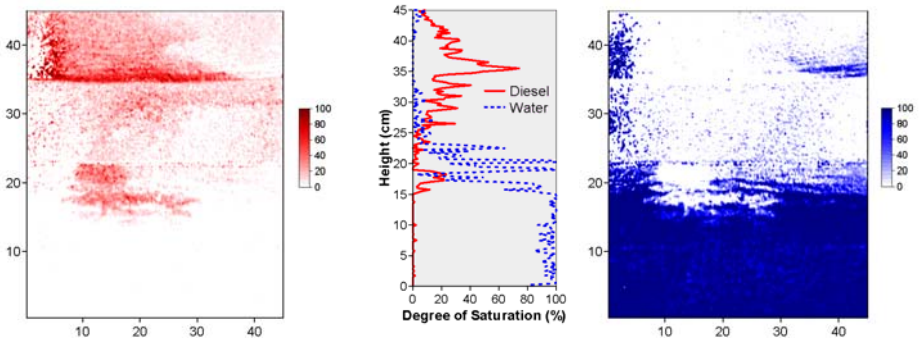

(e) t = 42 hour

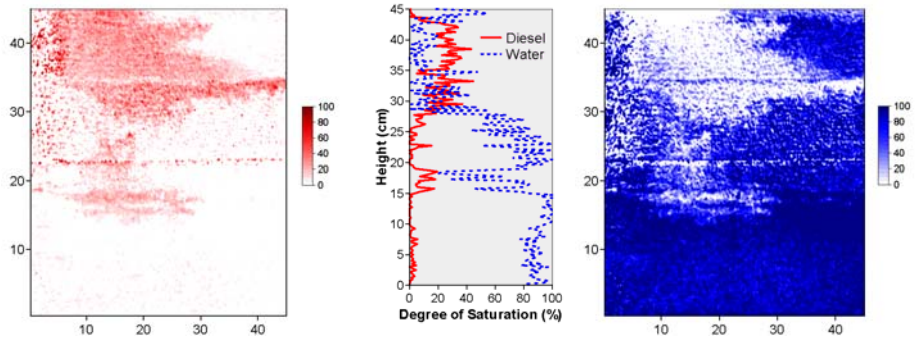

(f) t = 54 hour

Figure 4.29 Diesel saturation contour (left), diesel and water saturation profiles (center) and water saturation contour (right) for test T-11 (i = 0.1)

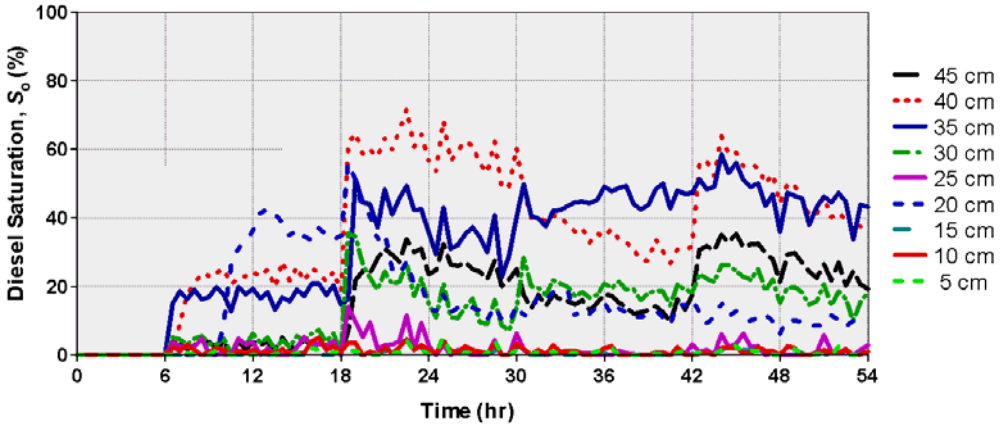

(a)

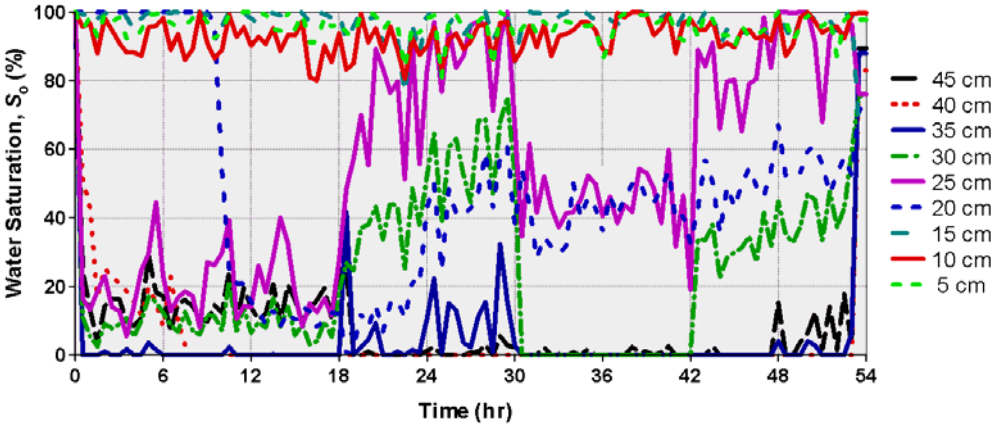

(b)

Figure 4.30 (a) Diesel saturation profiles vs. time for test T-11 and (b) Water saturation profiles vs time for test T-11

Test T-12: Ottawa#3821sand/Ottawa#3820 sand, i = 0.2

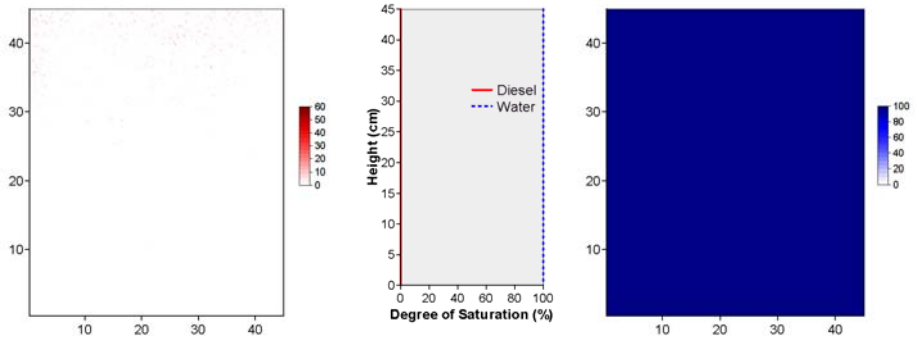

(a) t = 0 hour

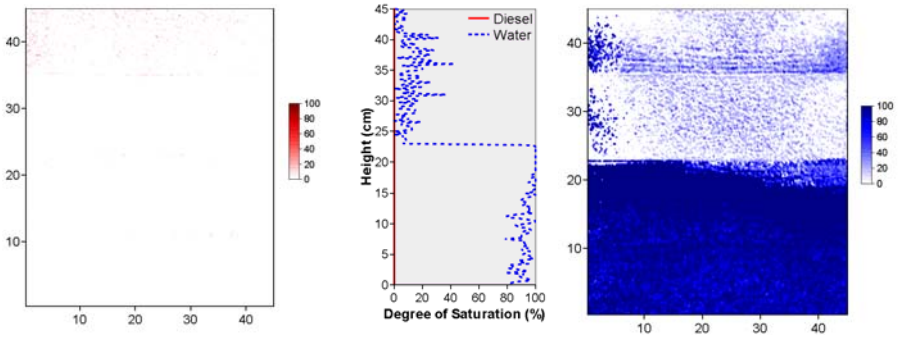

(b) t = 6 hour

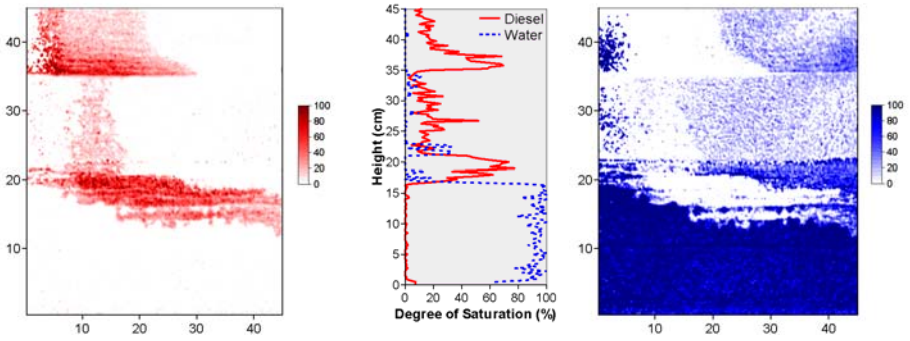

(c) t = 18 hour

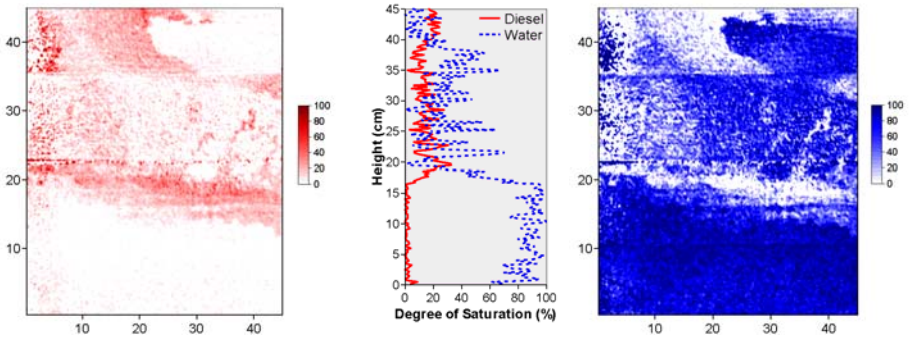

(d) t = 30 hour

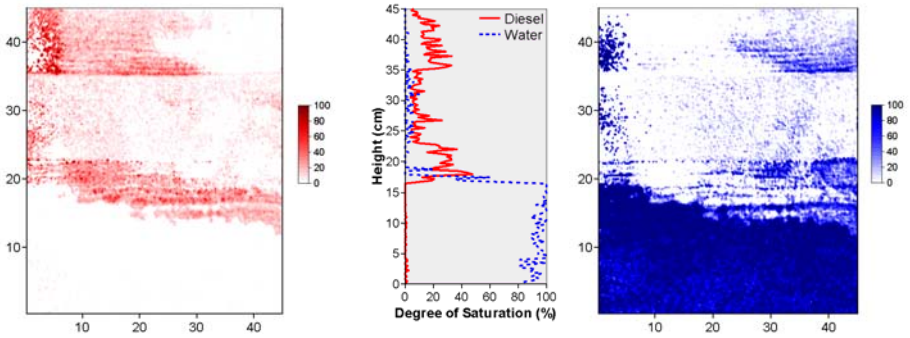

(e) t = 42 hour

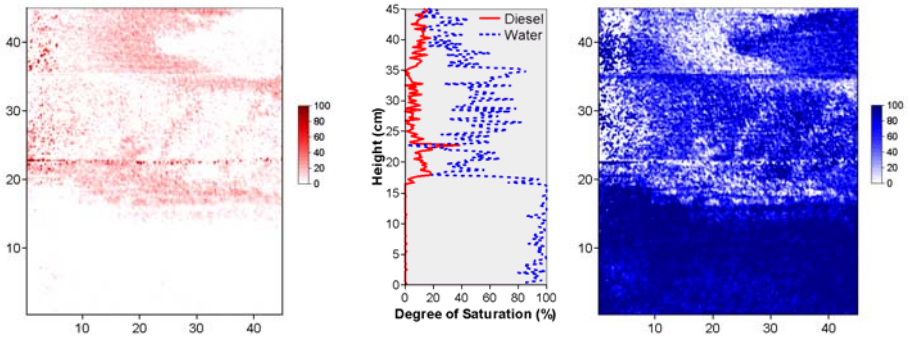

(f) t = 54 hour

Figure 4.31 Diesel saturation contour (left), diesel and water saturation profiles (center) and water saturation contour (right) for test T-12 (i = 0.2)

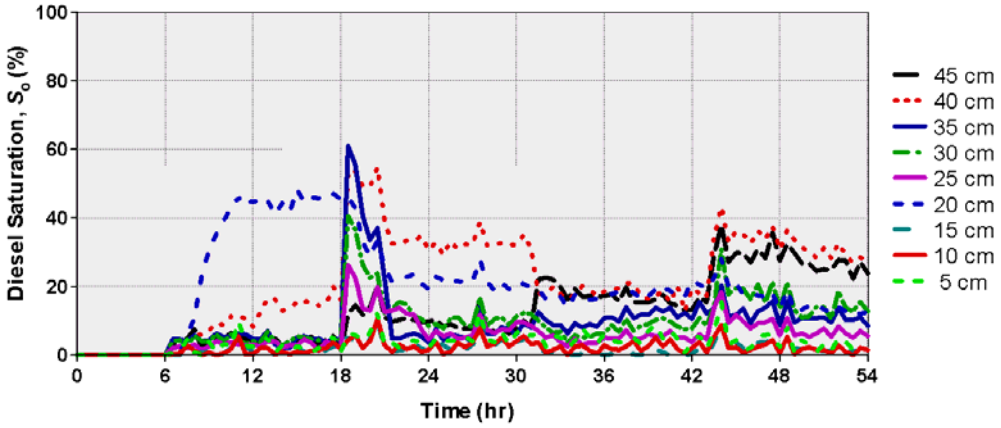

(a)

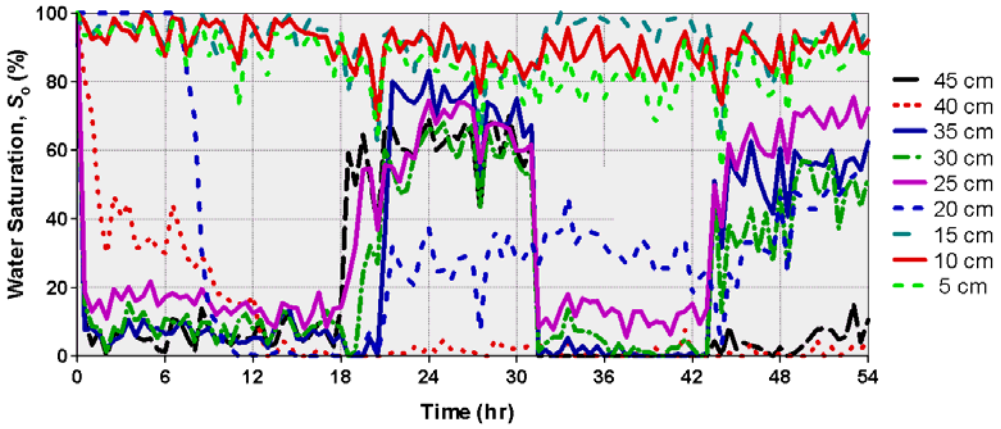

(b)

Figure 4.32 (a) Diesel saturation profiles vs. time for test T-12 and (b) Water saturation profiles vs time for test T-12

4.3.6 Discussions

From test T-7, T-8 and T-9, Ottawa#3820 sand laid over Ottawa#3821 sand when diesel introduce into the layer-4 (Figure 4.21) it migrated vertically downward following the lower of water table. At the interface between coarser layer (Ottawa#3820) and finer layer (Ottawa#3821), gravity force overcome the pore entry pressure of finer sand layer then most of diesel penetrate pass thorough this layer and accumulate at the interface between finer layer to coarse layer. Some of diesel starts to move laterally but at the end of 1st drainage stage most of diesel can infiltrated pass through coarser layer (layer-3) and mobile diesel were observed at this stage.

Symmetry lateral movement of mobile diesel was observed in test T-7 (i = 0) but in test T-8 (i = 0.1) and test T-9 (i = 0.2) mobile diesel were move laterally following the horizontal groundwater flow direction. During the 1st imbibition in test T-7, mobile diesel that accumulated in layer-2 in the 1st drainage moves vertically following the rise up of water table pass through layer-3 and accumulate again at finer/coarser interface (Layer-3/Layer-4) but in test T-8 and test T-9 mobile diesel can migrated pass through finer/coarser interface because of the horizontal groundwater flow transported those mobile diesel pass through that interface. For 2nd drainage and 2nd imbibition, Diesel repeated the same behavior but because of effect of horizontal ground water flow some of diesel in test T-8 and test T -9 were spilled out from the system.

From test T-10, T-11 and T-12, Ottawa#3821 sand laid over Ottawa#3820 sand when diesel infiltrate through finer layer (layer-4) it accumulate at the interface between finer/coarser and migrate laterally however finally excess diesel from finer layer move vertically downward pass through Ottawa#3820 sand layer (layer-3) and move toward to capillary fringe and water table. Some of diesel retains above the groundwater table. Similar as previous test diesel approach the water table, a large amount of diesel accumulates above the water table and resulted in collapse of the capillary fringe and it migrates laterally and lateral migration is controlled by diesel head distribution. There are less effect of horizontal ground water flow in test T-10, T-11 and T-12 because water table during drainage stage and imbibition stage are located at the finer sand layer (Ottawa#3821).

4.4 Conclusions

In this chapter we have conducted the diesel migration in two-dimensional tank test in both homogeneous and heterogeneous porous media under the coupling effect from horizontal groundwater flow and water table fluctuating condition.

Ottawa#3820 sand and Ottawa#3821 sand were used as porous media in this study. Simplified image analysis method was applied to obtain degree of liquid saturation in the study as proven in previous chapter that there is linear relationship

existed between average optical density and degree of diesel saturation and degree of water saturation in porous media.

The experiment demonstrated that diesel shown typical behavior of LANPL. Diesel move vertically downward under the gravity force and it migrate through the partially water saturated zone toward capillary fringe and water table. Some of diesel retains above the groundwater table. As diesel approach the water table, a large amount of diesel accumulates above the water table and resulted in collapse of the capillary fringe and it migrates laterally and lateral migration of mobile diesel is controlled by diesel head distribution. In general, migration may be expected to be greatest in the direction of ground-water flow. During the 1st imbibition stage mobile diesel that presented in the 1st drainage stage moves vertically as the water table rise up and redistribution of diesel was observed during the 2nd drainage, it again migrate downward follow the lowering of water table until it reach the capillary fringe and water table and move laterally following horizontal ground water flow. During the 2nd imbibition mobile diesel was move up following the same behavior with the 1st imbibition.

In conclusion, the effects of water table fluctuation are influenced by the hysteresis of the water retention curves and the fluid entrapment in the porous media and also depend on the wetting and drying history of the porous media. Diesel migration is influenced by heterogeneity in subsurface media and may be complex. From the experiments we found that it preferentially migrates laterally through more permeable pathways or accumulate and migrate along low permeability layers above the water table and it shows that the higher horizontal groundwater flow rate renders the larger diesel-contaminated area comparing with lower flow rate.

CHAPTER V

CONCLUSIONS

5.1 Major conclusions

In this study we have verified the validity of Simplified Image Analysis Method (Flores, 2010) in different porous media. The linear relationship existed between Average Optical Density (AOD) and degree of diesel saturation and water saturation were exhibited for Ottawa#3820 sand, Ottawa#3821 sand and Toyoura sand. Due to the availability of Toyoura sand in Thailand we have selected Ottawa#3820 and Ottawa#3821 as a porous media in One-dimensional column test and Two-dimensional tank test. The main results and conclusions are summarized as follow;

- Chapter 1

In chapter one, research background and objective of study were clarified.

- Chapter 2

In chapter 2 the basic concepts of NAPL migration in porous media were presented and the most important saturation measurement techniques for measuring water and NAPL in laboratory were discussed.

- Chapter 3

In chapter 3 we have proven that there is a linear relationship existed between Average Optical Density and degree of diesel saturation and degree of water saturation in different porous media so that simplified image analysis method can be applied as a non-intrusive and non-destructive technique to measure temporal and spatial distribution of fluid saturations in a whole domain in the dynamic behavior of diesel migrating in porous media under water table fluctuating conditions.

Ottawa#3820 sand and Ottawa#3821 sand were selected to use as porous media in this study. Two-phase (air-water and air-diesel) experiment was conducted in both Ottawa#3820 sand and Ottawa#3821 sand.

Three-phase (air-water-diesel) experiment was conducted in both homogeneous and heterogeneous porous media. In homogeneous porous media case, Diesel shown a typical LNAPL behavior under the water fluctuating condition It migrated downward following the lowering of water table during the drainage stage until it reach equilibrium and during the imbibition stage it float over the water table however some trapped diesel were observed during the experiment. In heterogeneous porous media case, Immobilized diesel was observed at the interface of finer sand (Ottawa#3821) and coarse sand (Ottawa#3820).

Diesel presents quite different flow pattern and distribution in different porous media indicating the difficulty in studying LNAPL movement in subsurface also engineering properties and configuration of porous media play a significant role in LNAPL distribution in heterogeneous porous media.

- Chapter 4

In chapter 4 we have conducted the diesel migration in two-dimensional tank test in both homogeneous and heterogeneous porous media under the coupling effect from horizontal groundwater flow and water table fluctuating condition.

Ottawa#3820 sand and Ottawa#3821 sand were used as porous media in this study. Simplified Image Analysis Method was applied to obtain degree of liquid saturation in the study as proven in previous chapter that there is linear relationship existed between Average Optical Density and degree of diesel saturation and degree of water saturation in porous media.

The experiment demonstrated that diesel shown typical behavior of LANPL. Diesel move vertically downward under the gravity force and it migrate through the partially water saturated zone toward capillary fringe and water table. Some of diesel retains above the groundwater table. As diesel approach the water table, a large amount of diesel accumulates above the water table and resulted in

collapse of the capillary fringe and it migrates laterally and lateral migration of mobile diesel is controlled by diesel head distribution. In general, migration may be expected to be greatest in the direction of ground-water flow. During the 1st imbibition stage mobile diesel that presented in the 1st drainage stage moves vertically as the water table rise up and redistribution of diesel was observed during the 2nd drainage, it again migrate downward follow the lowering of water table until it reach the capillary fringe and water table and move laterally following horizontal ground water flow. During the 2nd imbibition mobile diesel was move up following the same behavior with the 1st imbibition.

In conclusion, the effects of water table fluctuation are influenced by the hysteresis of the water retention curves and the fluid entrapment in the porous media and also depend on the wetting and drying history of the porous media. Diesel migration is influenced by heterogeneity in subsurface media and may be complex. From the experiments we found that it preferentially migrates laterally through more permeable pathways or accumulate and migrate along low permeability layers above the water table and it shows that the higher horizontal groundwater flow rate renders the larger diesel-contaminated area comparing with lower flow rate.

5.2 Further research

This research we have studied the behavior of diesel migration in porous media in both one-dimensional column and two-dimensional tank by using the Simplified Image Analysis Method. There are three experiments that will be conducted in the future to improve the accuracy of Simplified Image Analysis Method and to fulfill the lack of knowledge about Remediation system.

5.2.1 Lighting test

We have found the difficulty for lighting setup during the experiments. Lighting condition is very importance parameter in the Simplified Image Analysis Method. The constant lighting condition has to be controlled during the test. In reality there is very tough to control the light source because the intensity of light is not stable. Every light bulb has it own life time. From this research we found that LED

light is the suitable light for Simplified Image Analysis Method therefore we need to confirm again with the better control lighting condition in the laboratory.

LED light will be used to test the stability of the light and light sensor will be installed in the system to make sure the lighting condition is stable during the experiment. The light intensity value from each sensor will be recorded for each photo taken and correction factor from lighting condition will be taking into account for Simplified Image Analysis Method.

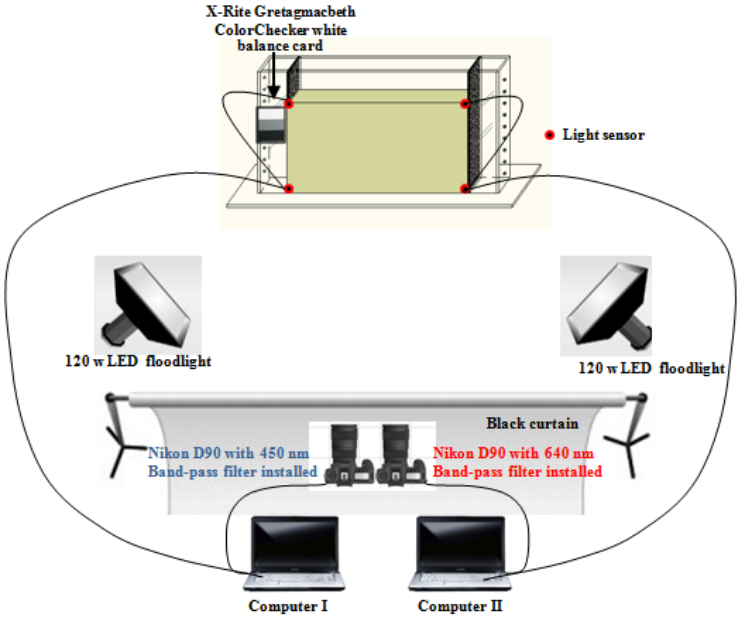

Figure 5.1 Lighting test experiment set up

5.2.2 Validity of SIAM in different porous media

In this study we have illustrated that linear relationship existed between AOD and degree of diesel saturation (S_o) and degree of water saturation ($S_{w)}$ in selected porous media. The sand that we used in this study (Ottawa sand) normally use in the field density test and it is not inexpensive sand and the engineering properties is rather different from reality porous media therefore we need confirm the linear relationship between AOD, S_o and S_w for different kind of porous media then we can study the LNAPL migration in more variety porous media. We may have to

change the band-pass filter to near infrared range (750-900 nm) following the study of Kechavarzi *et al* (2005).

5.2.2 Air sparging and soil vapor extraction test.

This study we have study to better understand the contaminant behavior. The remediation processed such as air-sparging and soil vapor extraction is suitable for cohesionless soil which is the one that we use in this study. To better understand the whole system from the point of contamination happened to the remediation is very importances especially there were many report regarded to LNAPL subsurface contamination and not many researchers in Thailand working in this topic. Local material will be used as a porous media to fulfill the knowledge about contamination and remediation for Thailand’s local porous media.

REFERENCES

Abdul, Abdpul S. 1998. Migration of petroleum products through sandy hydrogeologic systems. Ground Water Monitoring Review 8 (4): 73-81

Anderson, W.G. 1986. Wettability literature survey, Part 1. Rock/oil/brine interactions, and the effects of core handling on wettability, J. Pet.Technol (10): 1125-1149

Bear. J. 1979. Hydraulics of Groundwater. McGraw Hill

Bear, J., and Verruijt, A. 1987. Modeling Groundwater Flow and Pollution. Dodrecht, Netherlands: D.Reidel Pub

Boulding, J.R. and Ginn, J.S. (2003) Practical Handbook of Soil, Vadose Zone and Groundwater Contamination Assessment, Prevention and Remediation. 2nd edition. Florida: CRC Press

Eckberg and Sunada. 1984. Non-steady three phase immiscible fluid distribution in porous media. Water Resource Research 20 (12): 1891-1897

Fagerlund, F., T.H. Illangasekare and A. Niemi. 2007. Nonaqueous-Phase Liquid Infiltration and Immobilization in Heterogeneous Media: 2.Application to Stochastically Heterogenoeus Formations. Vadose Zone Jounal (6): 483-495

Farr, A.M., Houghtalen, R.J., and McWhorter, D.B. 1990. Volume Estimation of Light Nonaqueous Phase Liquids in Porous Media. Groundwater. 28(1): 48-56.

Fetter, C.W. 1999. Contaminant hydrogeology. New Jersey: Prentice hall Upper Saddle River

Flores, G. 2010. A Simplified Image Analysis Method To Evaluate LNAPL Saturation Under Fluctuating Groundwater Conditions. Global Environmental Studies, Kyoto University. Doctoral Degree**:** 168.

Freeze, R.A., and Cherry, J.A. 1979. Groundwater. New Jersey: Prentice-Hall

Kechavarzi, C., Soga, K. and Wiart, P. 2000. Multispectral image analysis method to determine dynamic fluid saturation distribution in two-dimensional three-fluid phase flow laboratory experiments. Journal of Contaminant Hydrology 46(3-4): 265-293.

Lenhard, R.J. and Parker, J.C. 1990. Estimation of free Hydrocarbon Volume from Liquids Level in Monitoring wells: Ground Water. V28 (1): 57-67

Luatua, S. 2010. Effects of physical properties on LNAPL migration in porous media under fluctuating groundwater conditions. Global Environmental Studies, Kyoto University. Master Degree**:** 74.

Mercer, J. W., and R. M. Cohen. 1990. A Review of Immiscible Fluids in the Subsurface: Properties, Models, Characterization and Remediation. Journal of Contaminant Hydrology. 6:107-163.

Nacalai Tesque. 2003. Material Safety Data Sheet: Sudan III. Japan

Nacalai Tesque. 2003. Material Safety Data Sheet: Brilliant Blue FCF. Japan

Number of service fuel service station in Thailand. [online]. Available from: http://www.doeb.go.th/info/info_sta_quarter.php. [2012, February 29]

PTT PLC MSDS. [online]. Available from: http://www.pttplc.com/TH/MSDS.aspx. [2008, December 25]

Quigley, R.M., Yanful, E.R., and Fernandez, F. 1987. Ion Transfer by Diffusion through Clay Barriers. Geotechnical Practice for Waste Diposal American Society of Civil Engineers Special Publication 13:137-158

Shakelford, C.D. 1989. Diffusion of Contaminants through Waste Containment Barrier Materials. Geotech. News. 6(2): 24-27

Sudaseng, S., Flores, G., Katsumi, T., Inui, T., Likitlersuang, S. and Yimsiri, S. 2010. Study of Diesel Migration in Porous Media by the Simplified Image Analysis Method. Proceeding of 23rd KKCNN Symposium on Civil Engineering. Taipei.

Sudaseng, S., Flores, G., Katsumi, T., Inui, T., Likitlersuang, S. and Yimsiri, S. 2011a. Experimental Study of Diesel Migration in Porous Media by the Simplified Image Analysis Method. Proceeding of Geo-Environmental Engineering 2011. Japan.

Sudaseng, S., Flores, G., Katsumi, T., Inui, T., Likitlersuang, S. and Yimsiri, S. 2011b. Experimental Study of Diesel Migration in Porous Media by the Simplified Image Analysis Method. Proceeding of The 2nd International Conference on Sustainable Future for Human Security. Japan.

The Basic. [online]. Available from: http://www.rtdf.org/public/napl/training/module1.pdf. [2009, January 30]

Van Genuchten, M.Th. 1980. A closed-form-equation for predicting the hydraulic

conductivity of unsaturated soil. Soil Science Society of America Journal 44: 892-98

BIOGRAPHY

Suwasan Sudsaeng

Mr.Suwasan Sudsaeng was born on July 31, 1980 in Udonthani Province, Thailand. He finished his primary school from Ban Wangphue-Khampom School in Khon Kaen province in 1994 and he continued his high school at Khon Kaen Wittayayon School and completed his high school in 1999, in the year 2000 He attended Department of Civil engineering, Faculty of Engineering at Burapha Univesity in Chonburi Province and He graduated from this faculty in 2003. From 2003 to 2004 he served as civil engineering and work for underground utility locating company based in Bangkok, Thailand. From 2004-2005 he served as underground utility survey department manager, the company based in Manama, Bahrain. He finished his duties and return back to Thailand in the year 2005 and work as civil engineering in environmental consultancy company base in Bangkok. In 2006, he applied for the scholarship for his PhD. and AUN/SEED-Net in the collaboration with Thailand Commission of Higher Education granted him a PhD. sandwich program (5 years) scholarship to study at Department of Civil engineering, Faculty of Engineering, Chulalongkorn University, Bangkok, Thailand. His publications are listed below;

S.Yimsiri&S.Sudsaeng, Effects of Ethanol content in Alternative Fuel on Soil-Liquid Characteristic Curves, 6th International Congress on Environmental Geotechnics, 8-12 November 2010, India,1405-1410

S. Sudsaeng, G. Flores, T. Katsumi, T. Inui, S. Likitlersuang& S.Yimsiri, Study of Diesel Migration in Porous Media by the Simplified Image Analysis Method, The 23rd KKCNN Symposium on Civil Engineering, 13-15 November, 2010, Taiwan, Published (KKCNN Best Presenter Award)

S. Sudsaeng, G. Flores, T. Katsumi, T. Inui, S. Likitlersuang& S.Yimsiri, Experimental Study of Diesel Migration in Porous Media by the Simplified Image Analysis Method, Geo-Environmetal Engineering 2011, May 2011, Japan, Published (Best Presentation Award)